Exotic Phenomena in Topological States of Matter

by

Mohammad Mahmoudzadeh Vazifeh

M.Sc., Sharif University of Technology, 2008

A THESIS SUBMITTED IN PARTIAL FULFILLMENT
OF THE REQUIREMENTS FOR THE DEGREE OF

Doctor of Philosophy

in

THE FACULTY OF GRADUATE AND POSTDOCTORAL
STUDIES
(Physics)

The University Of British Columbia
(Vancouver)

October 2014

Abstract

Electronic states in band insulators and semimetals can form nontrivial topological structures which can be classified by introducing a set of well defined topological invariants. There are interesting experimentally observable phenomena tied to these topological invariants which are robust as long as the invariants remain well-defined. One important class manifesting these topological phenomena in the bulk and at the edges is the time reversal invariant topological band insulators first discovered in HgTe in 2007. Since then, there have been enormous efforts from both the experimental and the theoretical sides to discover new topological materials and explore their robust physical signatures.

In this thesis, we study one important aspect, i.e., the electromagnetic response in the bulk and at the spatial boundaries. First we show how the topological action, which arises in a time reversal invariant three dimensional band insulator with nontrivial topology, is quantized for open and periodic boundary conditions. This confirms the Z2 nature of the strong topological invariant required to classify time-reversal invariant insulators. Next, we introduce an experimentally observable signature in the response of electronic spins on the surface of these materials to the perpendicular magnetic field. We proceed by considering electromagnetic response in the bulk of topological Weyl semimetals in a systematic way by considering a lattice model and we address important questions on the existence or absence of the Chiral anomaly. In the end, we show how a topological phase in a one dimensional system can be an energetically favourable state of matter and introduce the notion of self-organized topological state by proposing an experimentally feasible setup.

Preface

I have written this thesis based on the results my supervisor and I have obtained by working on various problems in the field of topological insulators throughout my program. Some sections of this thesis are based on the notes written by my research supervisor Professor Marcel Franz, and also publications authored by me and him.

Chapter 1 gives a brief introduction to the subjects that we have studied during the course of my program in the field of topological insulators. This is entirely based on my understanding of the topics which is of course limited but I have tried to convey the most important concepts of the field to people who are not very familiar with these novel topics. I have also tried to show why we think the problems that we have considered in this thesis are among important ones in the field.

Chapter 2 starts with an introduction to the topological Axion response. I also provide a simple proof of the quantization of the associated topological action term which are based on the short article entitled "Quantization and 2π Periodicity of the Axion Action in Topological Insulators" which we have published in Physical Review B, 82, 233103 (2010). The quantization proof is based on the notes written by my supervisor and I. Providing a proof for the quantization based on the electromagnetic field decomposition was my supervisor's idea. He proved that using a certain field decomposition one can write a second Chern number as a product of two first Chern numbers which are quantized. I provided an argument for the quantization of the first Chern numbers on tori based on the fact that single-valued electronic wave-functions must be well-defined. I wrote the initial draft of the manuscript based on my supervisor's and my own notes. He then edited and

modified the short report before we submitted it to Physical Review B.

Chapter 3 is based on my calculations while working on magnetic response of the mobile electrons at the surface of a topological insulator and some sections are based on the article we have published in Physical Review B 86, 045451 (2012). The problem statement was provided by my supervisor, I carried out the calculations. He provided extensive guidance during the time I was carrying out the calculations and resolved all the problems I encountered. I wrote the initial draft of the manuscript. He then edited the entire manuscript and we submitted the paper entitled "Spin Response of Electrons on the Surface of a Topological Insulator" to Physical Review B.

Chapter 4 is based on my notes while working on this project. The idea was mine and I carried out the calculations and wrote the paper entitled "Weyl Semimetal from the Honeycomb Array of Topological Insulator Nanowires", published in Euro Physics Letters 102, 67011 (2013). My supervisor encouraged me a lot during the course of this project and he provided some calculations and hints to put me in the right direction. In the end, he suggested that I publish this article on my own since he thought it was my idea even though his contribution was significant in this project and he helped me by reading the paper and providing constructive comments before the submission.

Chapter 5 is based on my supervisor's and my own notes while working on this project. We addressed a controversial question which was an open question at the time. We published a paper entitled "Electromagnetic Response of Weyl Semimetals" in Physical Review Letters 111, 027201 (2013) based on our numerical and analytical results. I carried out most of the numerical computations and we worked on the theory together. In the end, he wrote the manuscript and then I read it and gave my comments before the submission. Most of the sections in this chapter are based on this published paper.

Chapter 6 is again based on the noted written by my supervisors and I. This project started with my supervisor's idea to find the phase diagram of a 1D superconductor model which could potentially be in a topological phase that supports Majorana fermions at its ends motivated by some previous works on similar setups [1, 2]. I carried out part of the calculations and also the numerical computations. My supervisor wrote the paper (based on our notes and results), which was

then published as a letter entitled “Self-Organized Topological State with Majorana Fermions” in Phys. Rev. Lett. 111, 206802 (2013). Again most of the sections in this chapter are based on the text of this published paper.

The calculations given in the appendices provide supplementary material to explain some of the concepts, approximations and calculations discussed in chapters 1 to 6.

Table of Contents

List of Tables

List of Figures

Glossary

OI Ordinary Insulator

TI Topological Insulator

TR Time Reversal

ARPES Angle Resolved Photo Emission Spectroscopy

STM Scanning Tunnelling Microscopy

QH Quantum Hall

LL Landau Level

QSH Quantum Spin Hall

TKNN Thouless-Kohmoto-Nightingale-Nijs

BZ Brillouin Zone

QCD Quantum Chromodynamics

MF Majorana Fermions

CME Chiral Magnetic Effect

SO Spin-Orbit

NN Nearest-Neighbour

Acknowledgments

It has been a wonderful journey from beginning to end of my PhD program in physics department at UBC. I am deeply grateful to awesome family members, friends and mentors who helped me during this time. Before anyone else, I would like to express my sincere gratitude to my research supervisor Prof. Marcel Franz for his tremendous guidance and encouragement. He played a key role in all of the academic accomplishments I have had since I started my PhD. I also wish to thank the members of my advisory committee, Prof. Ian Affleck, Prof. Rob Kiefl, and Prof. Moshe Rozali. My grateful thanks are also extended to Prof. Allan H. MacDonald, Prof. Abdollah Langari, and Dr. Gilad Rosenberg for their support and assistant in my Four-Year Fellowship (4YF) application. Being on a 4YF enabled me to carry out research with the least amount of financial pressure.

During my years in Vancouver I made wonderful friends whom I shared some of the best moments of my life. I would like to specially thank, Dr. Kamran Alba for being an amazing friend for me during this time.

Finally, I would like to dedicate this thesis to my mother, MS. Farah Emami, a very special person whose support and encouragement is beyond what words can explain. I have been extremely lucky to have great relatives and friends. Special thanks goes to Mr. Khalil Vazifeh for being a great caring father, Mr. Ehsan Vazifeh, Ms. Sahar Vazifeh, Dr. Alireza Emami, Mr. Mohammad Reza Emami, and Ms. Mahjabin Emami for their support and love. Special thanks also goes to Atomic Racing cycling club members particularly Mr. Andrew Wilson for admitting me to their great community of cyclists in Vancouver.

Let me also extend my gratitude to the rest of family and friends for their support and guidance. My special thanks goes to Dr. Azizeh Mahdavi, Mr. Ramin

Hatam, Dr. Reza Behafarin, Dr. Reza Asgari, Dr. Haik Koltoukjian, Dr. Masoud Jazayeri, Dr. Rouhollah Aghdaee, Dr. Hessameddin Arfaei.

Chapter 1

Introduction to Topological Phases of Matter

1.1 Overview

Topology is one of the important fields of mathematics which has far-reaching applications in major fields of science such as biology, computer science and physics [3, 4]. One can use the basic concepts developed in this field to classify and characterize seemingly different systems. The main idea is that usually an important global property of a system under study remains invariant under a class of "smooth" deformations and this makes it possible to successfully distinguish between distinct structures by means of the theory of topological classification. A simple example is classifying closed differentiable surfaces in three spatial dimensions. It is easy to see that one cannot smoothly deform a donut-shape manifold to a sphere without tearing or puncturing it; therefore, the number of holes in a closed surface can be interpreted as a global property of the system which is robust under smooth deformations and infinite possible variations from the ideal sphere can still be considered as one distinct class of manifolds. The same simple idea applies to other examples of topological classification in science including condensed matter physics as we describe here. In physics, these classifications become important especially when the global property used to categorize possible phases is tied to some important phenomena that can be observed directly or indirectly in experiments. This con-

cept will become more clear once we introduce the first example in the next section. As we will see, establishing a good topological classification requires defining relevant global features in a proper quantitative fashion in order to understand why they are robust under local changes in a system. To see how this is possible in a systematic way and in the language of mathematics, in the next section we describe the concept of topological invariants by discussing Gauss-Bonnet theorem used to classify closed differentiable surfaces.

1.2 Topological classification via topological invariants

Topological invariants are the building blocks of any classification based on basic concepts of topology. In the case of closed two dimensional differentiable manifolds this invariant is the genus which is defined as the number of existing holes in the closed manifold embedded in a three dimensional space. It is important to note that this property is a global feature of the object under study and does not manifest itself directly in any local property of the system. However, as we will see one can establish a connection between the topological invariant in this case and the integral of a local property over the entire system. The Euler-Poincare characteristic is a good example to better understand this concept [5]. Euler first defined this invariant for polyhedra. A polyhedron is a solid geometrical object in three dimensions which has flat faces, straight edges and sharp corners. Euler showed that for all polyhedra, subtracting the number of edges (E) from the sum of the number of vertices (V) and faces (F) yields the number 2. Surprisingly, he observed that although this quantity which is now called Euler character is related to local features, it remains invariant under adding edges, faces and vertices.

A generalization of this invariant in the case of differentiable two dimensional manifolds is a special case of the more general Gauss-Bonnet theorem which can be expressed as

$$\int_{\mathbb{M}} K dS = 2\pi(2-2g), \tag{1.1}$$

this relates the genus to the local curvature, K which is defined for all the points forming the closed manifold. However, even though this connection exists, the genus remains invariant if one locally changes the curvature (see Fig. 1.1). The

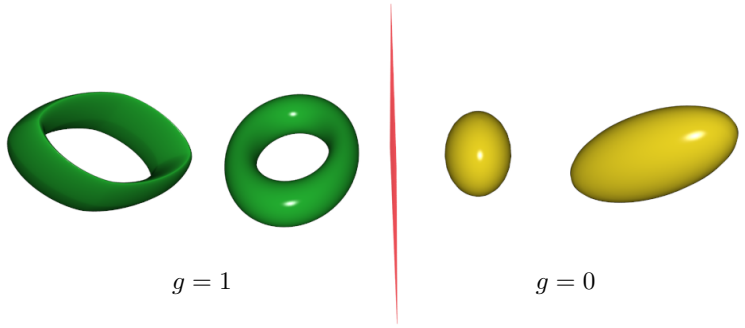

Figure 1.1: Both manifolds on the left side have a genus equal to one, i.e., $g = 1$ and those on the right have $g = 0$ which is equal to the number of their holes which is a robust global property under smooth deformations.

only requirement is that the deformation must be smooth in such a way that the manifold remains differentiable at all times during the deformation.

This is indeed the essence and the beauty of topological classifications from which one or several topologically "robust" quantities emerge. In the next section, we describe how this concept entered on to the scene of condensed matter systems in the context of Quantum Hall (QH) systems more than two decades ago and revisited the scene again during the last years.

1.3 Topological invariants in condensed matter systems

First discovery of the quantized Hall conductance in two dimensional electronic quantum-well heterostructure in a strong magnetic field by von Klitzing, Dorda, and Pepper in 1980 [6] stimulated a series of theoretical works aimed to describe the robust precisely quantized values of the transverse conductivity. The open question at the time was why these conductance values are exactly multiples of e^2/h with extremely high precision although the experimental setups were prone to imperfections which exist in all real crystalline structures. [7–10] The robustness to local impurities and perturbations suggested that there might be some fundamental connections to a global structure in the underlying many-body electron system which remains unchanged in the course of local changes in the same fashion as a

topological invariant does. Of course this is not as obvious as it is in the case of differentiable manifolds. Thouless and collaborators established this connection two years after the original discovery of the QH effect [11]. They studied a two dimensional electron gas in a periodic potential and calculated the transverse conductivity by performing a linear response (Kubo) [12] calculation and they found that the transverse conductivity has a simple expression as an integral over the entire Brillouin Zone (BZ) given as

$$\sigma_{xy} = \frac{ie^2}{4\pi h} \sum_{occn} \oint d^2k \int d^2r \left(\frac{\partial u_n^\star(\vec{k},\vec{r})}{\partial k_1} \frac{\partial u_n(\vec{k},\vec{r})}{\partial k_2} - \frac{\partial u_n^\star(\vec{k},\vec{r})}{\partial k_2} \frac{\partial u_n(\vec{k},\vec{r})}{\partial k_1} \right), \quad (1.2)$$

in which $u_n(\vec{k},\vec{r})$s are the generalized single electron Bloch functions (see A.4) and the sum is over the occupied electron bands. They showed that the above quantity is always an integer multiple of e^2/h whenever the chemical potential is in the gap, consistent with the values reported in the experiments. This equation which relates the transverse conductivity to a global structure of the underlying Bloch states is a milestone of the topological classification in condensed matter physics. To understand how this quantization arises, we can use the Dirac notation and show that the above quantity is an integral of the Berry curvature (see appendix. (A.1)) over the two dimensional torus of the BZ.

One can define the following gauge field

$$\vec{A}(\vec{k}) = i \sum_{\text{occ } \alpha} < u_{\vec{k}\alpha} | \nabla_{\vec{k}} | u_{\vec{k}\alpha} > . \quad (1.3)$$

From the properties of the Bloch states one can argue that the total flux corresponding to the pseudo-magnetic field, $\vec{B}(\vec{k}) = \nabla_{\vec{k}} \times \vec{A}(\vec{k})$, is quantized

$$\int \vec{B}(\vec{k}) \cdot d^2\vec{k} = 2\pi n, \quad (1.4)$$

in which the integer n can be thought of as the number of the pseudo-magnetic monopoles that can be imagined to exist inside the BZ torus responsible for the quantized net flux of the pseudo-magnetic field. In other words, the phase of the Bloch wave-functions can form $U(1)$ vortices in the BZ and the transverse conduc-

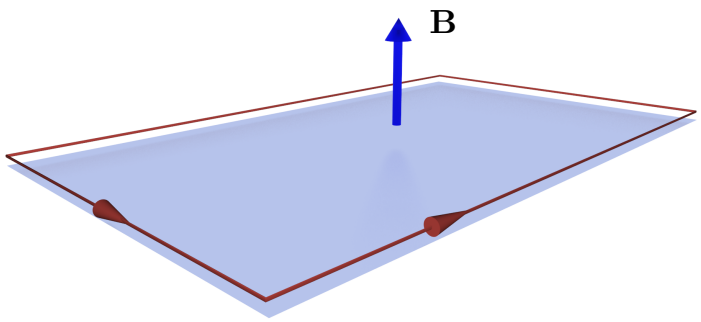

Figure 1.2: Two dimensional electron gas under applied perpendicular magnetic field in a QH phase with topological invariant $n = 1$. According to the bulk-edge correspondence, there are doubly degenerate chiral edge modes propagating counter-clock wise. The conductance of this edge mode is quantized and local impurities cannot change the conductivity as long as the bulk remains gapped.

tance is linearly proportional to the total vorticity [13].

It is easy to realize that Eq.(1.2) and Eq.(1.4) exactly describe the same quantity. This observation explains the quantization of the transverse Hall conductance. The robustness of the transverse conductivity arises since the above quantity is indeed a topological invariant and does not change as long as the bands are filled and the chemical potential is inside the gap keeping the gauge field well-defined [14]. In the language of mathematics this classification distinguishes different topological structures on a tangent bundle formed on the BZ torus as the base manifold and the tangent space is the Hilbert space of the electronic Bloch states. The above invariant classifies all the possible nontrivial topological structures on this tangent bundle which can arise due to the vortices in the $U(1)$ Berry phase of the Bloch states [11, 15].

This profound observation is important because conventionally in condensed matter physics the categorization of phases of matter has been based on symmetry classification. However, in QH systems all the integer QH states belong to the same symmetry group and therefore the symmetry classification fails to distinguish

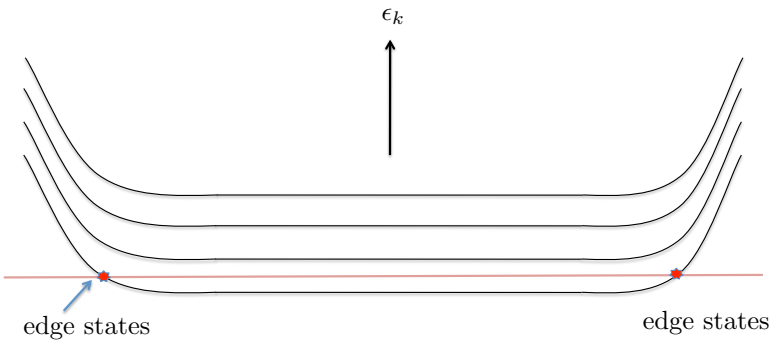

Figure 1.3: Schematic energy spectrum of a two dimensional electron gas in an integer QH phase when there is a periodic boundary condition along one of the directions. The system has two edges in this cylindrical configuration. The edge states' energy spectrum crosses the chemical potential for all chemical potentials inside the gap and the two branches at the two sides of the spectrum correspond to the spatially separated gapless one dimensional modes localized at the two sides of the system.

between different QH states. This also explains the extraordinary robustness of the quantized conductance, since as long as the above invariants remain well-defined the quantization holds. In fact the invariant remains well-defined as long as there is a gap in energy between the many-body ground-state and the first excited states. By changing the magnetic field one can close the gap and at the critical point where the bands touch, the topological invariant is no longer well defined and that is how the conductance can change so that we can see different integer plateaus in the transverse conductivity as a function of the applied magnetic field.

Another interesting aspect of a topologically nontrivial QH state is the existence of linearly dispersing chiral one dimensional modes at the boundary. In fact, according to Laughlin's argument, transverse conductance would not be possible without the existence of such states at the edges because there must be gapless states to accommodate the electrons that are being pumped between edges [8]. The edges are important in fact because they are the interface which separates two topologically distinct regions and in fact the existence of linearly dispersing modes can be associated with this topological mismatch. Remember that a classical vacuum can be viewed as a topologically trivial gapped state with infinite energy gap. These

chiral one dimensional modes are robust to local perturbations and they cannot be gapped out as long as the bulk remains to be in the same topological class [16]. The number of such doubly degenerate modes (considering spin degeneracy if one neglects the Zeeman effect) is the same as the value one gets from calculating the Thouless-Kohmoto-Nightingale-Nijs (TKNN) topological invariant, n, defined in Eq. (1.4). Indeed, this is another signature of the nontrivial topological state as it has been seen and confirmed in a number of multichannel transport experiments [7].

1.4 Quantum Spin Hall phase

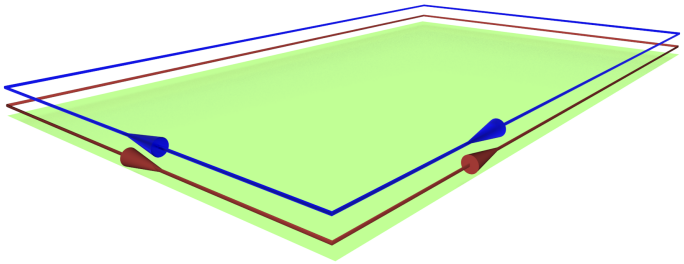

Figure 1.4: Schematic of a two dimensional electron gas in a QSH phase. According to bulk-edge correspondence, there is an odd number of pairs of counter propagating chiral edge modes. The spin conductance is conserved and therefore well-defined in the absence of Rashba SO coupling. In this case the spin conductance of the edge mode is quantized and local impurities that respect TR invariance cannot change the conductivity as long as the bulk remains gapped.

As we showed in the previous section, integer QH states are TR broken topological phases of matter which can be classified with a single topological invariant [14]. A legitimate question that arises here is whether it is possible or not to have a nontrivial topological state in two dimensions when there is no net uniform applied magnetic field. In other words, whether it is possible or not to get a nonzero quantized Hall response in the absence of a net uniform magnetic field. Haldane

answered this question in 1988 by introducing a simple two dimensional lattice model. He showed that in theory this is possible and one can have a QH state without a net uniform perpendicular magnetic field [17]. The model he introduced consists of a honeycomb lattice with modulating magnetic flux going through its hexagons in a way that the net magnetic flux going through each hexagon is zero. Then in a tight-binding approximation he showed that under certain conditions the system can in fact form a QH state with $n = \pm 1$ as its many-body ground-state.

A next-nearest neighbour (NNN) tight-binding model used by Haldane for a honeycomb lattice leads to distinct Dirac fermion modes in the low energy electronic spectrum [18, 19]. In the continuum limit, one can evaluate the TKNN topological invariant for a single massive Dirac mode in two dimensions and see that this quantity can only be either $+0.5$ or -0.5 by considering a proper regularization (see Appendix A.2). The sign depends on the sign of the product of the mass and the chirality of the corresponding two dimensional Hamiltonian ($= \mathrm{sgn}(m\upsilon_x\upsilon_y)$). Since two Dirac modes around the two distinct points in the BZ have opposite chirality, inducing equal mass for these Dirac modes always guarantees that the net transverse conductivity is zero in the absence of the magnetic field. However, Haldane came up with the modulating magnetic field configuration on the honeycomb lattice and realized that the associated term in the tight-binding Hamiltonian gives rise to opposite masses for these Dirac modes, and therefore, one can consider a situation where the net transverse conductivity is nonzero. In fact, by considering the full BZ states one can show that the TKNN invariant can be ± 1 in the presence of the Haldane term. This model was considered as an interesting toy model for more than two decades and remained unrealistic even after the discovery of Graphene in 2004 [20], since inducing magnetic field that modulates at lattice scale is something that is not experimentally plausible. However, this model inspired Kane and Mele [21] to realize that graphene can possibly be driven into a nontrivial topological phase in two dimensions if one considers the effect of SO interaction. The transverse conductivity is zero for this novel phase, since the TR symmetry is respected in the system (remember σ_{xy} is odd under TR so it can only be zero if the system has this symmetry). However, they showed that this phase is totally distinct from an Ordinary Insulator (OI) in a sense that there is no smooth deformation of the Hamiltonian to the one that describes an OI as long as TR symmetry is respected

and the system is gapped. The general Hamiltonian they considered can be written as

$$H = t\sum_{\langle ij\rangle} c_i^\dagger c_j + i\lambda_{SO}\sum_{\langle\langle ij\rangle\rangle} \nu_{ij} c_i^\dagger s^z c_j + i\lambda_R \sum_{\langle ij\rangle} c_i^\dagger (\mathbf{s}\times\hat{\mathbf{d}}_{ij})_z c_j + \lambda_v \sum_i \xi_i c_i^\dagger c_i.$$

in which $c_i^\dagger(c_i)$ are the creation (annihilation) operators on site i. λ_{SO} is the strength of the SO interaction, λ_R is the strength of Rashba interaction, and λ_v is the staggered potential strength. $\hat{\mathbf{d}}_{ij}$ is the position vector connecting two sites from site i to site j. ν_{ij} is either $+1$ or -1 [22].

In the most simple case of $\lambda_R = 0$, this nontrivial topological phase can be viewed as two copies of the Haldane state with $n = +1$ for $S_z = \hbar/2$ states and $n = -1$ for $S_z = -\hbar/2$ states. In fact the form of the Hamiltonian is the same as the one studied by Haldane for each spin flavour. Now, since in this case the spin sectors are disconnected, each of them supports chiral edge modes which propagate oppositely for opposite spins. The robustness is guaranteed by the fact that TR symmetry prevents mixing of states with opposite spins, therefore the counter-propagating spin filtered chiral edge states are protected by a combination of TR symmetry at the surface and the topological properties of the bulk states (see Fig. (1.4)). Also, the system exhibits quantized spin Hall effect which can be defined as the difference between the transverse charge current in the two spin sectors [21–23]. Therefore, this phase is called the Quantum Spin Hall (QSH) phase.

The more interesting situation is when the Hamiltonian does not commute with S_z which can happen in the presence of a finite Rashba SO coupling. Kane and Mele showed that even in this case, for a wide range of system parameters the ground-state can still be a nontrivial topological state with counter propagating modes at the boundary [21, 22].

One can define a $\mathbb{Z}_2$ topological invariant to classify all TR invariant insulators in two dimensions which has various formulations [24–27]. This invariant is defined as a sum of a surface and a line integral of the Berry curvature that appeared in the TKNN invariant over half of the BZ and its boundary and can be written as

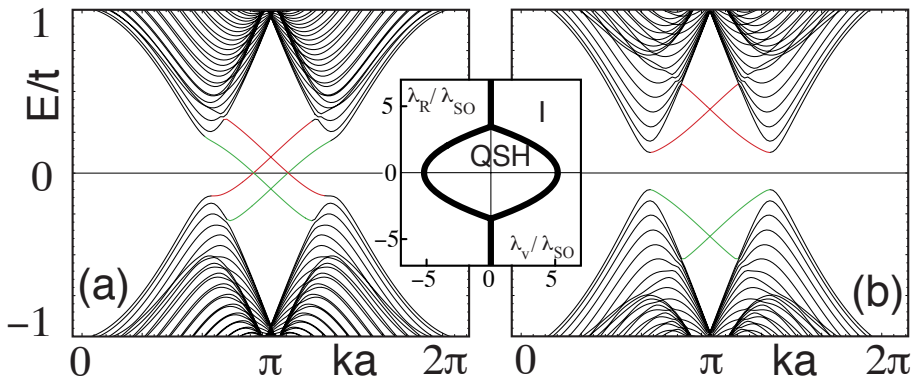

Figure 1.5: Energy bands for a one dimensional "zigzag" strip in the (a) QSH phase $\lambda_v = .1t$ and (b) the insulating phase $\lambda_v = .4t$. In both cases $\lambda_{SO} = .06t$ and $\lambda_R = .05t$. The edge states on a given edge cross at $ka = \pi$. The inset shows the phase diagram as a function of λ_v and λ_R for $0 < \lambda_{SO} \ll t$. Figure and caption from Ref. [22]

$$\nu_0^{2D} = \frac{1}{2\pi}\left(\oint_{\partial \mathrm{EBZ}} \vec{A}(\vec{k})\cdot d\vec{k} - \int_{\mathrm{EBZ}} \vec{B}(\vec{k})\cdot d^2\vec{k}\right) \mod 2. \tag{1.5}$$

When ν_0^{2D} is zero the system would be in a trivial topological phase, and whenever this invariant is equal to 1, it would be in a topological QSH insulator phase which supports counter-propagating modes at its edges (see Fig. (1.5)). Of course establishing a physical meaning for this invariant or understanding its connection with any physical observable like the edge states is not as easy as it was for the TKNN invariant defined for the integer QH systems. However, one can use an alternative picture to see why this phase is non-trivial and cannot be smoothly connected to a trivial insulator. If we can prove that no such path exists, then the existence of the edge modes follows from the same argument we used before for QH states, i.e., they arise due to the topological mismatch between the two sides of the boundary as can be seen in the most simple case of two copies of Haldane states with opposite magnetic flux configurations. We come back to this point in the next section.

Clean graphene was not a good candidate for the QSH phase due to its sub

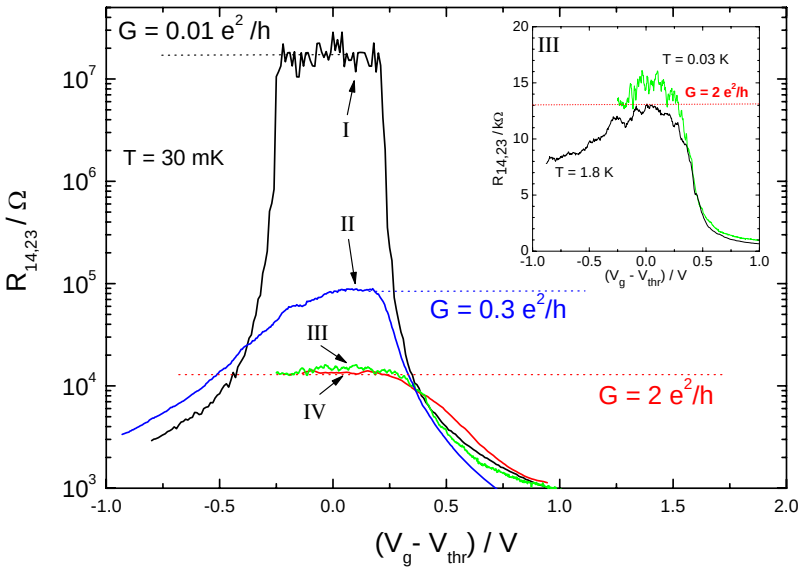

Figure 1.6: When the film thickness is large enough the HgTe quantum well undergoes a phase transition to a spin Hall insulator phase which supports robust counter-propagating edge modes. The longitudinal four channel resistance, $R_{1,2,3,4}$ of various normal ($d = 5.5$mm) (I) and inverted (d = 7.3) (II, III, IV) QW structures as a function of gate voltage is measured for $\vec{B} = 0$T at $T = 30$ mK. Figure and caption from Ref. [28]

meV spin-orbit gap despite the fact that it was the main inspiration for the theoretical development and the introduction of this topological phase. What was obvious in those theoretical works was that SO plays an important role in driving the system into a topological phase so naturally one had to look for materials with heavy elements to realize this phase. It was proposed in 2003 by Shou-Cheng Zhang's group that Mercury-Telloride (HgTe) might be a good candidate in that sense [29, 30]. Using a $\mathbf{k}.\mathbf{p}$ model they showed that thin films of HgTe sandwiched between (Hg,Cd)Te barriers can be driven into a QSH phase by increasing the thickness of the thin film, d, and going through a quantum phase transition. At the critical point, $d = d_c$, the bands of the electronic spectrum touch and as one

increases the d further, the system enters the topological phase when the bands are inverted. In 2007, the same group reported the discovery of this phase in HgTe in the experiments done by the group of Laurens Molenkamp [28]. They observed quantized conductance which arise due to the existence of counter-propagating edge modes in a transport measurement (see Fig. (1.6)). HgTe remains the only example of the QSH phase discovered until now although it has been suggested recently that graphene can also become a QSH insulator in the presence of heavy adatoms [31, 32].

1.5 Topological insulators in three dimensions

Similar to two dimensional QSH systems, TR invariant band insulators with non-trivial topological structure exist. It turns out that in fact there are 16 distinct topological phases and 4 invariants are required to fully characterize all band insulators with TR symmetry [26, 33, 34]. One of these invariants, ν_0 which is called the 'strong' topological invariant is directly related to various physical properties of the system and is robust to all local perturbations that preserve TR symmetry.

Again, similar to the two dimensional case, there are various formulations of this strong invariant. One way to express this invariant is the following [26]

$$\nu_0^{3\mathrm{D}} = \frac{1}{2\pi^2}\int \varepsilon_{ijk}\mathrm{Tr}[\mathcal{A}_i\partial_j\mathcal{A}_k - i\frac{2}{3}\mathcal{A}_i\mathcal{A}_j\mathcal{A}_k] \mod 2, \tag{1.6}$$

where we have

$$\mathcal{A}_i^{\alpha\beta} = -i < u_{\vec{k}\alpha}|\partial_i|u_{\vec{k}\beta} >, \quad i = 1,2,3 \tag{1.7}$$

which is the non-Abelian gauge field matrix defined for Bloch states. In the inversion symmetric cases this invariant takes a simpler form [35] and can be obtained by evaluating the Pffafian of the inversion operator's representation in the Hilbert space of the occupied states at certain high symmetry momenta in the BZ. In this case this invariant can be expressed as

$$(-1)^{\nu_0^{3\mathrm{D}}} = \prod_{i=1}^{8}\delta_i, \quad \delta_i = \prod_{m=1}^{N}\xi_{2m}(\Gamma_i), \tag{1.8}$$

where Γ_is are the TR invariant momenta and $\xi_{2m} = \xi_{2m-1}$ is the parity eigenvalue of the $2m$-th occupied energy band at the TR invariant momenta. Using one of these two expressions for the different band insulator models, one can find out whether a system can be in a strong topological phase or not. Several systems have been proposed to be in a Topological Insulator (TI) phase based on this characterization. In a 'strong' TI phase, the quantum states have been formed in a non-trivial fashion so that the system belongs to a different topological class than the class of OIs, meaning that there is no fully gapped deformation path in the phase space of the Hamiltonians that connects the Hamiltonian of the system to that of an OI, preserving the TR symmetry [36]. Any phase space path connecting two topologically distinct points in the phase space would contain a point where the associated Hamiltonian is gapless. This intuitively explains the presence of the robust topological surface states at the interfaces between these systems and OIs. It can be understood from the fact that one can establish a mapping between any path connecting a point in the bulk of a TI to a point in the vacuum and the TR symmetry preserving paths connecting two topologically distinct regions. Therefore these paths must contain a critical point where the system is locally gapless and is in the metallic phase. All such critical points span the metallic surface connecting the two topologically distinct phases. Therefore, any local perturbation on the surface that respects the TR symmetry cannot destroy the gapless surface modes. These gapless surface modes are then protected by the coexistence of TR symmetry on the surface and the non-trivial topological structure in the bulk of the system [24, 37].

In the case of a 'strong' TI there is an odd number of Dirac points at any surface and, importantly, they are not spin degenerate. Furthermore, they exhibit a unique spin-momentum locking [38, 39] as a result of the strong SO interaction in the underlying 'strong' TI which is essential for the formation of the topologically non-trivial insulator phase with TR symmetry. These properties make electronic surface states in a 'strong' TI very distinct from those of graphene with a pair of spin degenerate Dirac bands near two special points in the Brillouin zone which exist as a result of the unique arrangement of carbon atoms in the honeycomb lattice [18, 19].

This novel phase of matter was discovered first in semiconducting alloy $Bi_{1-x}Sb_x$ by observing these unusual gapless linearly dispersing modes in an Angle Re-

solved Photo Emission Spectroscopy (ARPES) experiment [38, 40]. Soon after this discovery, a single Dirac surface mode with unique spin texture was observed in Bi_2Se_3 with spin-resolved ARPES experiments [41]. In this case it is easier to see why the system is in a TI phase by calculating the strong topological invariant using a low-energy Dirac Hamiltonian. We discuss this in more detail in the next section.

Many of the interesting features of the surface states in a TI also can be captured, at least qualitatively, using a simple non-interacting Dirac Hamiltonian

$$H = \sum_{\vec{k}} \Psi^{\dagger}_{\vec{k}} [\hbar \upsilon_F \boldsymbol{\sigma} \cdot (\hat{z} \times \vec{k}) + \Delta_0 \sigma_z] \Psi_{\vec{k}}, \tag{1.9}$$

where $\hat{z}$ is the unit vector perpendicular to the surface, $\Psi^{\dagger}_{\vec{k}} = (c^{\dagger}_{\uparrow\vec{k}}, c^{\dagger}_{\downarrow\vec{k}})$ and $c^{\dagger}_{\uparrow(\downarrow)\vec{k}}$ is the fermionic creation operator of the spin up(down) states with wave vector $\vec{k}$. Δ_0 is the intrinsic gap in the surface spectrum which might be nonzero when the TR symmetry is spontaneously broken due to magnetic ordering. The latter can arise due to the presence of magnetic dopants with spin $\boldsymbol{S}$ in the proximity of the surface exchange-coupled to the electronic spins [42–44] or as a result of electron-electron interaction [45].

The coupling between spin and the momentum in these surface modes has interesting consequences in the electromagnetic response. In chapter 3 we consider TI surface modes and we address one interesting feature of these surface modes which happens in response to an applied out-of-plane magnetic field and can be used to probe small intrinsic gaps on the surface using an experimental technique which is called $\beta-$NMR [46, 47].

1.6 A lattice model for topological insulators

A three dimensional Dirac Hamiltonian can be expressed in terms of two sets of Pauli matrices $\tau = (\tau_1, \tau_2, \tau_3)$ and $\sigma = (\sigma_1, \sigma_2, \sigma_3)$ acting on a two level orbital and spin degrees of system. In momentum space, the gapless Hamiltonian in terms of these matrices can be written as

$$H(\vec{k}) = \tau_3(\upsilon_1 \sigma_1 k_y - \upsilon_2 \sigma_2 k_x) + \upsilon_3 \tau_2 k_z. \tag{1.10}$$

It is easy to consider a tight-binding cubic lattice model which, near specific points in the BZ and at low energies, can be described effectively by the above Hamiltonian. In a Fourier transformed tight-binding Hamiltonian, the momentum dependent Hamiltonian matrix can only depend on crystal wave-vector $\vec{k}$ via $\cos(\vec{a}_i \cdot \vec{k})$ and $\sin(\vec{a}_i \cdot \vec{k})$ terms therefore one can immediately find the corresponding Hamiltonian matrix. This can be expressed by replacing (k_x, k_y, k_z) by their lattice versions, i.e., $(\sin k_x a_1, \sin k_y a_2, \sin k_z a_3)$. Assuming that the lattice is cubic with $a_1 = a_2 = a_3 = a$ we get

$$H(\vec{k}) = \tau_3 \lambda (\sigma_1 \sin k_y a - \sigma_2 \sin k_x a) + \tau_2 \lambda_z \sin k_z a, \tag{1.11}$$

This Hamiltonian is invariant under the time-reversal meaning that $\Theta^\dagger H(\vec{k})\Theta = H(-\vec{k})$ where the time reversal operator, $\Theta = i\sigma_2 K$, in which K is complex conjugation operator, acts on σ and τ operators in the following way

$$\Theta^\dagger(\tau_1, \tau_2, \tau_3)\Theta = (\tau_1, -\tau_2, \tau_3), \tag{1.12}$$

$$\Theta^\dagger(\sigma_1, \sigma_2, \sigma_3)\Theta = (-\sigma_1, -\sigma_2, -\sigma_3). \tag{1.13}$$

There are eight distinct Dirac points at the time-reversal invariant momenta given as

$$\vec{\Gamma}_i = \frac{\pi}{2}(1,1,1) + \frac{\pi}{2}(\pm 1, \pm 1, \pm 1). \tag{1.14}$$

In general, there are various ways to open up a gap in the spectrum of the Hamiltonian given in Eq. (1.11) by adding combinations of the Pauli matrices. However, there is only one way to open up a gap respecting the time-reversal symmetry. It is not hard to find this term by forming various possible combinations of the Pauli matrices and seeing which one is invariant under time-reversal and at the same time anti-commutes with all the terms in the Hamiltonian. By this consideration the massive time-reversal invariant Dirac Hamiltonian can be written as

$$H(\vec{k}) = \lambda \tau_3 (\sigma_1 \sin k_y a - \sigma_2 \sin k_x a) + \lambda_z \tau_2 \sin k_z a + M(\vec{k})\tau_1. \tag{1.15}$$

In a nearest-neighbour tight-binding Hamiltonian, the most general form of $M(\vec{k})$ can be written as

$$M(\vec{k}) = \varepsilon - 2t\cos k_x a - 2t\cos k_y a - 2t\cos k_z a, \tag{1.16}$$

Note that in the above $\sin\vec{k}\cdot\vec{a}_i$ terms cannot exist since TR symmetry requires that the function must be even under $\vec{k}$ to $-\vec{k}$ so the only allowed $\vec{k}$ dependence is via cosine functions. One can compute the strong topological invariant using the expression given in Eq. (1.8) since the system is inversion symmetric. It turns out that the system can be in a topological insulator phase for a wide range of system parameters. Another way to see how the system can be in a topological insulator phase is to calculate the strong topological invariant analytically in the continuum limit and considering a proper regularization for a three dimensional Dirac Hamiltonian to resolve the integral divergences arising from the Dirac sea. It turns out that in this case each of the eight existing Dirac modes contribute to the total value of this invariant which can either be zero or one. This lattice model which is a regularized minimal model for Bi_2Se_3 has been studied before in the context of the magnetic response of the topological insulators [44, 48].

For a single Dirac Hamiltonian of mass m and Fermi velocity components $(\upsilon_1, \upsilon_2, \upsilon_3)$, the contribution turns out to be

$$\delta\nu_0^{3\mathrm{D}} = \frac{1}{2}\mathrm{sgn}\,(m\upsilon_1\upsilon_2\upsilon_3). \tag{1.17}$$

The 'strong' invariant, $\nu_0^{3\mathrm{D}}$ can be obtained by summing the contribution from all these Dirac points. It turns out that for $2t < \varepsilon < 6t$ the system is in a topological phase ($\nu_0^{3\mathrm{D}} = 1$).

An alternative characterization of a 'strong' TI follows from its unusual response to applied electromagnetic fields which is encoded in a bulk 'axion' term [26, 37] of the form

$$\mathscr{L}_{\mathrm{axion}} = \theta\left(\frac{e^2}{2\pi hc}\right)\vec{B}\cdot\vec{E}, \tag{1.18}$$

with $\theta = \pi$. The axion term (1.18) appears in the electromagnetic Lagrangian in addition to the standard Maxwell term. Eq. (1.18) underlies the topological magnetoelectric effect [26, 37] in which electric (magnetic) polarization is induced by

external magnetic (electric) field, as well as the Witten effect [48, 49] that attaches a fractional electric charge to a magnetic monopole.

The axion term (1.18) has been introduced in the context of high-energy physics decades before the discovery of STIs to resolve the CP non-violation problem in Quantum Chromodynamics (QCD) [50–52]. The corresponding $\theta(\vec{x},t)$ field is known to particle physicists as the axion field [53]. The action of the uniform axion field can be viewed as a topological term for the θ vacuum in QCD arising from nontrivial topology of such a vacuum.

For a generic value of θ the axion term breaks $\mathscr{T}$ as well as parity $\mathscr{P}$. This is because under time-reversal $\vec{B} \to -\vec{B}$, $\vec{E} \to \vec{E}$, while under spatial inversion $\vec{B} \to \vec{B}$, $\vec{E} \to -\vec{E}$. What allows the $\mathscr{T}$- and $\mathscr{P}$-invariant insulators to possess an axion term with $\theta = \pi$ is the 2π-periodicity of the axion action $S_{\text{axion}} = \int dt d^3x \mathscr{L}_{\text{axion}}$ in parameter θ. Specifically, on periodic space-time (that is used to model an infinite bulk crystal), the integral in the axion action is quantized,

$$\left(\frac{e^2}{2\pi hc}\right) \int dt d^3x \vec{B} \cdot \vec{E} = N\hbar, \tag{1.19}$$

with N integer. All physical observables depend on $\exp(iS_{\text{axion}}/\hbar)$ and are thus invariant under a global transformation $\theta \to \theta + 2\pi$. Consequently, $\theta = \pi$ and $\theta = -\pi$ are two equivalent points and describe a $\mathscr{T}$- and $\mathscr{P}$-invariant system. Conversely, in a system invariant under $\mathscr{P}$ or $\mathscr{T}$ the value of θ is quantized to 0 or π.

The statement regarding the quantization of the expression (1.19) on periodic space-times has been made in several influential papers [26, 37, 53, 54] but no simple physical explanation has been given of its validity. In chapter 2, we will present our simple proof of quantization using simple arguments based on single particle quantum mechanics and classical electrodynamics.

1.7 Weyl and Dirac semimetals

The topological protection is not restricted to just one and two dimensional metallic systems which arise at the interface of topological insulators. Indeed one can generalize this idea to find a three dimensional metallic system where the band crossing

is protected by the underlying nontrivial topological structure of the quantum states rather than the discrete symmetries such as the inversion or the TR. Recently, experimentally feasible proposals to realize such 3D metallic phases has been made where linear energy crossings (Dirac Points) exist in the band dispersion and are protected by global topological properties of the electronic states [55–59]. In this case there is no discrete symmetry involved in protecting the Dirac point from the gap opening as opposed to the 1D and the 2D TI edge and surface cases where we still need to keep the TR symmetry in order to maintain the band crossings [42, 44]. The existence of this nontrivial topological structure associated with the isolated linear touching points would lead to some interesting transport phenomena in the bulk and on the surface of such systems. A topological axion term with a non-uniform axion field is predicted to emerge in the effective electromagnetic Lagrangian which is related to the chiral anomaly in these systems [60–63].

The low energy theory of an isolated Weyl point is given by the Hamiltonian

$$h_W(\vec{k}) = b_0 + \upsilon_F \boldsymbol{\sigma} \cdot (\vec{k} - \vec{b}), \tag{1.20}$$

where υ_F is the characteristic velocity, $\boldsymbol{\sigma}$ a vector of the Pauli matrices, b_0 and $\vec{b}$ denote the shift in energy and momentum, respectively. Because all three Pauli matrices are used up in $h_W(\vec{k})$, small perturbations can renormalize the parameters, b_0, $\vec{b}$ and υ_F, but cannot open a gap. This explains why the Weyl semimetal forms a stable phase [36]. Although the phase has yet to be experimentally observed there are a number of proposed candidate systems, including pyrochlore iridates [58], TI multilayers [55–57, 64], and magnetically doped TIs [65].

When such topological protection of band touching exists, the system is in a topological semi-metal phase even in the presence of weak disorder or other types of interactions that preserve the momentum conservation. These band crossing points in the BZ can only exist in pairs [62]. Near an isolated Weyl point the low lying states can be described by the 2-by-2 Dirac Hamiltonian given in Eq. (1.20). Therefore, any local perturbation that does not violate the momentum conservation can only shift the position of such a point in the BZ and is not sufficient to gap out the spectrum unless it is strong enough to merge two such points with opposite chirality and make the system unstable towards becoming an insulator. These

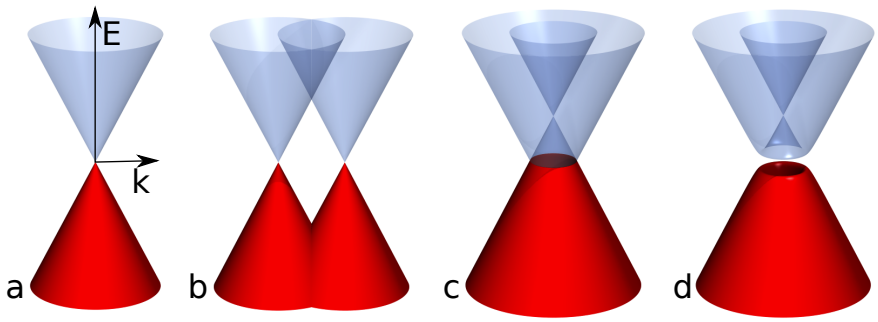

Figure 1.7: a) Doubly degenerate massless Dirac cone at the transition from a TI to a band insulator. Weyl semimetals with the individual cones shifted in b) momenta and c) energy. Panel d) illustrates the Weyl insulator which can arise when the excitonic instability gaps out the spectrum indicated in c). In all panels two components of the 3D crystal momentum $\vec{k}$ are shown.

points can be thought of as topological defects in the fibre bundle formed by the electronic states in the BZ as the base manifold and are the magnetic monopoles of the pseudo-magnetic field (Berry curvature) associated with the gauge field defined for the Bloch states. Only the pairwise annihilation of such points with opposite chirality is possible as one can define a well-defined charge for these monopoles which is a conserved quantity in the regime where the crystal momentum is still a good quantum number. The topological charge defined for a Weyl point can be expressed as the surface integral of the Berry curvature on the Fermi surface sphere.

In theory, it is possible to choose a physical parameter to adiabatically drive a system to a TI phase from an OI or vice versa by tuning such a parameter. This phase transition can happen for the lattice model introduced in the previous section in Eq. (1.15) by changing a single lattice parameter. As one fine tunes such a parameter to the critical point where the gap closes (which is inevitable when we have TR or inversion symmetry) the system becomes an unstable bulk metal if the TR and inversion symmetry is preserved at the same time. At this critical point the system would be in an unstable 3D metallic phase with degenerate bands near the crossing points. This gapless metallic phase is susceptible to local perturbations

and instabilities that drive the system to either TI or OI phases. Now if another parameter in the Hamiltonian is tuned in such a way that it separates the degenerate bands at the crossing points in the BZ (by breaking the inversion and/or the TR symmetry) then the system would be in a topological semi-metal phase with gapless modes dispersing in three spatial dimensions which are "robust" against momentum conserving perturbations. The topological nature of the phase reflects itself in the appearance of a nontrivial term in the effective Lagrangian of the electromagnetic fields [63]. This topological term is very similar to what appears in the effective electromagnetic response of TIs as an abelian axion term, however in this case the axion field is a non-homogeneous field as opposed to being a constant field with $\theta = 0(\text{OI})$ or $\pi(\text{TI})$. This topological term can be expressed as

$$S_{\text{axion}} = C \int \theta(\vec{x}) \mathscr{F} \wedge \mathscr{F}, \tag{1.21}$$

where C is a constant and $\theta(x)$ modulates in space and time with wave-vector that depends on the separation of the Weyl nodes in momentum and energy. For a single pair of Weyl nodes it is given by $\theta(\vec{x}) = \vec{q} \cdot \vec{x} - b_0 t$ in which $\vec{q}$ is a vector of the separation of the pair of the Weyl nodes in the crystal momentum and b_0 is the energy offset between two Weyl points [60–63]. This topological term in the effective electromagnetic Lagrangian is closely related to the topological transport phenomena that is present in these systems [63]. This unusual response is a consequence of the chiral anomaly, well known in the quantum field theory of Dirac fermions [61, 62, 66], now potentially realized in a Weyl semimetal. The physical manifestations of the above topological term can be best understood from the associated equations of motion, which give rise to the following charge density and current response,

$$\rho = \frac{e^2}{2\pi^2} \vec{b} \cdot \vec{B}, \tag{1.22}$$

$$\vec{j} = \frac{e^2}{2\pi^2} (\vec{b} \times \vec{E} - b_0 \vec{B}). \tag{1.23}$$

Eq. (1.22) and the first term in Eq. (1.23) encode the anomalous Hall effect that is expected to occur in a Weyl semimetal with broken $\mathscr{T}$ [55, 56, 58]. The second term in Eq. (1.23) describes the Chiral Magnetic Effect (CME), whereby a

ground-state dissipationless current proportional to the applied magnetic field $\vec{B}$ is generated in the bulk of a Weyl semimetal with broken $\mathscr{P}$ [67].

These observations are based on field theoretical considerations which requires specific regularizations, so the important question is whether in a lattice system these effects can still survive when two opposite chirality Weyl points are connected via high energy modes of the lattice. In chapter 5 we address this important question.

1.8 One dimensional topological phase with Majorana fermions

So far we have only discussed the nontrivial topological phases in two and three dimensional systems. It turns out that even in one dimension nontrivial topological phases exist. The most interesting example has been introduced by Alexei Kitaev in 2001 [69]. He showed that spin-less electrons in a Nearest-Neighbour (NN) tight-binding model with a p-wave pairing can form an interesting topological phase which supports exotic zero-dimensional states near their ends. These states have exactly the same properties as the elusive Majorana Fermions (MF). Hypothesized by Ettore Majorana in 1937, MFs are interesting Dirac states which are their own anti-particles. The creation and annihilation operators of the Majorana state are the same and they follow non-abelian statistics.

Kitaev's model still remains experimentally unfeasible since electrons are spin-half particles. A p-wave superconductor in two-dimensions also supports Majorana fermions in the vicinity of the magnetic vortex. However, this model did not resolve the problem since p-wave superconductivity does not occur easily in condensed matter systems and its existence in Sr_2RuO_4 is still under debate [70].

In 2008, Fu and Kane showed that it is possible to realize a topological phase with Majorana fermions from s-wave pairing order at the surface of a topological insulator [68, 71]. This was an important step towards realizing Majorana fermions in condensed matter systems since all the previous models were based on p-wave superconducting ordering. The main ingredients in the Fu and Kane two dimensional topological superconductor model was a combination of magnetic ordering, spin-orbit coupling and the proximity induced s-wave superconductivity. In 2010

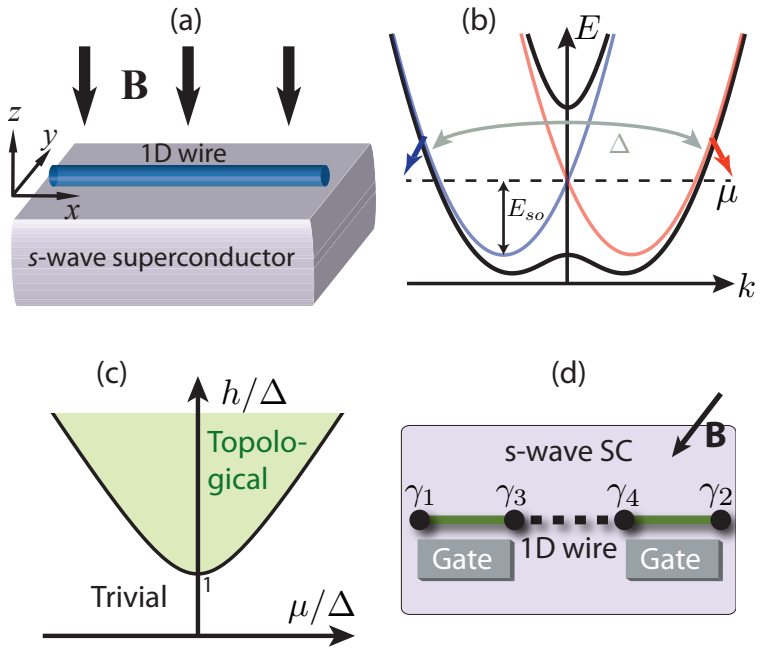

Figure 1.8: (a) Basic architecture required to stabilize a topological superconducting state in a 1D spin-orbit-coupled wire. (b) Band structure for the wire when time-reversal symmetry is present (red and blue curves) and broken by a magnetic field (black curves). When the chemical potential lies within the field-induced gap at $k = 0$, the wire appears 'spinless'. Incorporating the pairing induced by the proximate superconductor leads to the phase diagram in (c). The endpoints of topological (green) segments of the wire host localized, zero-energy Majorana modes as shown in (d). Figure and caption from Ref. [68]

Refael and von Oppen used all these ingredients to propose a quantum wire as a topological superconductor with MFs [72]. Their setup consisted of a semiconductor quantum wire placed on top of an s-wave superconductor under applied in-plane magnetic field to produce a Zeeman field. This was ground breaking proposal since all the ingredients of this model are already realizable in experimental setups. The only challenge was tuning the chemical potential to the desired mid-gap configuration where the gap arises from the Zeeman field which is normally of the order of 1 meV. In 2012, a group of experimentalists at Delft University of Technology

reported robust zero-bias peak in their experimental setup based on the Refael and von Oppen proposal [73]. This interesting observation has been under debate and it is now believed that there are other scenarios which can equally explain the existence of zero-bias peaks and a smoking-gun proof of the existence of Majorana fermions in an experimental system still remains to be found. Another interesting proposal is magnetic chain of adatoms placed on top of an s-wave superconductors. Magnetic nuclei on top of superconductors have been shown to bind localized mid-gap electron modes. Forming a chain of these atoms, which is experimentally plausible, can potentially lead to a one dimensional topological phase. It turns out that the topological phase can arise naturally due to the existence of a magnetic instability in the one dimensional electron systems. In chapter 6 we consider this proposal and we address how this can arise in detail using a simple minimal model.

Chapter 2

Axion Angle Periodicity in Topological Insulators

2.1 Overview

The electromagnetic response of TIs is highly affected by the nontrivial topological structure of the underlying electrons. One can see this by integrating out massive Dirac electrons coupled to a classical electromagnetic gauge field. Apart from the usual Maxwell terms in the action, an extra term exists which arises solely due to the twist in one of the Dirac masses which is essential for driving a system into a TR symmetric TI. This term in the action modifies the Maxwell equations and explains the quantized magneto-electric effects in the bulk and at the surface of a three dimensional TI. Since the quantization of the axion term and the related θ-periodicity underlies the essential element of the theory of topological insulators, it is important to have a clear physical understanding of its origin. In the rest of this chapter we provide a direct and simple proof of the axion action quantization on periodic space-time. We also consider a non-periodic case where the axion action remains quantized. Our proof is based on the electromagnetic field decomposition into an 'externally imposed' uniform constant part which we show can have non-zero contribution to S_{axion} and a part generated by space-time periodic charge and current configurations whose contribution to S_{axion} vanishes. The quantization condition (1.19) follows from the requirement that the underlying vector potential

be consistent with the single-valuedness of the electron wave-functions [74]. In our proof we assume that no magnetic monopoles are present but we comment on the situation with monopoles in the end.

2.2 Electromagnetic field decomposition

In a covariant formulation with the speed of light $c = 1$ the axion action can be written as [53]

$$\frac{1}{\hbar} S_{\text{axion}} = \frac{\theta}{8\Phi_0^2} \int d^4x \, \varepsilon^{\mu\nu\alpha\beta} F_{\mu\nu}(x) F_{\alpha\beta}(x), \tag{2.1}$$

where $F_{\mu\nu} = \partial_\mu A_\nu - \partial_\nu A_\mu$ is the electromagnetic field tensor and $\Phi_0 = h/e$ is the quantum of the magnetic flux. In the following we consider a space-time hypercube of side L with periodic boundary conditions imposed on $F_{\mu\nu}(x)$ in all directions.

In the absence of monopoles integration by parts gives

$$\frac{1}{\hbar} S_{\text{axion}} = \frac{\theta}{4\Phi_0^2} \int d^4x \, \varepsilon^{\mu\nu\alpha\beta} \partial_\alpha \left[F_{\mu\nu}(x) A_\beta(x) \right], \tag{2.2}$$

At first glance, from the periodicity of space and time one might conclude that the integral in (2.2) vanishes for a general electromagnetic field tensor since it can be written as a three dimensional hyper-surface integral of $F_{\mu\nu} A_\beta$ which is zero if this function is periodic in space-time coordinates. However, a simple example of constant uniform fields $\vec{E} \| \vec{B}$ shows this conclusion to be erroneous. The point is that in general the gauge field 4-vector of a periodic electromagnetic field is not periodic in space and time. As an example consider a lower dimensional case of T^2 torus with a magnetic flux through its hole increasing linearly with time (Fig. 2.1a). This induces an electric field on the torus which is constant and therefore periodic in time and the coordinates that parametrize the torus. However the line integral of the gauge field over the non-contractible loop enclosing the magnetic flux is nonzero which means that the gauge field cannot be chosen periodic. For the field configurations of this type, containing field lines along non-contractible loops, S_{axion} will be non-vanishing and we must consider these with special care.

A question arises here: in general for what kind of periodic electromagnetic field configurations in 3 spatial dimensions, the gauge field cannot be chosen peri-

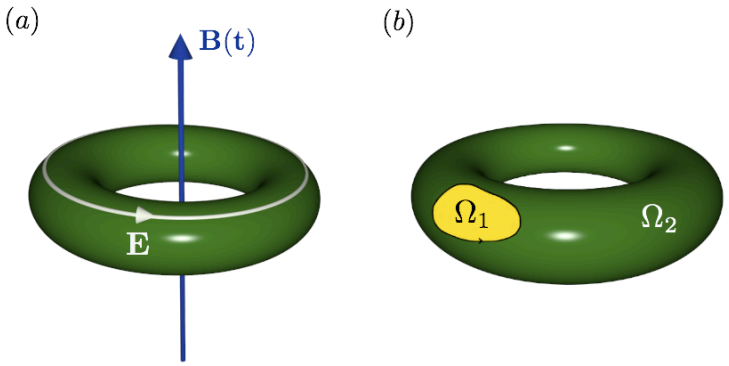

Figure 2.1: (a) A magnetic field increasing linearly with time and confined to a torus hole produces a uniform and constant electric field along the torus. (b) A closed path on the torus can be thought of as enclosing two areas, Ω_1 and Ω_2.

odic? A gauge potential A_μ cannot be chosen periodic if

$$\oint_\square d\ell \cdot A \neq 0 \tag{2.3}$$

where the line integral is over any $L \times L$ square located in one of the coordinate planes $x_\mu x_\nu$ with $\mu \neq \nu$ on the hyper-cube. We note that the above integral (2.3) is gauge invariant and, due to the periodicity of $F_{\mu\nu}(x)$, its value is independent of the position of the $L \times L$ square, i.e. it is invariant under any space-time translation. In terms of the field tensor Eq. (2.3) can be written as

$$\int_\square dx_\mu dx_\nu F_{\mu\nu} \neq 0, \tag{2.4}$$

with no summation over μ, ν. Physically, this means that the total magnetic flux through one of the spatial faces of the hypercube is non-zero and a similar condition for the electric field (see below).

The above considerations motivate a decomposition of the gauge potential into two pieces,

$$A_\mu(x) = A^0_\mu(x) + \delta A_\mu(x), \tag{2.5}$$

such that

$$\oint_{\square} d\ell \cdot \delta A = 0. \tag{2.6}$$

Hence δA_μ can be chosen periodic, while $A^0_\mu(x)$ contains any non-periodic part. Similarly, we write

$$F_{\mu\nu}(x) = F^0_{\mu\nu}(x) + \delta F_{\mu\nu}(x), \tag{2.7}$$

with $F^0_{\mu\nu} \equiv \partial_\mu A^0_\nu - \partial_\nu A^0_\mu$. To make this decomposition unique (up to a gauge transformation) we furthermore impose a condition that components of $F^0_{\mu\nu}$ are uniform and constant,

$$F^0_{\mu\nu} = \frac{1}{L^2} \int_{\square} dx_\mu dx_\nu F_{\mu\nu}. \tag{2.8}$$

In terms of electric and magnetic field vectors our decomposition corresponds to

$$\vec{E} = \vec{E}_0 + \delta\vec{E}, \quad \vec{B} = \vec{B}_0 + \delta\vec{B}, \tag{2.9}$$

where $\vec{E}_0$, $\vec{B}_0$ are constant uniform fields while $\delta\vec{E}$, $\delta\vec{B}$ are space-time varying fields derived from the periodic gauge potential $\delta A_\mu(x)$. The constant fields can only be produced by magnetic and electric fluxes through the holes in the T^3 torus embedded in a four dimensional space, and it is not possible to devise non-singular charge and current sources within the periodic three dimensional space to produce them [75].

Fields $\delta\vec{E}$ and $\delta\vec{B}$ are produced by ordinary charge and current sources. They have the following physical properties: (i) Magnetic fluxes associated with these magnetic fields through each spatial face vanish,

$$\varepsilon^{ijk} \int_{\square} dx_i dx_j \delta B_k = 0 \qquad i,j,k = 1,2,3. \tag{2.10}$$

There is no summation on indices and the equation holds for all x_k and x_0. (ii) The integral over any space-time face

$$\int_{\square} dx_0 dx_i \delta E_i = 0, \tag{2.11}$$

with no summation on $i = 1,2,3$. (i) and (ii) are properties of the fields produced by a general space-time periodic charge and current sources. With this preparation

we can now proceed to evaluate the axion action.

It is most convenient to employ Eq. (2.2) where in view of our decomposition (2.6,2.7) the expression $F_{\mu\nu}A_\beta$ is replaced by

$$F^0_{\mu\nu}A^0_\beta + 2F^0_{\mu\nu}\delta A_\beta + \delta F_{\mu\nu}\delta A_\beta. \tag{2.12}$$

An integration by parts has been performed on $\delta F_{\mu\nu}A^0_\beta$ to obtain the factor of 2 in the middle term. Now the second and the third term in the above expression (2.12) are explicitly space-time *periodic* and therefore their contribution to S_{axion} identically vanishes. The only contribution to the action comes from the first term which represents the uniform constant part of the electromagnetic fields. Thus,

$$\frac{1}{\hbar}S_{\text{axion}} = \frac{\theta}{\Phi_0^2}\int d^4x\, \vec{E}_0 \cdot \vec{B}_0. \tag{2.13}$$

It remains to be demonstrated that the action is quantized for these constant and uniform fields.

2.3 Quantization of the Chern numbers

Our arguments thus far have been purely classical. At the level of classical electrodynamics, clearly, the integral in Eq. (2.13) can attain any desired value and is not quantized. To proceed, we must recall that in the present context the axion term results from integrating out the electron degrees of freedom in a topological insulator. Electron behaviour is inherently quantum mechanical. The axion action quantization then follows from the requirement that the gauge potential A_μ that couples to the electron wave-functions, be consistent with the quantum theory of electrons in periodic space-time.

In the following we assume for simplicity that our fields are pointed along the x_3 direction, $\vec{E}_0 = E_3\hat{x}_3$ and $\vec{B}_0 = B_3\hat{x}_3$. Other components can be treated in an identical fashion. For this configuration we may decompose our space-time torus T^4 into a direct product $T^2_{12} \times T^2_{03}$ and write

$$\frac{1}{\hbar}S_{\text{axion}} = \frac{\theta}{\Phi_0^2}\int_\square dx_1 dx_2 B_3 \int_\square dx_0 dx_3 E_3. \tag{2.14}$$

It remains to show that each of these integrals is an integer multiple of the magnetic flux quantum Φ_0. The first integral represents the total magnetic flux through the x_1x_2 face of the hypercube. The quantization of this term follows from the standard arguments for the electron motion in applied magnetic field, which we now briefly review for completeness.

Imagine an arbitrary closed path $\mathscr{C}$ on the T^2_{12} torus. As illustrated in Fig. 2.1b it encloses area denoted as Ω_1. Alternately, it can be viewed as enclosing its complement on T^2_{12} denoted as Ω_2. Using Stokes' theorem we may write

$$\int_{\Omega_1} \vec{B}\cdot d\mathbf{S} = \oint_{\mathscr{C}} \vec{A}\cdot d\mathbf{l} \tag{2.15}$$

$$\int_{\Omega_2} \vec{B}\cdot d\mathbf{S} = -\oint_{\mathscr{C}} \vec{A}'\cdot d\mathbf{l}, \tag{2.16}$$

where the prime on the vector potential signifies the subtle but important fact that the equality is required to hold only up to a gauge transformation $A_\mu \to A'_\mu = A_\mu - \partial_\mu f$, with $f(x)$ a scalar function. Now the line integral of $\vec{A}$ along a closed path is normally thought of as a gauge invariant quantity in which case adding Eqs. (2.15) and (2.16) immediately implies $\int_{\Omega_1+\Omega_2} \vec{B}\cdot d\mathbf{S} = 0$. This suggests that $S_{\text{axion}}/\hbar$ is indeed quantized but the only value allowed is 0. However, there exists a class of 'large' gauge transformations $f(x)$ which change the value of the line integral but leave the wave-function single valued. The latter transforms as $\Psi(x) \to \Psi'(x) = e^{ief(x)}\Psi(x)$ and the relevant $f(x)$ contains a vortex (a Dirac string) at some point of the T^2_{12} torus, i.e. $e^{ief(x)} \sim e^{in\varphi}$ where φ is an angle in x_1x_2 plane measured from the vortex center and n is an integer. Since $\oint_{\mathscr{C}} \nabla f\cdot d\mathbf{l} = 2\pi n$ the inclusion of large gauge transformations of this type can be seen from Eqs. (2.15) and (2.16) to allow for non-zero quantized values $\int_\square dx_1dx_2B_3 = n\Phi_0$.

One can advance the same argument to establish the quantization of the second surface integral in Eq. (2.14). Consider a closed path, this time on T^2_{03}, enclosing Ω_1 and Ω_2 regions. It is straightforward to check that all steps proceed exactly as before. The large gauge transformations now involve space-time vortices in $f(x)$ (i.e. vortices in the x_0x_3 plane) and lead to the analogous result $\int_\square dx_0dx_3E_3 = m\Phi_0$ with m integer.

Combining the above results we find

$$\frac{1}{\hbar}S_{\text{axion}} = N\theta, \tag{2.17}$$

with $N = nm$. Eq. (2.17) shows that the axion action for electromagnetic field is quantized on periodic space-time and, consequently, the amplitude $\exp(iS_{\text{axion}}/\hbar)$ is invariant under the shift of the axion angle θ by any integer multiple of 2π.

A more abstract and rigorous way to think of the quantization of these quantities is using fibre bundle mathematics mentioned briefly in the beginning. The fibre bundles [3] can be classified in terms of the so called Chern characters. These are forms whose integral over closed base space of the bundle always return an integer number. One consequence is that the integral of a first Chern character of the Abelian $U(1)$ gauge theory, $F_{\mu\nu}/\Phi_0$ on the closed base space $T^2_{\mu\nu}$ must always be an integer. On the other hand the axion action is a second Chern character integral evaluated for this abelian gauge theory. We showed that this can be written as a product of the two first Chern character integrals whose quantization, as we discussed, has a clear physical interpretation.

2.4 Open boundaries case

Assuming periodic boundary conditions in all directions is the simplest way to avoid edges and to concentrate on the bulk response. However, in real experimental setup one must deal with a situation where the the fields are present in a finite portion of space and over a finite time duration. The question arises whether the axion action remains quantized under these non-periodic conditions. The answer is "yes" provided that one additional condition on the gauge potential is satisfied. Specifically, it is possible to show that Eq. (1.19) remains valid if (i) the fields $\vec{B}$ and $\vec{E}$ vanish outside a space-time volume $\mathscr{V}$ and (ii) the underlying gauge field A_μ is such that its presence cannot be detected by any Aharonov-Bohm type experiment performed using charge e particles outside $\mathscr{V}$. For the magnetic field this implies, for example, that the total flux enclosed by any closed trajectory is $n\Phi_0$ with n integer. In that case the Aharonov-Bohm phase acquired by charge e particle is $2\pi n$ and thus indistinguishable from 0.

2.5 Abelian versus non-abelian gauge fields

Table 2.1: Chern Character for Abelian and non-Abelian gauge fields

	Abelian gauge	non-Abelian gauge
Base space	Minkowski Space	Four-dimensional BZ
Gauge field	$A^{\mu} = (\phi, \vec{A})$	$\mathcal{A}_i^{\alpha\beta} = -i < \alpha, \vec{k} \vert \partial_i \vert \beta, \vec{k} >$
Field strength	$F^{\mu\nu} = \partial^{\mu} A^{\nu} - \partial^{\nu} A^{\mu}$	$\mathcal{F}_{ij}^{\alpha\beta} = \partial_i \mathcal{A}_j^{\alpha\beta} - \partial_j \mathcal{A}_i^{\alpha\beta} + i[\mathcal{A}_i, \mathcal{A}_j]^{\alpha\beta}$
First Chern	Φ/Φ_0	σ_{ij}/σ_0
Second Chern	S_{axion}/θ	C_2

As we discussed in the beginning, the electromagnetic response of the TIs can be studies by considering a Dirac field coupled to a classical electromagnetic gauge field. Chern characters and numbers can be defined for this abelian gauge field as they are shown in the table. Apart from the abelian gauge field, one can define Chern characters in the same fashion for the non-abelian pseudo magnetic gauge field of the electronic Bloch states.

All the possible configurations for the occupied electronic states can be characterized in terms of invariants which are the integral of the so called Chern Characters over the closed base space (the BZ). In this case, first Chern numbers can be defined by integrating the first Chern character over a 2D closed sub-manifold ($\equiv T^2$) as discussed in the quantization of the magnetic flux in the second chapter.

$$C_1^{\mathrm{A}} = \frac{1}{\Phi_0} \int dx \int dy F_{xy} = \frac{1}{\Phi_0} \oint \vec{B} \cdot d\mathbf{a} = \frac{\Phi}{\Phi_0}, \tag{2.18}$$

One can also define the second Chern number which can take integer values and can be factorized in terms of two first Chern characters defined on two 2D sub-manifolds as we showed in our proof of the quantization of the axion action. Till now all the Chern characters we discussed were defined for the QED's Abelian $U(1)$ gauge field over real space that couples to the Dirac field via minimal coupling.

In (3+1) we can define three first Chern numbers $(\sigma_{xy}, \sigma_{yz}, \sigma_{xz})$ which all vanish for a time-reversal invariant system. For such a system with zero first Chern numbers we can have a non-zero second Chern number which is related to the θ

axion field [37]. This quantity is an integral of the second Chern character for a non-Abelian gauge field evaluated over a 4-dimensional BZ. Table (2.1) compares the Abelian and non-Abelian cases.

2.6 Effect of magnetic monopoles

In passing from Eq. (2.1) to (2.2) we have assumed that a term $A_\beta \varepsilon^{\mu\nu\alpha\beta} \partial_\alpha F_{\mu\nu}$ that appears in the integration by parts vanishes on the account of partial derivatives commuting and $\varepsilon^{\mu\nu\alpha\beta}$ being antisymmetric. This assumption would appear to fail in the presence of magnetic monopoles. Consider *e.g.* the $\beta = 0$ component of the above expression which equals $2A_0 \nabla \cdot \vec{B}$. In the presence of the non-vanishing monopole density $\nabla \cdot \vec{B} \neq 0$ such term will give non-zero contribution to S_{axion} whenever A_0 is non-zero. Similarly, $\beta = 1,2,3$ terms correspond to monopole currents and may be non-vanishing as well. Careful evaluation of S_{axion} in the presence of monopoles leads to a contribution that appears to violate the global symmetry $\theta \to \theta + 2\pi$ of S_{axion} on periodic space-time.

One nevertheless expects the axion action to remain a valid description of topological insulators in the presence of monopoles. For instance the occurrence of the Witten effect, [49] *i.e.* electric charge $-e(\theta/2\pi + n)$ bound to the fundamental monopole, has been recently verified using a model topological insulator [48].

We believe that the problem with the apparent violation of the $\theta \to \theta + 2\pi$ symmetry lies in the fact that the presence of magnetic monopoles contradicts the description of the system in terms of the gauge potential A_μ. It is well known [75] that it is mathematically impossible to find a globally defined vector potential $\vec{A}$ that would give rise to non-vanishing $\nabla \cdot \vec{B}$. Vector potentials commonly used to describe monopole-like field configurations [76] invariably contain a singularity. For example the usual choice of the vector potential $\vec{A} = -\Phi_0(1 + \cos\vartheta)\nabla\varphi$, with (ϑ, φ) the spherical angles, is singular along the positive z-axis. Physically, this singularity can be viewed as an infinitely thin solenoid, a "Dirac string", that brings one quantum of the magnetic flux to the location of the monopole. The string can either extend to infinity or terminate at an anti-monopole. A Dirac string can be thought of as a limiting case of a solenoid with the radius approaching zero. Such

a thin solenoid carrying integer number of flux quanta is invisible to electrons as it imparts Aharonov-Bohm phase that is an integer multiple of 2π. Nevertheless if we include the fields inside the solenoid in the computation of S_{axion} then the condition $\nabla \cdot \vec{B} = 0$ is upheld, all magnetic field lines are closed, and the term $A_\beta \varepsilon^{\mu\nu\alpha\beta} \partial_\alpha F_{\mu\nu}$ identically vanishes. Our original argument therefore goes through as before and implies symmetry under $\theta \to \theta + 2\pi$ of S_{axion} on periodic space-time even in the presence of Dirac monopoles.

2.7 Conclusions

We have presented a simple and intuitive proof of the quantization of the topological axion action on periodic space-time. Our considerations show that the theory is invariant under a global $\theta \to \theta + 2\pi$ transformation consistent with the $\mathbb{Z}_2$ character of the fundamental 'strong' invariant describing the physics of time-reversal invariant band insulators. An important observation was that for $U(1)$ Abelian gauge field the second Chern number is a direct product of two first Chern numbers and once a first Chern number vanishes the second will vanish too but in the $SU(2)$ non-abelian case even when the first Chern numbers vanish the second Chern number can be non-zero as it can be the case in a TI [37].

Chapter 3

Response of Surface Dirac States

3.1 Overview

Topologically protected electronic states residing on the surface of topological insulators (TI) [33, 38, 38, 40, 41, 77–79] form a unique 2D metal distinct from those so far realized in solid state systems. Similar to the low energy electronic states in a single layer graphene [19], the robust 2D metal on an TI surface has conic branches touching (in the absence of the intrinsic gap) at high-symmetry points in the first Brillouin zone. This resemblance in the energy dispersion is responsible for some common properties between these metallic systems, such as the square-root dependence of Landau Level (LL)s spacing to the applied magnetic field. However, there are important differences between these systems, as a result of the topological nature of the surface states in TIs.

One of the interesting aspects in which these 2D metallic systems behave uniquely is their magnetic response [80]. Here, motivated by the recent progress in the experimental methods and the importance of the spin susceptibility for our understanding of electronic systems, we study the spin response of electrons on the surface of a TI and show that it exhibits interesting features even in a simple non-interacting limit. We find that the characteristic spin-momentum locking of these electrons leads to a unique spin response that is distinct from spin-degenerate systems like graphene and 2DEG. Instead of the oscillatory behaviour of the susceptibility as a function of the chemical potential found in spin degenerate systems,

in TIs our work predicts a plateau-type behaviour which arises from the strong correlation between spin and orbital degrees of freedom. In addition we find that the existence of a special LL with full spin polarization leads to a jump in the magnetization as the chemical potential crosses the energy of this LL. When an intrinsic magnetic ordering is present there is also a jump in the magnetization as a function of the applied magnetic field. Our results can therefore assist in detection of such intrinsic magnetization [42, 43] which is known to have profound consequences for the nature of the surface state; the magnetized surface state of a TI is predicted to become a quantum Hall liquid with half-integer quantized Hall conductivity [35, 37] and many unusual [54, 81–85] and potentially useful [85, 86] physical properties.

There are various ways of measuring the weak magnetization produced by electrons on a metallic surface. The SQUID scanning magnetometry is a highly sensitive probe which can detect tiny magnetization on the surfaces. However, it is a challenge to use this device to probe magnetization when there is a large applied magnetic field which interferes with the superconducting part of the SQUID and causes noise. A variant of this method using a superconducting pickup coil has been developed in order to study deHaas-van Alphen oscillations of the 2D metallic systems in a large perpendicular magnetic field [87, 88]. High-sensitivity micro-mechanical cantilever magnetometry [89] is another way of measuring electronic magnetization, however, this method measures the magnetization of the whole sample and it is difficult to isolate the contribution from the electrons on a single surface.

The nuclear magnetic resonance (NMR) is another powerful experimental technique which can be used to study electronic spin magnetic response in a bulk metal [90]. Through the so-called Knight shift of the nuclear resonance peak, it is possible to probe the spin part of the magnetic susceptibility of the electrons as they interact with the resonating nuclei in their proximity. Unfortunately, this method, in its conventional form, fails to be useful in very thin films and 2D metallic systems due to the limitation in the number of available nuclei and the resulting weakness of the signal. Thanks to the progresses made by experimentalists in controlling and implementing high energy beams of unstable ions, an experimental technique, the so-called β-NMR, has been recently developed to overcome the above limitations.

Briefly, in this exotic variety of NMR, unstable radioactive ions such as ^{8}Li and ^{11}Be are implanted in the sample surface. The nuclear spin precession signal is then detected through the products of the beta decay of the radioactive nucleus. Since the ion implantation depth can be controlled by tuning the beam energy it is possible to acquire information about the behaviour of the electronic spins in very thin metallic films [46, 47]. Experiments are currently underway to study the surface magnetic response of TI crystals Bi_2Se_3 and Bi_2Te_3 using β-NMR [46].

This chapter is organized as follows. First we introduce a simple model known to describe the electrons on the surface of a TI in the presence of a perpendicular magnetic field. We review the exact solutions of its eigenvalue problem which has been studied previously in various contexts [80, 91]. We then calculate the spin magnetization and susceptibility assuming that the chemical potential lies inside the gap between positive and negative energy eigenstates. We discuss the magnetic response of the surface as one tunes the magnetic field and the chemical potential for various values of the intrinsic gap. In the end, we explain how a β-NMR experiment might be able to detect these effects through Knight shift measurements.

3.2 Dirac modes in out-of-plane applied magnetic field

Turning on a perpendicular magnetic field adds two terms to the above Hamiltonian. One is the minimal coupling of the magnetic vector potential, $\hbar\vec{k} \to \hbar\vec{k} + e\vec{A}$ (electron charge $-e$). The other is the coupling of the spins to the magnetic field, the Zeeman effect, expressed as $\delta H_Z = -g_s \mu_B \hbar^{-1} \vec{B} \cdot \vec{s}$, where g_s is the effective electron gyromagnetic constant. In the bulk Bi_2Se_3 crystal $g_s \simeq 30$ (Ref. [92]) although much smaller values have been reported for electrons near the surface [93]. In our calculations below we use two representative values, $g_s = 8$ and $g_s = 30$, which yield qualitatively similar results with some interesting differences.

In the continuum limit, the leading order Hamiltonian describing these surface states in the presence of the applied magnetic field, $\vec{B} = B_0\hat{z}$, in the Landau gauge $\vec{A} = -(B_0 y, 0)$, can be written in the following form

$$H = \sum_{k_x} \int dy \, \Psi^\dagger_{k_x}(y) \mathscr{H}(k_x, y) \Psi_{k_x}(y), \tag{3.1}$$

where $\Psi^{\dagger}_{k_x}(y)$ is the creation operator for the spinor mode extended along the x direction and localized at y. $\mathscr{H}(k_x,y)$ for $B_0 > 0$ is defined as

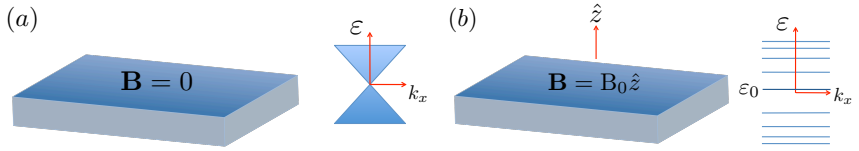

Figure 3.1: The surface spectrum of a strong topological insulator in the absence of magnetic dopants ($\Delta_0 = 0$), (a) in the absence of the external magnetic field, (b) in the presence of an applied perpendicular magnetic field.

$$\mathscr{H}(k_x,y) = \begin{pmatrix} \Delta & i\varepsilon_c a_{k_x} \\ -i\varepsilon_c a^{\dagger}_{k_x} & -\Delta \end{pmatrix}, \tag{3.2}$$

where $\varepsilon_c = \upsilon_F\sqrt{2e\hbar|B_0|}$ and

$$\Delta = \Delta_0 - \frac{g_s\mu_B B_0}{2}. \tag{3.3}$$

The term in Δ proportional to the magnetic field is the Zeeman contribution. a_{k_x} is the one-dimensional harmonic oscillator Bosonic operator defined as

$$a_{k_x} = \frac{1}{\sqrt{2}}\left(\frac{y}{l_B} + l_B(\partial_y - k_x)\right), \quad l_B^2 = \frac{\hbar}{e|B_0|}. \tag{3.4}$$

Note that varying k_x shifts the position of the localized state, produced by the application of $a^{\dagger}_{k_x}$ on the vacuum state, along the y direction. In the $B_0 < 0$ case, $\mathscr{H}(k_x,y)$ can be obtained from the one given for $B_0 > 0$ in Eq. (3.2) by exchanging the off-diagonal elements and replacing k_x by its time reversed counterpart $-k_x$.

The eigenstates for $B_0 > 0$ and $n > 0$ are given by [80, 91]

$$\phi^{+}_{k_x,n}(y) = \begin{pmatrix} \cos(\delta_n/2)\varphi_{n-1}(y - k_x {l_B}^2) \\ \\ -i\sin(\delta_n/2)\varphi_n(y - k_x {l_B}^2) \end{pmatrix}, \tag{3.5}$$

$$\phi^{-}_{k_x,n}(y) = \begin{pmatrix} \sin(\delta_n/2)\varphi_{n-1}(y - k_x {l_B}^2) \\ \\ i\cos(\delta_n/2)\varphi_n(y - k_x {l_B}^2) \end{pmatrix}, \tag{3.6}$$

while for $n = 0$ we have

$$\phi_{k_x,0}(y) = \begin{pmatrix} 0 \\ \\ \varphi_0(y - k_x {l_B}^2) \end{pmatrix}. \tag{3.7}$$

In the above $\cos\delta_n = \Delta/\varepsilon_n^+$ and φ_n are the one-dimensional harmonic oscillator eigenstates, i.e., $a^\dagger a\varphi_n = n\varphi_n$. We remark that the $n = 0$ eigenstate in Eq. (3.7) is very special since it is fully *spin polarized*. This will have important consequences for the magnetic response discussed below.

The eigenvalues associated with $\phi^{\pm}_{k_x,n}(y)$ eigenstates are given by

$$\varepsilon_n^{\pm} = \pm\sqrt{n\varepsilon_c^2 + \Delta^2}, \qquad n > 0, \tag{3.8}$$

and for the fully spin-polarized $n = 0$ eigenstates

$$\varepsilon_0 = -\mathrm{sgn}(B_0)\Delta. \tag{3.9}$$

Note that the form of the eigenstates for $B_0 < 0$ is different from that given in Eq.(3.5-3.7) since the Hamiltonian is different in that case.

3.3 Spin susceptibility and magnetization

The electronic magnetic moment due to spin is proportional to the spin operator

$$\boldsymbol{\mu}_e = -\gamma_e \boldsymbol{s}, \qquad (\gamma_e = -g_s\mu_B/\hbar), \tag{3.10}$$

Therefore, to calculate the spin part of the magnetic moment for the eigenstates given in the previous section, we only need to find the expectation value of the spin operator. A straightforward evaluation using Eqs. (3.5-3.7) shows that all the electronic states within the same LL contribute equally to the magnetization. For

each of them we have

$$\mathscr{M}^{\alpha}_{x,n} = \mathscr{M}^{\alpha}_{y,n} = 0, \tag{3.11}$$

$$\mathscr{M}^{\alpha}_{z,n} = \frac{g_s \mu_B}{2} \cdot \frac{\Delta}{\varepsilon^{\alpha}_n}, \tag{3.12}$$

$$\mathscr{M}_{z,0} = -\frac{g_s \mu_B}{2} \mathrm{sgn}\,(B_0), \tag{3.13}$$

The total magnetization for each Landau level can be obtained by multiplying the above quantities by the Landau level degeneracy $L^2/(2\pi l_B^2)$, representing the total number of states with characteristic length l_B that the surface area L^2 can accommodate. Since the magnetization contribution computed above for each eigenstate is an explicit function of its energy, we can perform the following integral to find the total magnetization density due to the electronic spins

$$M_s = \int d\varepsilon \, D(\varepsilon) \mathscr{M}_s(\varepsilon) n_F(\varepsilon), \tag{3.14}$$

where $\mathscr{M}_s(\varepsilon) = g_s \mu_B \Delta/(2\varepsilon)$ is the magnetization of the eigenstate with energy ε and $n_F(\varepsilon) = 1/[e^{(\varepsilon-\mu)/k_B T} + 1]$ is the Fermi-Dirac distribution function. The electronic density of states associated with the surface states is $D(\varepsilon)$. For the Hamiltonian we used in the previous section it takes the following form

$$D(\varepsilon) = \frac{1}{2\pi l_B^2} \left[\delta(\varepsilon - \varepsilon_0) + \sum_{n>0,\alpha=\pm}^{n_c} \delta(\varepsilon - \varepsilon^{\alpha}_n) \right], \tag{3.15}$$

where $n_c \equiv (\Lambda^2 - \Delta^2)/\varepsilon_c^2$ is the Landau level index beyond which the energy exceeds the cutoff energy Λ. The cutoff can be chosen to be the energy where the surface band becomes degenerate with the bulk bands and here we assume $\Lambda = 300$ meV. Using this density of states function to perform integration in Eq. (3.14) yields

$$\frac{M_s}{B_0} = \chi_0 \left[-n_F(\varepsilon_0) + \mathrm{sgn}\,(B_0) \sum_{n=1}^{n_c} \frac{n_F(\varepsilon^+_n) - n_F(\varepsilon^-_n)}{\varepsilon^+_n/\Delta} \right], \tag{3.16}$$

where $\chi_0 \equiv (e g_s \mu_B)/2h$.

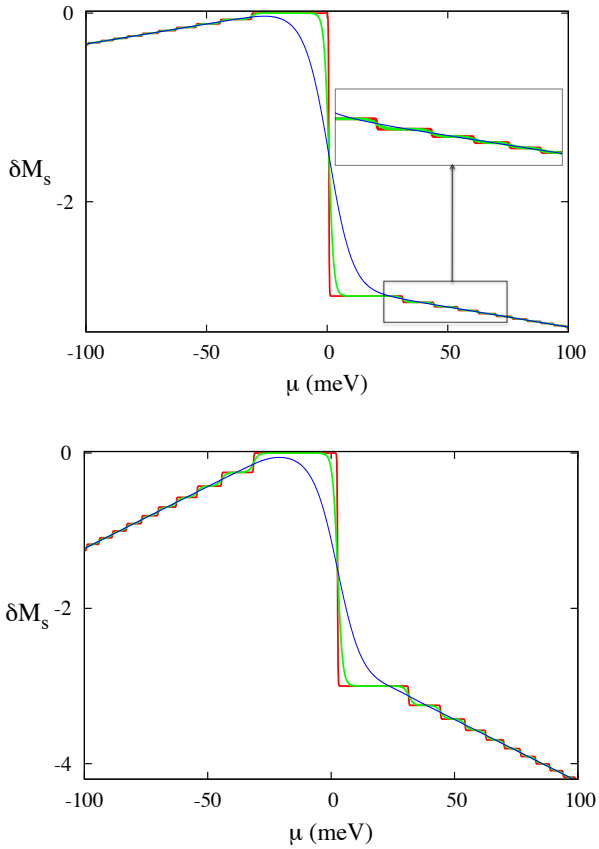

Figure 3.2: Spin magnetization $\delta M_s = M_s(T,\mu) - M_s(0,0)$ in units of ($\chi_0 \cdot$ Tesla) as a function of the chemical potential for a nonmagnetic surface ($\Delta_0 = 0$) at $B_0 = 3.0$ Tesla, $g_s = 8$ (top panel) and 30 (bottom panel). $k_B T = 0.1, 1.0, 5.0$ meV (red, green, blue).

For a constant magnetic field B_0 the magnetization of a single TI surface given by Eq. (3.16) shows an interesting behaviour as a function of chemical potential μ illustrated in Fig. 3.2. In order to avoid ambiguity associated with the high-energy cutoff we choose to display $\delta M_s = M_s(T,\mu) - M_s(0,0)$, i.e. spin magnetization relative to the neutrality point at $T = 0$. For the negative values of μ magnetization initially decreases reflecting the fact that the negative-energy surface states exhibit negative spin polarization, as can be seen from Eq. (3.12). The large jump in δM_s

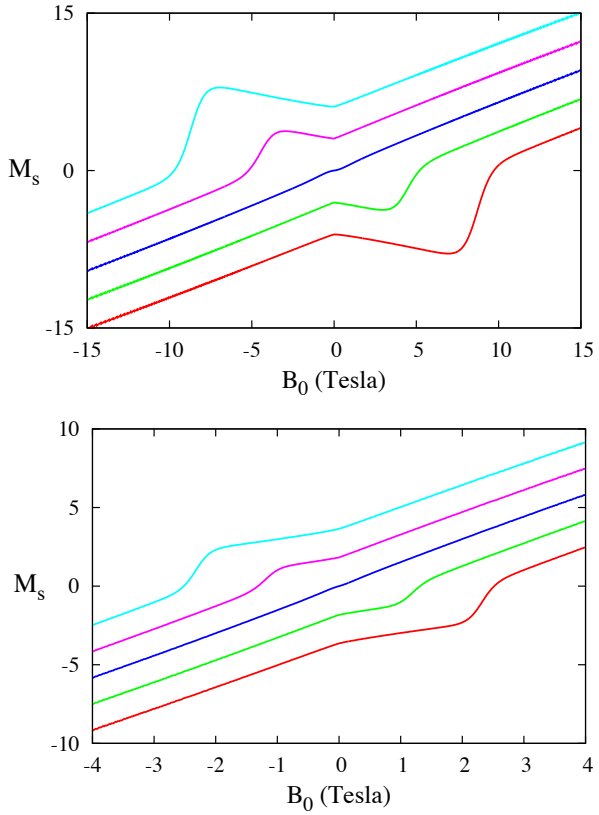

Figure 3.3: Spin magnetization in units of (χ_0· Tesla) as a function of the magnetic field for (from left to right) $\Delta_0 = -2,-1,0,1,2$ meV and $k_BT = 0.1$meV. $g_s = 8$ (top panel) and 30 (bottom panel).

near $\mu = 0$ results from electrons filling the fully spin-polarized $n = 0$ Landau level. Further increase in μ results in increase of δM_s now reflecting the fact that the positive-energy surface states exhibit positive spin polarization. To get a better sense of the order of the magnitude, assuming $g_s = 30$ and $B_0 = 1$Tesla, the jump in the spin magnetization on the surface area of size $1cm^2$ is of the order of $10^7\mu_B$.

The above behavior is unique to topological insulators for it results from the Landau level structure in a single Dirac point (or more generally an odd number thereof). In a TI the 'other' Dirac point is located on the opposite surface where the magnetic field points in the direction opposite relative to the surface normal, see

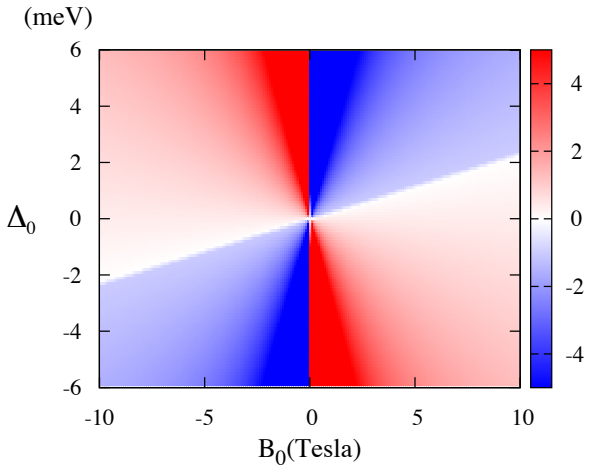

Figure 3.4: The color at each point (B_0, Δ_0) represents the magnitude of the spin susceptibility in the linear response regime, i.e., $\chi = M_s/B_0$, in units of χ_0. The step (diagonal white line) is given by Eq. (3.18) and results from $n = 0$ Landau level crossing the chemical potential. The discontinuity evident at $B_0 = 0$ reflects the fact that susceptibility χ diverges as $B_0 \to 0$. We have assumed $g_s = 8$ and $k_B T = 0.01$meV in this graph.

Fig. 3.1. The contribution of this surface to δM_s would be the same. We emphasize that for a relatively thick TI slab β-NMR will be sensitive to a single surface facing the beam and the behaviour predicted here is in principle observable, except that continuous tuning of the chemical potential in a crystal might be difficult to achieve.

A much more feasible experiment involves varying magnetic field B_0 while keeping μ constant. We now show that a unique signature of the fully polarized $n = 0$ Landau level still exists in samples with intrinsic magnetic ordering, when the chemical potential resides in the gap (i.e. both the bulk and the surface are insulating in the absence of the field). In his situation we can set $\mu = 0$ in our model. Now consider the effect of the applied magnetic field. Since the gap between the adjacent energy levels in which the Fermi energy is located is fairly large (~ 100 K for a 1T field), at sufficiently low temperatures we can replace the Fermi function

in Eq. (3.16) by the step function $n_F(\varepsilon) \to \Theta(-\varepsilon)$ and write

$$\frac{M_s}{B_0} = \chi_0 \left[-\Theta(-\varepsilon_0) - \mathrm{sgn}\,(B_0) \sum_{n=1}^{n_c} \frac{\Delta}{\sqrt{\varepsilon_c^2 n + \Delta^2}} \right], \tag{3.17}$$

We have assumed that the chemical potential remains pinned at zero energy and does not change as we tune the magnetic field. With these assumptions the magnetization has an interesting discontinuity at a finite magnetic field. The discontinuity in M_s occurs since tuning the magnetic field forces the fully spin polarized Landau level energy to evolve according to Eq. (3.3) and cross the chemical potential. The critical magnetic field at which the jump happens is given by

$$B_c = \frac{2}{g_s \mu_B} \Delta_0. \tag{3.18}$$

Assuming that the intrinsic gap Δ_0 remains independent of B_0, we plot the resulting magnetization in Fig. 3.3. This predicted behaviour could be employed to experimentally detect the intrinsic magnetization gap in the surface of a magnetically doped TI and measure the size of Δ_0 through Eq. (3.18). Although this signature only occurs when the chemical potential lies very close to the surface state Dirac point, we note that magnetically doped samples satisfying this requirement have been grown and studied [42].

It is important to note that Δ_0 is in general not independent of B_0, since magnetic moments of dopants will tend to align with the applied field. Thus, like in a ferromagnet, there will be a hysteresis effect whose features will depend on the material details [42]. One possible scenario is shown schematically in Fig. 3.5. In the case when Δ_0 depends on the field, the equation (3.18) continues to hold but must now be viewed as an implicit equation for the critical field B_c. It is also important to note that the behaviour of the magnetization as a function of B_0, will be modified if we assume that Δ_0 depends on the magnetic field. Assuming that Δ_0 remains uniform with a change in the magnetic field, one can obtain the behaviour of the spin magnetization as a function of the magnetic field by extracting the values of the magnetization on the corresponding hysteresis path in the (Δ_0, B_0) plane using Eq. (3.16).

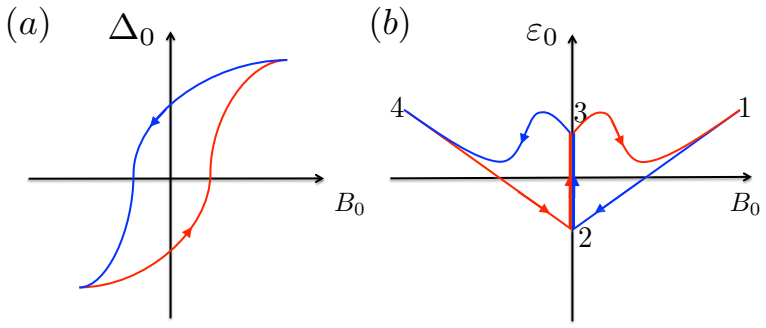

Figure 3.5: (a) Schematic behaviour of Δ_0, i.e., the intrinsic magnetization gap on the surface in a system with a slab geometry shown in Fig. 3.1 versus the applied magnetic field. (b) The energy of the $n = 0$ Landau level versus the magnetic field. Starting at the point 1 and by decreasing the magnetic field gradually, the energy would follow the path shown by the blue curve, i.e., $1 \to 2 \to 3 \to 4$, this happens if Δ_0 is described by the blue part of the cycle in (a). Now by increasing the magnetic field from a negative value, corresponding to the point 4, the energy would follow the path given by the red curve, i.e., $4 \to 2 \to 3 \to 1$, since this time Δ_0 would be given by the red curve in the hysteresis cycle.

Another question that arises has to do with the origin of the electrons that fill the $n = 0$ Landau level upon changing the field through B_c. One may wonder where the extra electrons come from in a fully gapped isolated system. The answer lies in the side surfaces which under generic conditions remain gapless and act as a reservoir of electrons. The model we consider here does not capture these states but they reflect themselves in solutions of the Hamiltonian which are not normalizable in an infinite system. These are fully spin polarized with opposite energy and spin direction. In fact they are the particle-hole conjugates of the fully spin polarized LL given in Eq. (3.7). Taking into account these electronic states and the fact that it is more favourable for electrons with higher energy to be transferred to the negative energy states the counting problem can be resolved.

3.4 Knight shift

We now outline how a β-NMR experiment can in principle be used to probe some of the physics discussed in the previous section. The valence and conduction elec-

trons in a metal posses magnetic moments arising from both their orbital motion and their spin degrees of freedom. Nuclear magnetic resonance technique can be used as a probe of the spin part of the total magnetization in the presence of the magnetic field by measuring the relative shift in the nuclear resonance peak with respect to the same resonance peak in a reference insulating system. This effect, which is due to the interaction between electronic spins and those of the nuclei, is known in the literature as the Knight shift and has been extensively studied in both theory and experiment [90].

The mobile electrons in a metal interact with the nuclei in their proximity and the Knight shift in the resonance peak of these nuclei can be described by a local Fermi contact interaction term given by $H_{\text{int}} = -\frac{8\pi}{3}\boldsymbol{\mu}_e \cdot \sum_i \boldsymbol{\mu}_i \delta(\boldsymbol{r} - \boldsymbol{R}_i)$ where $\boldsymbol{R}_i$ is the position of the ith nucleus and $\boldsymbol{\mu}_i = \gamma_N \boldsymbol{I}_i$ is its magnetic moment. The magnitude of γ_N, the gyromagnetic ratio, depends on the nuclear quantum state. The nucleus total spin, $\boldsymbol{I}_i$, couples to the applied magnetic field and therefore the position of the peak depends on the magnitude of the total magnetic field experienced by the nucleus which has a contribution due to the interaction with electrons. It turns out that this shift is proportional to the spin susceptibility. The constant of proportionality, known as the hyperfine coupling, can be computed using first principle calculations for the implanted nuclei. On the other hand, if we assume that the presence of the nuclei does not significantly alter the electronic states, then it is possible to approximate the shift for them by taking the expectation value of the aforementioned interaction term using the unperturbed electronic states. This is the lowest order approximation in the perturbative treatment of the interaction term. For metallic systems with spin degenerate bands this shift is proportional to the spin susceptibility, as can been seen from a simple calculation considering the fact that the spatial and spin degrees of freedom are uncorrelated [90].

The spin-momentum locking on the surface of a TI along with the energy dependence of the penetration depth can in principle change the above simple physics. Since it is not possible anymore to separate spin and orbital degrees of freedom, one might question the validity of the linear relation between the Knight shift and the spin susceptibility. We devote the rest of this section to addressing this issue by considering a very simple model. We assume that the nuclei do not alter the electronic states around them. It is important to note that this assumption may break

down for the implanted nuclei if they modify the electronic states around them significantly and computing the Knight shift would then require a first principle calculations.

The field experienced by the ith nucleus due to the interaction with the proximate electrons is given by

$$\boldsymbol{\delta}\vec{B}_i \equiv -\frac{8\pi}{3}\gamma_e\langle\boldsymbol{\sigma}\delta(\vec{r}-\vec{R}_i)\rangle_T, \tag{3.19}$$

where $\langle ...\rangle_T$ is the expectation value over electronic states at temperature T. Therefore, the effective Hamiltonian for the ensemble of nuclei takes the form

$$\boldsymbol{H}_N^{\text{eff}} = -\hbar\gamma_N\sum_i \boldsymbol{I}_i\cdot(\vec{B}_0+\boldsymbol{\delta}\vec{B}_i). \tag{3.20}$$

This way, the ith nucleus would have a resonance peak $\omega_i = \gamma_N(B_0+\delta B_{iz})$. The Knight shift is then defined by comparing the resonance frequency with the frequency in a similar material without these electronic states

$$K_i = \frac{\omega_i-\omega_0}{\omega_0} = \frac{B_0+\delta B_{iz}-B_0}{B_0} = \frac{\delta B_{iz}}{B_0}. \tag{3.21}$$

The shift in the resonance peak of the nuclei ensemble is the average of the Knight shift from each individual nucleus and is given by

$$K = \frac{1}{N}\sum_i \frac{\delta B_{iz}}{B_0}, \tag{3.22}$$

where N is the number of the implanted nuclei. Using the electronic eigenstates given in Eq. (3.5-3.7) we get the following expression for K

$$-\frac{8\pi\gamma_e}{3NB_0}\sum_i\sum_{k_x,n,\alpha}^{\text{occ}}|\psi_n^\alpha(z_i)|^2(|\phi_{n,\uparrow}^\alpha|^2(\vec{R}_{\perp i})-|\phi_{n,\downarrow}^\alpha|^2(\vec{R}_{\perp i})). \tag{3.23}$$

Here $|\psi_n^\alpha(z)|^2$ appears as a factor in the realistic 3D electronic wave functions of the surface electrons reflecting the fact that the electrons have an energy dependent penetration depth into the bulk. The nuclei implanted in the system have a spatial probability distribution $P_{\text{Nuc}}(z,\boldsymbol{r}_\perp)$, which depends on the energy and diameter of

the beam of the ions used in the β-NMR experiment. If the distribution function is known, we can replace the above summation with a 3D integral over the crystal volume

$$\frac{1}{N}\sum_i \rightarrow \int dz d^2\boldsymbol{r}_\perp P_{\mathrm{Nuc}}(z,\boldsymbol{r}_\perp). \tag{3.24}$$

Assuming that the distribution is uniform in the plane of the surface, i.e., $P_{\mathrm{Nuc}}(z,\boldsymbol{r}_\perp) = P(z)$, we get

$$K = \frac{8\pi}{3l_B^2 B_0}\sum_{n,\alpha}^{\mathrm{occ}} f_n^\alpha \cdot \mathscr{M}_{z,n}^\alpha, \tag{3.25}$$

where we have performed the integration over the in-plane degrees of freedom and replaced the summation over k_x with the LL degeneracy. We have also defined the nth LL weight, f_n^α, as

$$f_n^\alpha \equiv \int dz |\psi_n^\alpha(z)|^2 P(z). \tag{3.26}$$

Now if we assume that different LL have the same penetration depth we have $f_n^\alpha = f_0$ for all $n < n_c$ and we obtain

$$K = \frac{8\pi f_0}{3B_0}\frac{1}{l_B^2}\sum_{n,\alpha}^{\mathrm{occ}} M_{z,n}^\alpha = \frac{8\pi f_0}{3}\chi_e^s. \tag{3.27}$$

We thus recover the linear proportionality of the Knight shift to the surface electronic spin susceptibility under reasonable assumptions. Note that if we relax the assumption that different LLs can now have different penetration depths, then the Knight shift would no longer be linearly proportional to the total spin susceptibility. Instead, it would be a weighted superposition of contributions from each individual LL to the spin susceptibility. Nevertheless, the Knight shift will still display the interesting behavior discussed in this study as long as f_n^α is a reasonably slowly varying function of n. We should emphasize once again that although above considerations elaborate on the differences caused by the spin-momentum locking and the energy dependent penetration depth, they do not take into account the fact that the electronic wave-functions could be altered by the presence of the implanted nuclei and the hybridization with the adjacent atoms.

3.5 Conclusions

The magnetic response of spins of the Dirac-like electrons on the surface of a topological insulator shows interesting features both in the absence and the presence of an intrinsic gap Δ_0. When the surface states are gapped owing to the time-reversal breaking perturbation (i.e. due to magnetic doping) the $n = 0$ LL, which is fully spin polarized, can have positive or negative energy depending on the sign of the intrinsic gap Δ_0 relative to that of the applied magnetic field. It will therefore be completely filled or empty when the chemical potential potential is tuned to zero energy. Our study shows that this structure results in an observable jump in the spin susceptibility, measurable e.g. through the β-NMR Knight shift, as one tunes the applied magnetic field through the critical value B_c given by Eq. (3.18). The effect may be used as a means to measure the magnitude of the intrinsic gap on the surface of a magnetically doped topological insulator if β-NMR or another surface-sensitive technique (e.g., LE-μsR, CE-Mossbauer, PAD [94–96]) could capture the magnetic response of the electronic spins on the surface. This behaviour is a unique feature of the topological insulator exotic surface states closely related to the special form of the spin-momentum entanglement.

Chapter 4

Models for Weyl Semimetals

4.1 Overview

As we discussed in the first chapter, the parent phase in a Weyl semimetal phase is a degenerate Dirac semimetal at the critical point in the transition between a topological and an ordinary insulator where time-reversal and inversion symmetries are preserved. Starting from this Dirac semimetal phase which has already been realized experimentally in Na_3Bi [97], one can drive the system to what is called a Weyl semimetal phase with a pair of isolated linear band-touching points. The Weyl points' separation in momentum space or energy has some interesting consequences that can potentially be observed in an actual experiment. Anomalous Hall current is one of these interesting consequences in which applying an electric current in the direction which is perpendicular to the direction of the Weyl separation leads to a current in the transverse direction which is proportional to the length of the vector that connects the two Weyl points. Another interesting but questionable prediction is the CME which arises if the form of the topological action predicted based on subtle field theoretical consideration is correct. It is important to study various lattice models that can be in a Weyl semimetal phase in order to understand the rich physical phenomena associated with this phase.

The original proposal is very simple and it is based on considering a layered heterostructure that is made by stacking thin films of ordinary magnetic insulators and topological insulators on top of each other [55]. This way one can realize a

Dirac Hamiltonian at low energies with proper term to separate Weyl points for a range of system parameters. One can generalize the cubic lattice model described in the introduction chapter to model a topological insulator and realize a Weyl semimetal by breaking the time-reversal and inversion symmetries at the critical point where the Dirac mass is zero. This system is the core model in our study of the electromagnetic response of Weyl semimetals on a lattice model as we are going to study in the next chapter. However, before that we introduce another toy model for Weyl semimetals where multiple pairs of Weyl nodes can exist and we show that the cumulative effect of these pairs on the transport can lead to different behaviours in the linear response theory.

4.2 Multiple Weyl pairs

It turns out that a system with more than one pair of Weyl fermions might have zero net anomalous Hall conductivity since pairs can have total cancelling contributions due to the exactly opposite separations in momentum space. Here we consider a simple theoretical model which can lead to a topological semi-metal phase with two Weyl pairs under certain circumstances. Although there are big challenges on the way to experimental realization of such a system, it can be used as a platform to study the bulk and the surface properties of a system in a Weyl semi-metal phase when there is more than one pair of Weyl nodes.

In the rest of this chapter we introduce a lattice model made by arranging parallel TI nano-wires in a honeycomb fashion with a lattice spacing which is small enough to allow a significant hopping of the electrons between these wires and then we discuss how one can achieve a topological semimetal phase with anomalous Hall charge and valley current from this arrangement.

We show that a Weyl semimetal phase with isolated Weyl nodes in momentum space can arise in a system of parallel topological insulator nano-wires arranged in a honeycomb fashion where the anomalous Hall response can be absent. This introduces another theoretical example of a topological semi-metal phase with more than one pair of Weyl nodes and due to the simple form of its Hamiltonian it can be used to study various interesting phenomena associated with this phase. Our results indicates that depending on the separation of the Weyl nodes a topological

electromagnetic charge response might or might not be present and two pairs can have overall cancelling contributions to the net anomalous Hall conductivity. We show that when the separation of the two Weyl pairs are exactly opposite, there is a non-zero anomalous Hall valley-current which is proportional to the length of the separation vector in momentum space.

4.3 TI nano-wires

The surface modes of a cylindrical topological insulator system can be described by a Dirac Hamiltonian in a curved space [98] ($\hbar = 1$)

$$H_k = \frac{\upsilon}{2}[\boldsymbol{\nabla}\cdot\hat{\boldsymbol{n}} + \hat{\boldsymbol{n}}\cdot(\vec{p}\times\boldsymbol{\sigma}) + (\vec{p}\times\boldsymbol{\sigma})\cdot\hat{\boldsymbol{n}}], \tag{4.1}$$

where $\boldsymbol{\sigma}$ is the Pauli matrix vector which acts on the spin Hilbert space. $\vec{p} = -i\boldsymbol{\nabla}$ is the momentum operator and $\hat{\boldsymbol{n}}$ is the unit vector normal to the surface. For a cylinder of radius R along $\hat{z}$ axis we have $\hat{n} = \cos\varphi\hat{x} + \sin\varphi\hat{y}$. The Hamiltonian that governs the TI surface modes in the presence of a sufficiently thin magnetic flux, $\phi = \eta\phi_0$, can then be written as

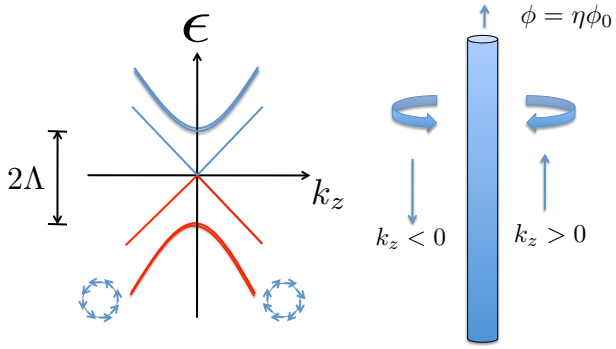

Figure 4.1: The surface spectrum of a wire made from a strong topological insulator in the presence of half integer multiple of the magnetic flux quantum along the wire. The bandwidth in which the spectrum is non-degenerate is $\Lambda = \hbar\upsilon_0/R$, where R is the radius of the wire. The spin texture is shown schematically for the states dispersing along k_z with the blue arrows.

$$H_k = \frac{1}{2R} + \begin{pmatrix} \frac{1}{R}(i\partial_\varphi + \eta) & -ik_z e^{-i\varphi} \\ ik_z e^{i\varphi} & -\frac{1}{R}(i\partial_\varphi + \eta) \end{pmatrix}, \tag{4.2}$$

We can simplify this Hamiltonian by a unitary transformation $\tilde{H}_k = U^\dagger(\varphi) H_k U(\varphi)$ in which $U(\varphi)$ is given by

$$U(\varphi) = \begin{pmatrix} 1 & 0 \\ 0 & e^{i\varphi} \end{pmatrix}, \tag{4.3}$$

using this transformation we can get rid of the phase in the off-diagonal components of the Hamiltonian matrix

$$H_k = \begin{pmatrix} \frac{1}{R}(i\partial_\varphi + \eta - \frac{1}{2}) & -ik_z \\ ik_z & -\frac{1}{R}(i\partial_\varphi + \eta - \frac{1}{2}) \end{pmatrix}, \tag{4.4}$$

The eigenstates of this Hamiltonian are given by $\psi_{kl}(\varphi) = e^{i\varphi l}\psi_{kl}$ where ψ_{kl} are eigenstates of the H_{kl} defined as

$$H_{kl} = k_z\sigma_2 - \frac{1}{R}\sigma_3(l + \frac{1}{2} - \eta). \tag{4.5}$$

When there is a magnetic flux through the wire equal to the odd multiple of the half quantum of the magnetic flux $\eta = n + 0.5$, we get a non-degenerate gapless band for $l = n$

$$H_0 = k_z\sigma_2, \tag{4.6}$$

We assume that R is small enough in a way that there exists a significant energy range, Λ, in which the gapless band does not overlap with other bands (See Fig. 4.1), then we can use this energy band as a building block of the model to realize a Weyl semimetal phase.

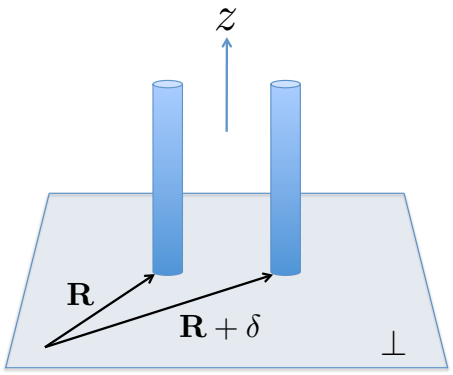

Figure 4.2: Two adjacent parallel wires. The electronic states on one can interact with those on the other via a finite hopping term t.

4.4 Honeycomb lattice of parallel wires

When the distance between two parallel nano-wires is sufficiently small, there would be an overlap between electronic wave-functions and this leads to a hopping between adjacent electronic states of the surface modes. This can also arise from the inter-wire electron-electron interactions in a mean-field approximation. Here we consider a honeycomb arrangement of these nano-wires by considering the nondegenerate gapless modes of these wires that can be achieved by exposing them to a static magnetic field along the wires. We assume that the spin-momentum locking that happen at the surface of topological insulators are in opposite directions for wires in the A and B sublattices. We should point out here that all the so far discovered topological insulators happen to have the same direction for the spin-momentum locking. In theory, one can get a system with an opposite spin-momentum locking by simply changing the sign of the spin-orbit coupling required to get the original topological insulator system. We also assume that the Dirac points for both A and B wires have the same energy, however, in the end we relax this assumption, and we discuss how this is essential in order to get a Weyl semimetal phase. On the other hand, these wires are multi-band systems, therefore, they must be sufficiently thin to allow a significant gap, Λ, in which the gapless band does not overlap with other subbands (see Fig. (4.2)). With these assumptions, and by considering only the non-degenerate lowest lying band in each

wire in the energy range 2Λ (see Fig. 4.1) we can split the Hamiltonian into two parts as follows

$$H = H_0 + H_{\rm t}, \tag{4.7}$$

in which H_0 sums up the gapless nondegenarate modes of each individual wire in a second quantized notation and is given in terms of the Fourier components as

$$H_0 = \int \frac{dk_z}{2\pi} \sum_{\vec{k}_\perp} \Psi^\dagger_{\vec{k}_\perp}(k_z)(\upsilon_0 k_z \tau_3 \sigma_2)\Psi_{\vec{k}_\perp}(k_z), \tag{4.8}$$

where τ_3 is the pauli matrix acting on the sublattice Hilbert space, k_z is the momentum along the wire (Fig. 4.1) and $\vec{k}_\perp$ spans the honeycomb's reciprocal lattice (similar to what one gets for graphene) and $\Psi^\dagger = (\psi^\dagger_{A+}, \psi^\dagger_{A-}, \psi^\dagger_{B+}, \psi^\dagger_{B-})$. The first (last) two components act on the spin space of the wire in the A (B) sub-lattice. $\psi^\dagger_{A/B\alpha}$ creates an electron in the α branch of the A/B wire when it acts on the vacuum state. Using this representation, $H_{\rm t}$ which represents the direct hopping between nearest-neighbour wires, can be written as

$$H_t = \int \frac{dk_z}{2\pi} \sum_{\vec{k}_\perp} \Psi^\dagger_{\vec{k}_\perp}(k_z) \left[\begin{pmatrix} 0 & g(\vec{k}_\perp) \\ g^\star(\vec{k}_\perp) & 0 \end{pmatrix} \otimes \mathbb{1} \right] \Psi_{\vec{k}_\perp}(k_z), \tag{4.9}$$

in which $g(\vec{k}_\perp) = -t\sum_{\delta_i} e^{-i\vec{k}_\perp \cdot \delta_i}$ and δ_i are three vectors that connect a site in honeycomb lattice to the three adjacent points. The energy spectrum of the total Hamiltonian would then be doubly degenerate

$$\varepsilon_\pm(k_z, \vec{k}_\perp) = \pm\sqrt{\upsilon_0^2 k_z^2 + |g(\vec{k}_\perp)|^2}, \tag{4.10}$$

$g(\vec{k}_\perp)$ vanishes at two inequivalent points in the two-dimensional reciprocal lattice, i.e., at $\vec{K}^\pm$ and is linear near these points. Therefore, we get two degenerate three-dimensional Dirac points at $(k_z, \vec{k}_\perp) = (0, \vec{K}^\pm)$. In order to get a topologically protected semimetal phase we need to break time-reversal or inversion symmetry in such a way that it separates the Dirac points. Breaking inversion symmety can be easily realized by relaxing the assumption we had in the beginning, i.e., allow the Dirac point at two sub-lattices to have different energies. By revising H_0 to

account for such an energy difference, V, we get

$$H_0 = \int \frac{dk_z}{2\pi} \sum_{\vec{k}_\perp} \Psi^\dagger_{\vec{k}_\perp}(k_z)(\upsilon_0 k_z \tau_3 \sigma_2 + V\tau_3)\Psi_{\vec{k}_\perp}(k_z), \tag{4.11}$$

In this case the degeneracy is lifted and we have four bands $\varepsilon_{sr}(k_z, \vec{k}_\perp)$ $(s, r = \pm)$ given by

$$\varepsilon_{sr}(k_z, \vec{k}_\perp) = r\sqrt{(\upsilon_0 k_z + sV)^2 + |g(\vec{k}_\perp)|^2}, \tag{4.12}$$

This spectrum has two pairs of Weyl points in the three dimensional BZ at which the bands cross linearly. Each pair consists of two Weyl points centred at $(k_z, \vec{k}_\perp) = (0, \vec{K}^\pm)$. They are separated along k_z axis by $Q = 2V/\upsilon_0$. According to the argument presented in the previous section, these crossings are topologically protected against various local momentum conserving perturbations as long as they are separated in the BZ. It is important to note that although these isolated Weyl nodes are robust against local momentum-conserving perturbations, the peculiarity in the Hall response that is present in a system with only one pair of Weyl nodes with broken time-reversal symmetry does not exist here since the separation of the Weyl points arise from breaking inversion symmetry and the system is time-reversal invariant. The transverse conductivity in the presence of the applied magnetic field along the wires, σ_{xy} is zero [17, 55] since the two pairs contribute oppositely to the Hall conductivity, as they are separated in the opposite way at two valleys considering their chirality. On the other hand, the topological nature of the system shows itself in the nonzero valley Hall current which can be defined as the anti-symmetric combination of the two valley contributions to the charge current in the system

$$\sigma^V_{xy} = \sigma^+_{xy} - \sigma^-_{xy} = \frac{2V}{\upsilon_0}\frac{e^2}{h} \tag{4.13}$$

There is also a possibility of a phase transition to an insulator phase due to the electron-electron interactions. This instability arises in a mean-field treatment of the inter-rod electron-electron interactions. When the wire radius, R, is much smaller than the honeycomb lattice constant, a, the Coulomb interaction between

electrons in adjacent wires can be written as

$$H_{e-e} = U \int_{-L/2}^{L/2} dz \int_{-\infty}^{\infty} du \frac{\hat{n}(\vec{R},z)\hat{n}(\vec{R}+\boldsymbol{\delta},z+u)}{\sqrt{1+(\frac{u}{a})^2}}, \tag{4.14}$$

where $\hat{n}$ is the electronic density operator and $U = e^2/(4\pi\varepsilon a)$. $\vec{R}$, $\boldsymbol{\delta}$ and z have been defined in the Fig. (4.2). In a mean-field treatment of the above term and by considering a Kekule type modulating order parameter with a wave-vector $\vec{G} = \vec{K}^+ - \vec{K}^-$, it is possible to connect the Weyl points separated by $\vec{G}$. This would then open up a gap and the system becomes an insulator. The critical coupling, U_c at which such a phase transition to an insulator phase occurs can be computed for this system. It is a function of the potential difference, V, as well as the hopping strength, t, and is given by

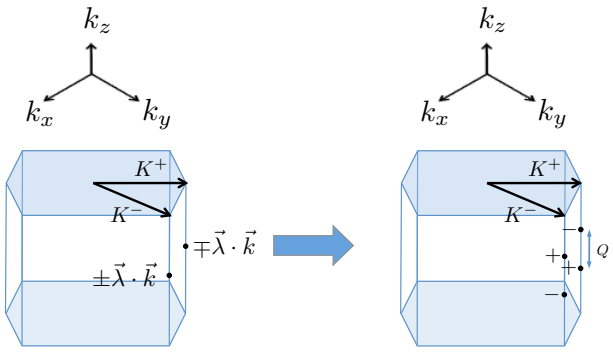

Figure 4.3: The three dimensional BZ before and after separating the Weyl nodes along the k_z. We have two inequivalent pairs of Weyl nodes.

$$U_c = \frac{4\Lambda}{3}\left(1+\ln\frac{\alpha V(\Lambda-V)}{t}\right)^{-1}, \tag{4.15}$$

in which $\alpha = (8/\sqrt{3}\pi)^{1/2}$. This critical coupling would be of the order of the single wire's non-degenerate bandwidth Λ (see Fig. 4.1) whenever the hopping strength is significant enough. For $U < U_c$ the system would remain in the topological semimetal phase and for $U > U_c$ the system would become a three-dimensional version of Kekule insulator which has been discussed previously in two dimensions for graphene [99]. It is possible to make the system stable against such a phase tran-

sition for all ranges of interactions at least in this mean-field channel by introducing a term in the Hamiltonian which separates the two Weyl nodes at each valley ($\vec{K}^+$ and $\vec{K}^-$) by a different amount. In this case the system becomes stable against the perturbation that connects two valleys since all the opposite chirality Weyl pairs would have incommensurate separation in momentum space after addition of such a term. This term can be induced by considering next nearest-neighbour inter-wire hopping of the electronic states. The hopping amplitude is imaginary considering a modulating magnetic flux with a zero net average through each hexagon (see Fig. 4.4). This can be achieved by applying a modulating magnetic field instead of the uniform magnetic field that is required to induce half-quantum magnetic fluxes in the wires. Such a term was first introduced for a honeycomb lattice to realize a quantum Hall phase in a system without a net uniform applied magnetic field [17]. The Hamiltonian for this next-nearest neighbor hopping in momentum space can be written as

$$H' = -t' \int \frac{dk_z}{2\pi} \sum_{\vec{k}_\perp} \Psi^\dagger_{\vec{k}_\perp}(k_z)(\mu(\vec{k}_\perp) + V(\vec{k}_\perp)\tau_3)\Psi_{\vec{k}_\perp}(k_z), \tag{4.16}$$

which is similar to the term which has been introduced in Eq. (4.11) but here the V which separates the Dirac nodes along k_z is a function of the $\vec{k}_\perp$ and takes different values at $\vec{K}^+$ and $\vec{K}^-$. The presence of $\mu(\vec{k}_\perp)$ separates the two pairs in energy since it also depends on $\vec{k}_\perp$ and can take different values at two valleys. In the original Haldane's [17] flux configuration $\mu(\vec{k}_\perp)$ and $V(\vec{k}_\perp)$ are given by

$$V(\vec{k}_\perp) = -2t' \sin\phi \sum_{i=1,2,3} \sin\vec{k}_\perp \cdot \boldsymbol{b}_i, \tag{4.17}$$

and

$$\mu(\vec{k}_\perp) = 2t' \cos\phi \sum_{i=1,2,3} \cos\vec{k}_\perp \cdot \boldsymbol{b}_i, \tag{4.18}$$

$\boldsymbol{b}_i$ and ϕ have been defined in the caption of Fig. 4 and t' is the next-nearest neighbor hopping amplitude.

Therefore, the distance between each pair of Weyl nodes is now an incommensurate wave-vector since the separations of Weyl nodes at two valleys, i.e., $\vec{q}_1 = 2V(\vec{K}^+)\hat{z}/\upsilon_0$ and $\vec{q}_2 = 2V(\vec{K}^-)\hat{z}/\upsilon_0$ are not exactly opposite. This makes

the system stable against charge density perturbations that connect quantum states of two valleys. The axion field is not zero in this case as the separations are not exactly opposite and instead it modulates in space [63].

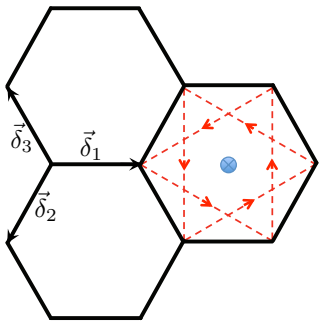

Figure 4.4: The modulations in the magnetic flux with a zero average through each hexagon introduces a complex next nearest neighbor hopping parameter, $t'e^{i\phi}$. The vectors that connect adjacent sites in the same sublattice are $\pm(\vec{b}_1,\vec{b}_2,\vec{b}_3) = \pm(\boldsymbol{\delta}_1-\boldsymbol{\delta}_2,\boldsymbol{\delta}_2-\boldsymbol{\delta}_3,\boldsymbol{\delta}_3-\boldsymbol{\delta}_1)$

Therefore in the presence of the Haldane term, the system breaks the time reversal symmetry and it would have a nontrivial topological response. In this case the transverse conductivity in the presence of the magnetic field in the z direction can be obtained by a summation over the transverse conductivity of the massive two-dimensional Dirac fermions for each k_z [17, 55] . At $\vec{k}_\perp = \vec{K}^+$ and $-q_1 < k_z < q_1$ the sign of the masses of two-dimensional Dirac states are in such a way that they contribute constructively to the transverse Hall conductivity. Similarly, at $\vec{k}_\perp = \vec{K}^-$ and $-q_2 < k_z < q_2$ the transverse Hall conductivity is nonzero. The net σ_{xy} can be obtained, when the chemical potential is inside the gap in the presence of an applied magnetic field in the z direction, by a summation over the contribution of all two-dimensional Dirac fermions labeled by k_z and the valley index, i.e., 1 and 2

$$\sigma_{xy} = \int_{-\Lambda}^{\Lambda} [\nu_1(k_z) - \nu_2(k_z)] \frac{dk_z}{2\pi} \frac{e^2}{h}, \tag{4.19}$$

in which $\nu_1 = \Theta(q_1 - |k_z|)$ and $\Theta(q_2 - |k_z|)$. Using Eq. (4.17) the transverse conductivity becomes

$$\sigma_{xy} = \frac{6\sqrt{3}t' \sin\phi \; e^2}{\pi h}, \tag{4.20}$$

This result highlights the fact that although the momentum conserving perturbations cannot gap out the system, this does not necessarily imply the existence of a topological electromagnetic response in the system and two pairs of Weyl nodes can have cancelling contributions to the electromagnetic response in special cases and therefore σ_{xy} can be zero even when the Weyl nodes are well separated in the BZ which is the case for our model in the absence of the Haldane term. Adding the next nearest hopping and introducing the Haldane term would lead to a nonzero net topological electromagnetic response since two Weyl pairs would now have different separations and therefore their contributions to the transverse conductivity do not sum up to zero.

4.5 Conclusions

To summarize, in order to realize multiple Weyl pairs, we considered a system of parallel nano-wires in the time-reversal invariant topological insulator phase and by breaking inversion and time-reversal symmetry, we found that it is possible to realize a topological semimetal phase with two pairs of Weyl nodes in the three dimensional BZ which are protected against local perturbations that conserve crystal momentum. A nontrivial topological electromagnetic response might arise under certain circumstances when the contributions from two pairs do not exactly cancel each other.

It is important to note that although experimentalists can grow large-scale vertically aligned nano-rods and nanopillars with various arrangements including honeycomb [100–102], realizing a system for which one can observe the robust Weyl energy crossings described in this chapter seems not to be experimentally plausible. One can name a few obstacles on the way of its experimental realization. First, wires are multi-band systems and the two-band model approximation used here requires a significant gap for the other existing subbands in the nano-wires. For the so far discovered topological insulators, the surface Fermi velocity [41], v_0,

is of the order of $10^5 m/s$ ($5 \times 10^5 m/s$ for Bi_2Se_3 [77]), therefore, the wire diameter required ($2R \lesssim 60$nm) to get a significant gap ($\Lambda \gtrsim 10$meV) is still out of the experimentally feasible sub-micron ranges [100–102]. Finally, another challenge to realize such a system is to find two types of topological insulators with opposite spin-momentum lockings. Although in theory it is possible to have systems with opposite chirality, in all the so far discovered topological insulators surface electrons' are directed around the Dirac point have the same handedness. We note that the direction of the spin-momentum locking is a material dependent property and in the theoretical lattice models for the topological insulators in three dimensions, it is possible to change it on the surface by varying physical parameters of the bulk.

Chapter 5

Electromagnetic Response of Weyl Semimetals

5.1 Overview

The anomalous Hall effect we discussed in the previous chapter is known to commonly occur in solids with broken time-reversal symmetry. In the present case of the Weyl semimetal its origin and magnitude can be understood from simple physical arguments [55, 56, 58, 103] applied to the bulk system as well as in the limit of decoupled 2D layers [104]. Understanding the chiral magnetic effect (CME) in a system with non-zero energy shift b_0 presents a far greater challenge. The issue becomes particularly intriguing in the case of a Weyl insulator, illustrated in Fig. 1.7d, which will generically arise due to the exciton instability in the presence of repulsive interactions and nested Fermi surfaces. According to Ref. [63] CME should persist even when the chemical potential resides inside the bulk gap. At the same time, standard arguments from the band theory of solids dictate that filled bands cannot contribute to the electrical current [105]. We remark that using a different regularization scheme for the Weyl fermions Ref. [106] found that CME occurs in the semimetal but is absent in the insulator, while Ref. [104] concluded that it only occurs when $\vec{b}^2 - b_0^2 \geq m_D^2$, where m_D denotes the gap magnitude. Semiclassical considerations [107] on the other hand predict a vanishing electrical current in the Weyl semimetal but non-zero 'valley current' proportional to $\vec{B}$.

CME, if present, could have interesting technological applications, as it constitutes a dissipationless ground state current, controllable by an external field. Disagreements between the various field-theory predictions, however, raise important questions about the existence of CME in Weyl semimetals and insulators. The implied contradiction with one of the basic results of the band theory calls into question whether the results based on the low-energy Dirac-Weyl Hamiltonians are applicable to the real solid with electrons properly regularized on the lattice. In this chapter we undertake to resolve these questions by constructing and analyzing a lattice model of a Weyl medium. Using simple physical arguments and exact numerical diagonalization, we confirm the existence of the anomalous Hall effect as implied by Eqs. (1.22,1.23) when $\vec{b} \neq 0$. We find, using the same model with $b_0 \neq 0$, that CME *does not* occur in either the Weyl semimetal or insulator, in agreement with arguments from the band theory of solids which we review in some detail.

5.2 Model

Our starting point is the standard model describing a 3D TI in the Bi_2Se_3 family [108, 109], regularized on a simple cubic lattice which we introduced in the introduction chapter. If we assume the lattice constant is $a = 1$ then we have

$$\begin{aligned} H_0(\vec{k}) &= 2\lambda\,\sigma_z(s_x \sin k_y - s_y \sin k_x) + 2\lambda_z \sigma_y \sin k_z \\ &+ \sigma_x M_{\vec{k}}, \end{aligned} \tag{5.1}$$

with $\vec{\sigma}$ and $\vec{s}$ the Pauli matrices in orbital and spin space, respectively, and $M_{\vec{k}} = \varepsilon - 2t\sum_\alpha \cos k_\alpha$. For $\lambda, \lambda_z > 0$ and $2t < \varepsilon < 6t$ the above model describes a strong topological insulator with the Z_2 index (1;000). In the following, we shall focus on the vicinity of the phase transition to the trivial phase that occurs at $\varepsilon = 6t$, via the gap closing at $\vec{k} = 0$.

It is easy to see that Weyl semimetal emerges when we add the following perturbation to H_0,

$$H_1(\vec{k}) = b_0 \sigma_y s_z + \vec{b} \cdot (-\sigma_x s_x, \sigma_x s_y, s_z). \tag{5.2}$$

Nonzero b_0 breaks $\mathscr{P}$ but respects $\mathscr{T}$ while $\vec{b}$ has the opposite effect. The two

symmetries are generated as follows, $\mathscr{P}$: $\sigma_x H(\vec{k})\sigma_x = H(-\vec{k})$ and $\mathscr{T}$: $s_y H^*(\vec{k})s_y = H(-\vec{k})$. For simplicity and concreteness we focus on the case $\vec{b} = b_z\hat{z}$, which yields

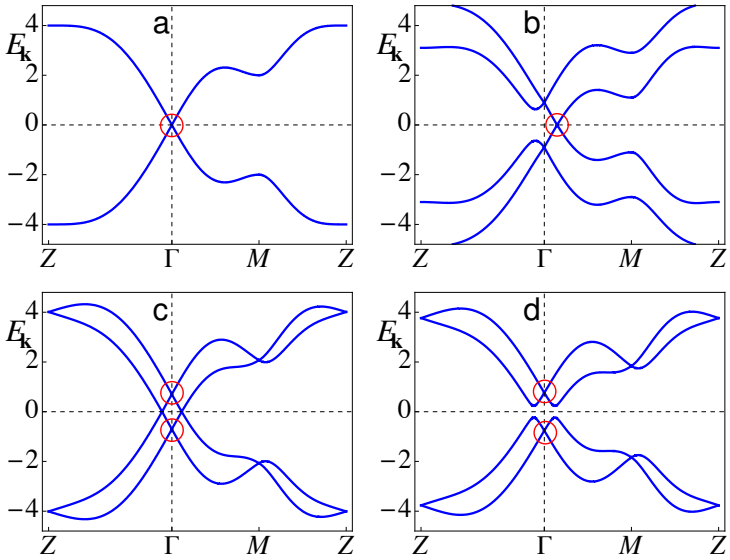

Figure 5.1: The band structure of the Weyl semimetal lattice model, displayed along the path $\vec{k}:\ (\pi,0,\pi)\to(0,0,0)\to(0,0,\pi)\to(\pi,0,\pi)$. a) Doubly degenerate 3D Dirac point when $H_1 = 0$ and $\varepsilon = 6t$. b) Momentum-shifted Weyl point for $b = 0.9$ and $b_0 = 0$. c) Energy-shifted Weyl points for $b_z = 0$ and $b_0 = 0.7$. d) Weyl insulator with $b_z = 0$ and $b_0 = 0.7$ and the exciton gap modeled by taking $\varepsilon = 5.9t$. In all panels we take $\lambda = \lambda_z = 1.0$, $t = 0.5$ and the energy is measured in units of λ. Red circles mark the location of the Dirac/Weyl points.

a pair of Weyl points at $\vec{k} = \pm(b_z/2\lambda_z)\hat{z}$. The band structure of $H = H_0 + H_1$ for various cases of interest is displayed in Fig. 5.1.

5.3 Anomalous Hall current

We now address the anomalous Hall current by directly testing Eq. (1.22). To this end we consider a rectangular sample of the Weyl semimetal with a base of $(L\times L)$ sites in the x-y plane and periodic boundary conditions, infinite along the z-direction. The effect of the applied magnetic field is included via the standard Peierls substitution, $t \to t\exp\left[2\pi i/\Phi_0 \int_i^j \vec{A}\cdot d\boldsymbol{l}\right]$, where $\Phi_0 = hc/e$ is the flux quan-

tum, $\vec{A}$ is the magnetic vector potential and the integral is taken along the straight line between sites $\vec{r}_i$ and $\vec{r}_j$ of the lattice. For $\vec{B} = \hat{z}B(x,y)$ we retain the translational invariance along the z-direction and the Hamiltonian becomes a matrix of size $16L^2$ for each value of k_z. We find the eigenstates $\phi_{n,k_z}(x,y)$ of H by means of exact numerical diagonalization and use these to calculate the charge density

$$\rho(x,y) = e \sum_{n\in \mathrm{occ}} \sum_{k_z} |\phi_{n,k_z}(x,y)|^2. \tag{5.3}$$

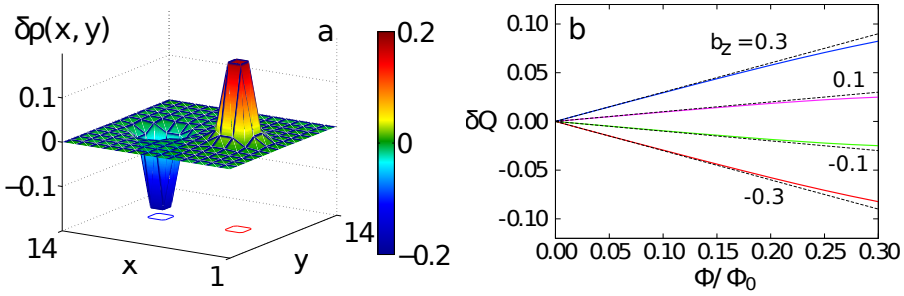

Figure 5.2: a) Charge density $\delta\rho(x,y)$ accumulated in the vicinity of the flux tubes $\Phi = 0.01\Phi_0$ in the Weyl semimetal. b) Total accumulated charge per layer δQ near one of the flux tubes, in units of $e/2\pi$ for indicated values of b_z. Dashed lines represent the expectation based on Eq (5.4). We use $\lambda = \lambda_z = t = 0.5$, $\varepsilon = 3.0$, $L = 14$ and $L_z = 160$ independent values of k_z.

Figure 5.2a displays ρ for the magnetic field configuration $B(x,y) = \Phi[\delta(x - L/4) - \delta(x + L/4)]\delta(y)$, i.e. two flux tubes separated by $L/2$ along the x direction. In accord with Eq. (1.22) charge accumulates near the flux tubes, although $\rho(x,y)$ is somewhat broadened compared to $B(x,y)$. We expect the total accumulated charge per layer δQ to be proportional to the total flux,

$$\delta Q = \frac{e}{\pi}\left(\frac{b_z}{2\lambda_z}\right)\frac{\Phi}{\Phi_0}, \tag{5.4}$$

where we have restored the physical units. Fig. 5.2b shows that this proportionality holds very accurately when the flux through an elementary plaquette is small compared to Φ_0. [When the flux approaches $\Phi_0/2$ we no longer expect Eq. (5.4) to hold

because of the lattice effects.] We have also tested the effect of a non-zero Dirac mass, $m_D = \varepsilon - 6t$, and non-zero b_0 on the anomalous Hall effect. These terms compete with b_z and for $m_D^2 + b_0^2 > b_z^2$ one expects the Hall effect to disappear [104, 106]. This is indeed what we observe in Figs. 5.3a,b. We have performed similar calculations for other field profiles $B(x,y)$ reaching identical conclusions for the anomalous Hall effect.

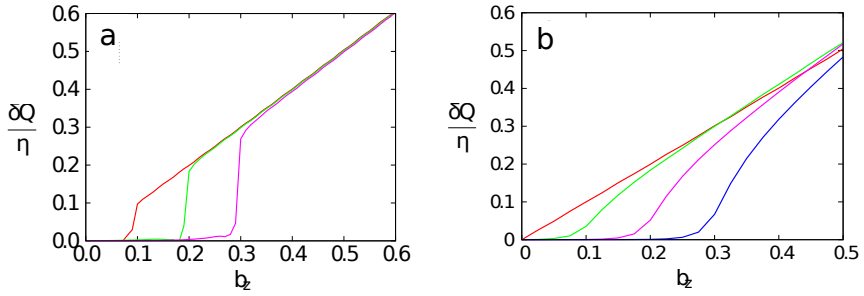

Figure 5.3: Charge accumulations as a function of b_z in the presence of non-zero Dirac mass and b_0. Parameters as above except $b_0 = 0.1, 0.2, 0.3$ in a) and $\varepsilon = 3.0, 2.9, 2.8, 2.7$ for the curves in b) from left to right.

5.4 Can CME exist in an equilibrium state?

We now address the chiral magnetic effect, predicted to occur when $b_0 \neq 0$. We consider the same sample geometry as above, but now with uniform field $\vec{B} = \hat{z}B$. In order to account for possible contribution of the surface states we study systems with both periodic and open boundary conditions along x. To find the current response we introduce a *uniform* vector potential A_z along the z-direction (in addition to A_x and A_y required to encode the applied magnetic field). The second-quantized Hamiltonian then reads

$$\mathscr{H}(A_z) = \sum_{k_z} H^{\alpha\beta}(k_z - eA_z) c^\dagger_{k_z\alpha} c_{k_z\beta}, \tag{5.5}$$

where α, β represent all the site, orbital and spin indices. The current operator is given by

$$\mathscr{J}_z = \frac{\partial \mathscr{H}(A_z)}{\partial A_z}\bigg|_{A_z\to 0} = -e\sum_{k_z} \frac{\partial H^{\alpha\beta}(k_z)}{\partial k_z} c^\dagger_{k_z\alpha} c_{k_z\beta}. \tag{5.6}$$

This leads to the current expectation value

$$J_z = -e\sum_{n,k_z} \left\langle \phi_{n,k_z} \left| \frac{\partial H(k_z)}{\partial k_z} \right| \phi_{n,k_z} \right\rangle n_F[\varepsilon_n(k_z)], \tag{5.7}$$

where n_F indicates the Fermi-Dirac distribution and $\varepsilon_n(k_z)$ the energy eigenvalues of $H(k_z)$. We note that Eq. (5.7) remains valid in the presence of the exciton condensate as long as it is treated in the standard mean field theory.

We have evaluated J_z from Eq. (5.7) for various system sizes, boundary conditions, field strengths and parameter values corresponding to energy- and momentum-shifted Weyl semimetals and insulators. In all cases we found $J_z = 0$ to within the numerical accuracy of our computations, typically 6-8 orders of magnitude smaller than CME expected on the basis of Eq. (1.23).

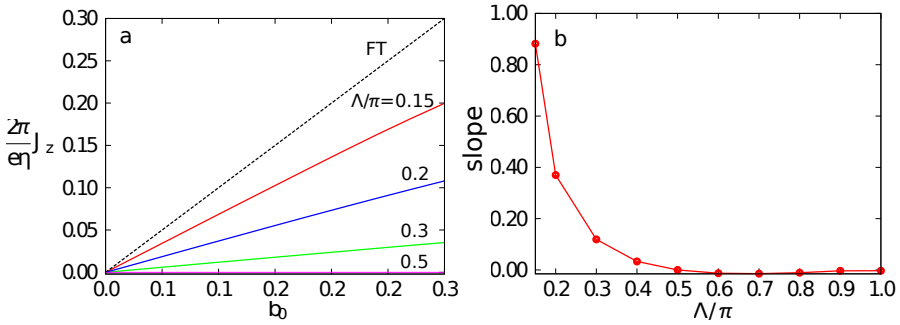

Figure 5.4: a) Chiral current J_z as a function of energy offset b_0 for various values of the momentum cutoff Λ. The dashed line indicates the field theory prediction Eq. (1.23). b) The slope dJ_z/db_0 in units of $e\eta/2\pi$ as a function of cutoff Λ. Slope 1.0 is expected on the basis of Eq. (1.23).

For an insulator, vanishing of J_z comes of course as no surprise. At $T = 0$ and

using the fact that $\partial_{k_z}\langle\phi_{n,k_z}|\phi_{n,k_z}\rangle = 0$ one can rewrite Eq. (5.7) as

$$J_z = -e\sum_{n\in\mathrm{occ}}\int_{\mathrm{BZ}}\frac{dk_z}{2\pi}\frac{\partial\varepsilon_n(k_z)}{\partial k_z}, \tag{5.8}$$

which vanishes owing to the periodicity of $\varepsilon_n(k_z)$ on the Brillouin zone. More generally, for a system at non-zero temperature and when partially filled bands are present we can rewrite Eq. (5.7) as

$$J_z = -e\sum_{n}\int_{\mathrm{BZ}}\frac{dk_z}{2\pi}\frac{\partial\varepsilon_n(k_z)}{\partial k_z}n_F[\varepsilon_n(k_z)], \tag{5.9}$$

where the sum over n extends over all bands. By transforming the k_z-integral in Eq. (5.9) into an integral over the energy it is easy to see that it identically vanishes for any continuous energy dispersion $\varepsilon_n(k_z)$ that is periodic on the Brillouin zone and for any distribution function that only depends on energy. This reflects the well-known fact that one must establish a non-equilibrium distribution of electrons to drive current in a metal, e.g. by applying an electric field.

5.5 Conclusions

Given these arguments we conclude that, as a matter of principle, CME cannot occur in a crystalline solid, at least when interactions are unimportant and the description within the independent electron approximation remains valid. There are several notable cases when filled bands *do* contribute currents. A superconductor can be thought of as an insulator for Bogoliubov quasiparticles and yet it supports a supercurrent. This occurs because Bogoliubov quasiparticles, being coherent superpositions of electrons and holes, do not carry a definite charge and consequently the current cannot be expressed through Eq. (5.7). In quantum Hall insulators non-zero σ_{xy} also implies non-vanishing current. In the standard Hall bar geometry, used in transport measurements, it is well known that the physical current is carried by the gapless edge modes, not through the gapped bulk. In the Thouless charge pump geometry the current indeed flows through the insulating bulk but this requires a time-dependent Hamiltonian (the magnetic flux through the cylinder is time dependent). Our considerations leading to Eq. (5.7) are only valid for

time-independent Hamiltonians. Finally, there are known cases [110] when the transition from Eq. (5.7) to (5.8) fails because the Hamiltonian is not self-adjoint on the space of functions that includes derivatives of ϕ. This can happen when the Hamiltonian is a differential operator but in our case $H(k_z)$ is a finite-size hermitian matrix with a smooth dependence on k_z, which precludes any such exotic possibility. In any case, our numerical calculations addressed directly Eq. (5.7) so self-adjointness cannot possibly be an issue.

Chapter 6

Self Organized Topological phase with Majorana Fermions

6.1 Overview

Topological phases, quite generally, are difficult to come by. They either occur under rather extreme conditions (e.g. the quantum Hall liquids [9], which require high sample purity, strong magnetic fields and low temperatures) or demand fine tuning of system parameters, as in the majority of known topological insulators [78, 108, 111]. Many perfectly sensible topological phases, such as the Weyl semimetals [58] and topological superconductors [70, 108], remain experimentally undiscovered.

The paucity of easily accessible, stable topological materials has been in a large part responsible for the relatively slow progress towards the adoption of topological phases in the mainstream technological applications. A question that naturally arises is the following: Is there a fundamental principle behind this "topological resistance"? Although unable to give a general answer to this question, we provide in this chapter a specific counterexample to this conjectured phenomenon of topological resistance. We consider a simple model system which, as we demonstrate, *wants* to be topological in a precisely defined sense. The key to this "topofilia" is the existence in the system of a dynamical parameter that adjusts itself in response to changing external conditions, so that the system self-tunes into the topological

phase.

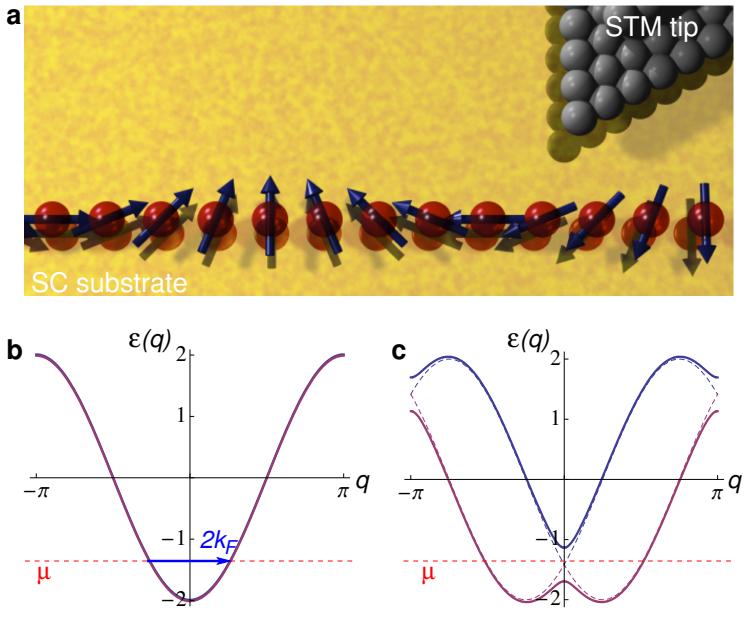

Figure 6.1: a) Schematic depiction of the system with the red spheres representing the adatoms and blue arrows showing their magnetic moments arranged in a spiral. b) Two spin-degenerate branches of the normal-state spectrum of the system in the absence of magnetic moments modelled by the nearest-neighbour tight-binding model Eq. (6.1). c) With the magnetic moments, the two branches shift in momentum by $\pm G$ and the gap JS opens at $q = 0, \pi$. Dashed lines show the shifted spectral branches indicated in panel (b) with no gap for comparison.

The specific model system we consider is depicted in Fig. 6.1a and consists of a chain of magnetic atoms, such as Co, Mn or Fe, deposited on the atomically flat surface of an ordinary *s*-wave superconductor. We note that scanning tunnelling microscopy (STM) techniques now enable fairly routine assembly of such and even much more complicated nanostructures [112, 113].

It has been pointed out previously [1, 114, 115] that if the magnetic moments in the chain exhibit a spiral order then the electrons in the chain can form a 1D topological superconductor (TSC) with Majorana zero modes localized at its ends

[69]. For a given chemical potential μ, however, the spiral must have the correct pitch in order to support the topological phase. This connection is illustrated in Fig. 6.1b,c and will be discussed in more detail below. Exactly how the pitch of the spiral depends on the system parameters and its thermodynamic stability are two key issues that have not been previously discussed. In this Letter we show that, remarkably, under generic conditions the pitch of the spiral that minimizes the free energy of the system coincides with the one required to establish the topological phase.

The physics behind the self-organization phenomenon outlined above is easy to understand and is similar to that leading to the spiral ordering of nuclear spins proposed to occur in 1D conducting wires [116, 117] and 2D electron gases [118]. Some experimental evidence for such an ordering has been reported [119, 120]. If we for a moment neglect the superconducting order and assume a weak coupling of the adatoms to the substrate then the electrons in the chain can be thought of as forming a 1D metal. The natural wavevector for the spiral ordering in such a 1D metal is $G = 2k_F$ where k_F denotes its Fermi momentum. This is because the static spin susceptibility $\chi_0(q)$ of a 1D metal has a divergence at $q = 2k_F$. Electron scattering off of such a magnetic spiral results in opening of a gap in the electron excitation spectrum but only for one of the two spin-degenerate bands [116, 117]. In the end, we are left with a single, non-degenerate Fermi crossing at $\pm 2k_F$, illustrated in Fig. 6.1c. According to the Kitaev criterion [69] this is exactly the condition necessary for a 1D TSC to emerge. In the following we will show that this reasoning remains valid when we include superconductivity from the outset and when we describe the chain by a tight-binding model appropriate for a discrete atomic chain.

6.2 Model

We begin by studying the simplest model of tight-binding electrons coupled to magnetic moments $\vec{S}_i$ described by the Hamiltonian

$$\mathscr{H}_0 = -\sum_{ij\sigma} t_{ij} c^\dagger_{i\sigma} c_{j\sigma} - \mu \sum_{i\sigma} c^\dagger_{i\sigma} c_{i\sigma} + J \sum_i \vec{S}_i \cdot (c^\dagger_{i\sigma} \boldsymbol{\sigma}_{\sigma\sigma'} c_{i\sigma'}) \tag{6.1}$$

Here $c^\dagger_{j\sigma}$ creates an electron with spin σ on site j, J stands for the exchange coupling constant and $\boldsymbol{\sigma} = (\sigma^x, \sigma^y, \sigma^z)$ is the vector of Pauli spin matrices. We assume that the substrate degrees of freedom have been integrated out, leading to a superconducting order Δ in the chain described by

$$\mathscr{H} = \mathscr{H}_0 + \sum_j (\Delta c^\dagger_{j\uparrow} c^\dagger_{j\downarrow} + \text{h.c.}). \tag{6.2}$$

We consider a co-planar helical arrangement of atomic spins as indicated in Fig. 6.1a,

$$\vec{S}_j = S[\cos(Gx_j), \sin(Gx_j), 0] \tag{6.3}$$

where G is the corresponding wavevector and the chain is assumed to lie along the x-axis. We note that Hamiltonian (6.2) is invariant under the simultaneous global SU(2) rotation of the electron and atomic spins so the discussion below in fact applies to any co-planar spiral.

To find the spectrum of excitations, it is useful to perform a spin-dependent gauge transformation [1],

$$c_{j\uparrow} \to c_{j\uparrow} e^{\frac{i}{2}Gx_j}, \quad c_{j\downarrow} \to c_{j\downarrow} e^{-\frac{i}{2}Gx_j}, \tag{6.4}$$

upon which the Hamiltonian becomes translationally invariant and can be written in the momentum space as

$$\begin{aligned} \mathscr{H} &= \sum_q \big[\xi(q) c^\dagger_{q\sigma} c_{q\sigma} + b(q) c^\dagger_{q\sigma} \sigma^z_{\sigma\sigma'} c_{q\sigma'} \\ &+ JS c^\dagger_{q\sigma} \sigma^x_{\sigma\sigma'} c_{q\sigma'} + (\Delta c^\dagger_{q\uparrow} c^\dagger_{-q\downarrow} + \text{h.c.})\big]. \end{aligned} \tag{6.5}$$

In the above $\xi(q) = \frac{1}{2}[\varepsilon_0(q - G/2) + \varepsilon_0(q + G/2)] - \mu$, and $b(q) = \frac{1}{2}[\varepsilon_0(q - G/2) - \varepsilon_0(q + G/2)]$ with $\varepsilon_0(q) = -\sum_j t_{0j} e^{iqx_j}$ the normal-state dispersion in the absence of the exchange coupling. We note that the Hamiltonian (6.5) is essentially a lattice version of the model semiconductor wire studied in Refs. [72, 121] with $b(q)$ playing the role of the spin-orbit coupling and JS standing for the Zeeman field. Its

normal state spectrum is given by

$$\varepsilon(q) = \xi(q) \pm \sqrt{b(q)^2 + J^2 S^2}, \tag{6.6}$$

and is displayed in Fig. 6.1c for the case of nearest-neighbour hopping with $\varepsilon_0(q) = -2t\cos q$.

If viewed as a rigid band structure then, according to the Kitaev criterion [69], the chain will support topological superconductivity when there is an odd number of Fermi crossings in the right half of the Brillouin zone. This requires μ such that $|\mu \pm 2t\cos(G/2)| < JS$. However, in the SU(2) symmetric model under consideration, G is a dynamical parameter that will assume a value that minimizes the system free energy. Taking $\vec{S}_i$ to be classical magnetic moments and working at $T = 0$, we thus proceed to minimize the ground state energy of the electrons $E_g(G)$ for a given value of μ and Δ. The result of this procedure is shown in Fig. 6.2a and confirms that at minimum $G \approx 2k_F$, as suggested by the general arguments advanced above. More importantly, for almost all relevant values of μ and Δ the self-consistently determined spiral pitch G is precisely the one required for the formation of the topological phase. This fails only close to the half filling ($\mu = 0$) where $G = \pi$ indicates an antiferromagnetic ordering. In this case the symmetry of the band structure prohibits an odd number of Fermi crossings, so the system must be in the trivial phase. Also, it is clear that no value of G can bring about the TSC phase when μ lies outside of the tight-binding band and the system is an insulator. The resulting topological phase diagram is displayed in Fig. 6.2b.

These results indicate that, as we argued on general grounds, the pitch of the magnetic spiral self-tunes into the topological phase for nearly all values of the chemical potential μ for which such a tuning is possible. The emergence of Majorana zero modes at the two ends of such a topological wire [69, 72, 121] and their significance for the quantum information processing have been amply discussed in the recent literature [68, 122, 123].

We now address the adatom coupling to the substrate in greater detail. We consider a more complete Hamiltonian $\mathscr{H} = \mathscr{H}_0 + \mathscr{H}_{\rm SC} + \mathscr{H}_{cd}$, where $\mathscr{H}_0$ is defined

in Eq. (6.1), while

$$\mathscr{H}_{\rm SC} = \sum_{\vec{k}} \left[\xi_0(\vec{k}) d^\dagger_{\vec{k}\sigma} d_{\vec{k}\sigma} + (\Delta_0 d^\dagger_{\vec{k}\uparrow} d^\dagger_{-\vec{k}\downarrow} + \text{h.c.}) \right] \tag{6.7}$$

describes the SC substrate with electron operators $d^\dagger_{\vec{k}\sigma}$. The substrate is characterized by a three-dimensional normal-state dispersion $\xi_0(\vec{k}) = k^2/2m - \varepsilon_F$ and the bulk gap amplitude Δ_0. The coupling is effected through

$$\mathscr{H}_{cd} = -r \sum_{j\sigma} (d^\dagger_{j\sigma} c_{j\sigma} + \text{h.c.}), \tag{6.8}$$

where $d_{j\sigma} = \frac{1}{\sqrt{N}} \sum_{\vec{k}} e^{-i\vec{k}\cdot\vec{R}_j} d_{\vec{k}\sigma}$, N is the number of adatoms in the chain and $\vec{R}_j$ denotes their positions.

We now wish to integrate out the substrate degrees of freedom and ascertain their effect on the magnetic chain. Since the Hamiltonian $\mathscr{H}$ is non-interacting this procedure can be performed exactly. As outlined in the Appendix of Ref. [68], a simple result obtains in the limit of the substrate bandwidth much larger than the chain bandwidth $4t$, which we expect to generically be the case. In this limit the Green's function of the chain reads

$$\mathscr{G}^{-1}_{\rm eff}(i\omega_n, q) = \mathscr{G}^{-1}_0(i\omega_n, q) - \pi\rho_0 r^2 \frac{i\omega_n - \tau^x \Delta_0}{\sqrt{\omega_n^2 + \Delta_0^2}}, \tag{6.9}$$

where $\omega_n = (2n+1)\pi T$ is the Matsubara frequency, $\rho_0 = ma^2/2\pi\hbar^2$ is the substrate normal density of states projected onto the chain, (with a being the atom spacing) and

$$\mathscr{G}^{-1}_0(i\omega_n, q) = -i\omega_n + \tau^z [\xi(q) + \sigma^z b(q)] + \sigma^x JS \tag{6.10}$$

the bare chain Green's function. The above Green's functions are 4×4 matrices in the combined spin and particle-hole (Nambu) space, the latter represented by a vector of Pauli matrices $\boldsymbol{\tau}$. In the low-frequency limit $\omega \ll \Delta_0$, relevant to the physics close to the Fermi energy, Eq. (6.9) implies two effects. First, the bare chain parameters t, μ and J are reduced by a factor of $\Delta_0/(\Delta_0 + \pi r^2 \rho_0)$. Second, a SC gap $\Delta = \pi r^2 \rho_0 \Delta_0/(\Delta_0 + \pi r^2 \rho_0)$ is induced in the chain. In the limit of a weak

chain-substrate coupling, $r^2 \ll \Delta_0/\rho_0$, the latter is seen to become $\Delta \simeq \pi r^2 \rho_0$, independent of the substrate gap Δ_0.

In order to visualize the above effects we display in Fig. 6.3 the relevant spectral function, defined as

$$A_{\text{eff}}(\omega, q) = -\frac{1}{2\pi} \text{Im Tr}[(1+\tau^z)\mathscr{G}_{\text{eff}}(\omega + i\delta, q)] \tag{6.11}$$

where δ represents a positive infinitesimal. The figure clearly shows how the bands self-consistently adjust to the changing chemical potential as well as the expected topological phase transitions taking place between the trivial and the TSC phases.

Our results thus far relied on the mean field theory and ignored interactions beyond those giving rise to superconductivity. There are several effects that can in principle destabilize the topological state found above but we now argue that the latter remains stable against both interactions and fluctuations. First, one may worry that the adatom magnetic moments would be screened by the Kondo effect at temperatures $T < T_K = \varepsilon_F e^{-1/\rho(\varepsilon_F)J}$, where $\rho(\varepsilon_F)$ is the density of states in the substrate at the Fermi level. For a normal metal, T_K can indeed be sizeable – tens of Kelvins – and the ground state is then non-magnetic [124]. In the presence of superconductivity, however, $\rho(\varepsilon_F) = 0$ and a more elaborate treatment of the Kondo problem in the presence of a gap shows that T_K is much reduced [125], possibly to zero when J is sufficiently small. Thus, generically, we expect the system to avoid the Kondo fixed point and remain magnetic at most experimentally relevant temperatures. Electron-electron interactions in the wire are additionally expected to enhance the magnetic gap [116, 118] compared to its non-interacting value JS, which will ultimately further improve the stability of the topological phase.

Second, one must consider thermal and quantum fluctuations which will tend to destroy any ordering present in a 1D wire. Since the SC order in the wire is phase-locked to the substrate we may ignore its fluctuations. However, fluctuations in the magnetic spiral order must be considered. In a realistic system spin-orbit coupling will induce a Dzyaloshinsky-Moriya interaction of the form $\mathbf{D}_{ij} \cdot (\vec{S}_i \times \vec{S}_j)$ in the effective spin Hamiltonian. The latter breaks the SU(2) spin symmetry and pins the spiral order so that the spins rotate in the direction perpendicular to $\mathbf{D}$. The

remaining low-energy modes of such a spiral are magnons. The relevant spin-wave analysis and the origin of the DM interaction are outlined in the next section. We find a single linearly dispersing gapless magnon $\omega_q = c|q|$ which will reduce the classical ordered moment according to

$$\langle S^x \rangle \simeq S - a \int_{\mathrm{BZ}} \frac{dq}{2\pi} \frac{1}{e^{\beta\hbar\omega_q} - 1}. \tag{6.12}$$

For an infinite wire the integral diverges logarithmically at long wavelengths, signaling the expected loss of the magnetic order in the thermodynamic limit. We are, however, interested in a wire of finite length L where the divergence is cut off at $q \sim \pi/L$. A crude estimate of the transition temperature in this case obtains by assuming $\beta\hbar\omega_q \ll 1$ over the Brillouin zone and setting $\langle S^x \rangle = 0$ in Eq. (6.12). This gives

$$k_B T^* \approx \frac{\pi S}{\ln N} \frac{\hbar c}{a}, \tag{6.13}$$

with $N = L/a$ the number of adatoms in the chain. For $N = 100$, $S = 5/2$ and typical model parameters $t = 10$meV, $J = 5$meV and μ appropriate for the topological phase we find T^* of tens of Kelvins as it is discussed in the next section. Due to the $\ln N$ factor T^* is only weakly dependent on the chain length.

6.3 Stability analysis of the spiral ground state

In this section we supply some of the technical details pertaining to the stability analysis of the spiral ground state. In this analysis it is useful to consider a spin-only effective theory that arises upon integrating out the electron degrees of freedom in the relevant Hamiltonian given e.g. by Eq. (6.1) in the previous section. More generally, we start from a Hamiltonian of the form

$$\mathscr{H} = \mathscr{H}_0 + J \sum_i \vec{S}_i \cdot (c^\dagger_{i\sigma} \boldsymbol{\sigma}_{\sigma\sigma'} c_{i\sigma'}) \tag{6.14}$$

where $\mathscr{H}_0$ describes the electrons in the absence of the exchange coupling to the magnetic moments $\vec{S}_i$. Assuming translational invariance we can integrate out the

electrons to obtain the effective spin-only Hamiltonian

$$\mathscr{H}_S = \frac{J^2}{2}\sum_q \chi^{\alpha\beta}(q) S^\alpha_q S^\beta_{-q} \tag{6.15}$$

where

$$\chi^{\alpha\beta}(q) = i\int_0^\infty dt \sum_{i,j} e^{-iq(x_i-x_j)}\langle [s^\alpha_i(t), s^\beta_j(0)]\rangle_0 \tag{6.16}$$

is the static spin susceptibility evaluated in the ensemble specified by $\mathscr{H}_0$ and $\vec{s}_i = c^\dagger_{i\sigma}\boldsymbol{\sigma}_{\sigma\sigma'}c_{i\sigma'}$. Given the electron Green's function $\mathscr{G}_0(i\omega_n,k)$ the spin susceptibility can be evaluated by analytical continuation of the Matsubara frequency susceptibility

$$\chi^{\alpha\beta}(i\nu_m,q) = k_B T\sum_{n,k}\mathrm{Tr}[\mathscr{G}_0(i\omega_n,k)\sigma^\alpha \mathscr{G}_0(i\omega_n-\nu_m,k-q)\sigma^\beta] \tag{6.17}$$

in the limit $\nu \to 0$.

In the simplest case of noninteracting electrons with $\mathscr{H}_0 = \sum_k(\hbar^2k^2/2m)c^\dagger_{k\sigma}c_{k\sigma}$ the $T=0$ susceptibility becomes $\chi^{\alpha\beta}(q) = \delta^{\alpha\beta}\chi_0(q)$ with one-dimensional Lindhard function

$$\chi_0(q) = \frac{L}{\pi}\frac{2m}{\hbar^2 q}\ln\left|\frac{2k_F-q}{2k_F+q}\right|. \tag{6.18}$$

The latter exhibits singularities at $q = \pm 2k_F$, as already noted in the main text. These peaks constitute the root cause behind the emergent spiral.

For the SU(2) symmetric model considered thus far the helical ordering can occur in any plane leading to a continuous ground-state degeneracy parametrized by a unit vector $\hat{\boldsymbol{n}}$ perpendicular to that plane. One possible mechanism that will break the global SU(2) spin symmetry and select a specific spiral plane is the Dzyaloshinski-Moriya (DM) interaction. It takes the form $\sum_{ij}\mathbf{D}_{ij}\cdot(\vec{S}_i\times\vec{S}_j)$ and arises in the presence of the spin-orbit coupling (SOC) when spatial inversion symmetry is broken, as is the case in our system of adatoms placed on a substrate. If we assume that the adatom chain lies along the x direction while the surface normal is along y then a Rashba-type SOC of the form $\lambda k\sigma^z$ is permitted in $\mathscr{H}_0$ with λ parametrizing the SOC strength. DM interaction arises in this situation because as a result of SOC Eq. (6.17) yields antisymmetric components of the susceptibility

$\chi^{\alpha\beta} \sim \mathrm{Tr}(\sigma^z\sigma^\alpha\sigma^\beta) = 2i\varepsilon^{3\alpha\beta}$. The D-vector points along the z direction and takes the form $\mathbf{D}_{ij} = D(\hat{\mathbf{y}} \times \vec{r}_{ij})$ where $\vec{r}_{ij}$ is a vector connecting sites i and j. To estimate the magnitude D we continue modelling our wire by the continuum free electron model with Rashba **SOC!** (**SOC!**), and evaluate Eq. (6.17) to obtain

$$\chi^{xy}(q) = \frac{1}{2}[\chi_0(q+Q_\lambda) - \chi_0(q-Q_\lambda)] \tag{6.19}$$

with $Q_\lambda = \lambda m/\hbar^2$ the characteristic SOC wave-vector. At long wavelengths, assuming $Q_\lambda \ll 2k_F$, one can expand

$$\chi^{xy}(q) \simeq \frac{L}{12\pi}\frac{qQ_\lambda}{\varepsilon_F k_F}. \tag{6.20}$$

This leads to an estimate $D \approx \frac{1}{12}\Lambda(J/\varepsilon_F)^2$ with $\Lambda = \lambda/a$ the SOC strength per adatom site. Taking $J/\varepsilon_F \approx 1$ and Λ of few meV we obtain D of the order of few degrees Kelvin. We expect the same result to qualitatively describe the tight-binding electrons when the chemical potential lies near the bottom of the band.

The DM interaction discussed above gives rise to a gap $\Delta_{\mathrm{DM}} \simeq DS$ towards the out-of-plane spin excitations and for a large adatom spin, e.g. $S = \frac{5}{2}$, to a characteristic temperature $T_{\mathrm{DM}} \simeq 10\mathrm{K}$ below which these can be ignored. We emphasize that the DM interaction represents only one possible mechanism by which the spiral plane can be pinned. Another possibility arises from an easy-plane anisotropy which is also allowed by symmetry.

We now address the effect of the remaining spin-wave fluctuations around the helical ground state pinned to a given plane. These remain gapless as $q \to 0$ and for a chain of a finite length L will destroy the helical order above the crossover temperature T^* given in Eq. (13) of the main text. Our goal here is to determine the spin-wave velocity c and estimate T^*. To this end we repeat the analysis given in Eqs. (1-6) but now including small adatom spin fluctuations $\delta\vec{S}_j$. We thus write

$$\vec{S}_j = R_j(S\hat{\mathbf{x}} + \delta\vec{S}_j) \tag{6.21}$$

where

$$R_j = \begin{pmatrix} \cos(Gx_j) & \sin(Gx_j) & 0 \\ -\sin(Gx_j) & \cos(Gx_j) & 0 \\ 0 & 0 & 1 \end{pmatrix} \tag{6.22}$$

is the rotation matrix. After the gauge transformation (4) we obtain

$$\mathscr{H} = \mathscr{H}_0 + J\sum_j \delta\vec{S}_i \cdot (c^\dagger_{j\sigma}\boldsymbol{\sigma}_{\sigma\sigma'}c_{j\sigma'}) \tag{6.23}$$

with $\mathscr{H}_0$ given by Eq. (5). We now pass to the bosonic magnon variables using the standard Holstein-Primakoff transformation for spin along the $\hat{\boldsymbol{x}}$ direction $S^x_j = S - a^\dagger_j a_j$ and $S^+_j = S^z_j + iS^y_j = \sqrt{2S}(1 - a^\dagger_j a_j/2S)^{1/2}a_j$. In the linear spin-wave theory we can neglect terms $O(1/S)$ and the Hamiltonian (6.23) becomes

$$\mathscr{H} = \mathscr{H}_0 + J\sum_j \left[-a^\dagger_j a_j s^x_j + \sqrt{S/2}(a_j s^-_j + a^\dagger_j s^+_j)\right], \tag{6.24}$$

where $s^\pm_j = s^z_j \pm is^y_j$. Once again we may integrate out the electrons to obtain the effective magnon Hamiltonian which takes the following form

$$\mathscr{H}_{\rm mag} = \sum_q \left[\Omega_q a^\dagger_q a_q + \frac{1}{2}\eta_q(a^\dagger_q a^\dagger_{-q} + a_q a_{-q})\right], \tag{6.25}$$

with $\Omega_q = J\langle -s^x\rangle_0 + 2J^2\chi^{+-}(q)$ and $\eta_q = 2J^2\chi^{++}(q)$. Here $\chi^{\alpha\beta}(q)$ is the static spin susceptibility tensor (6.16) evaluated for the Hamiltonian $\mathscr{H}_0$. The magnon spectrum follows from diagonalizing $\mathscr{H}_{\rm mag}$ via the Bogoliubov canonical transformation and reads

$$\omega_q = \sqrt{\Omega_q^2 - \eta_q^2}. \tag{6.26}$$

We have evaluated the relevant components of $\chi^{\alpha\beta}(q)$ for $\mathscr{H}_0$ given by Eq. (5) numerically; some representative results are displayed in Fig. 6.4. For simplicity and concreteness we focus here on the non-superconducting state. For $J = 0$ the susceptibility shows divergences at $q = 0, \pm 2G$ inherited from the free-electron Lindhard function (6.18). For $J > 0$ the divergence at $q = 0$ is quenched, reflecting the gap that has opened in the electron excitation spectrum at $k = 0$ (see Fig. 6.1c). The remaining peaks at $q = \pm 2G$ reflect the fact that a state exists with the

opposite helicity (i.e. described by a rotation matrix R_j with G replaced by $-G$) which is also a classical ground state of the system. This second ground state, being in a different topological sector, is separated from our chosen ground state by a large energy barrier and will be ignored in our subsequent analysis, which by construction focuses on small fluctuations in the vicinity of a single classical ground state.

To study the long-wavelength magnons we note that it is possible to evaluate the spin susceptibility in the vicinity of $q = 0$ analytically. The dominant contribution to the momentum summation in Eq. (6.16) here comes from the vicinity of $k = 0$ where the Hamiltonian (5) can be well approximated by a 1D Dirac theory with mass $m_D = JS$ and electron velocity v_F. To the leading order in q the susceptibility evaluates to $\chi^{\alpha\beta}(q) = \alpha\beta\chi_q$ with $\alpha, \beta = \pm$,

$$\chi_q = \frac{aS}{4\pi v_F}\left[\ln\left(1+\frac{\Theta^2}{J^2S^2}\right) - 1 - \frac{v_F^2 q^2}{2J^2S^2}\right], \tag{6.27}$$

and $\Theta \sim \varepsilon_F$ representing the high-energy cutoff for the Dirac theory. In addition we find $\langle -s^x \rangle_0 = 4J\chi_0$ as must be the case to satisfy the Goldstone theorem which requires a gapless mode as $q \to 0$. Substituting these results into Eq. (6.26) yields the magnon spectrum

$$\omega_q = 4J^2\sqrt{\chi_0(\chi_0 - \chi_q)} = cq \tag{6.28}$$

with the spin-wave velocity

$$c = \frac{Ja}{\pi\hbar}K, \tag{6.29}$$

and $K = \sqrt{\frac{1}{2}[\ln(1+\Theta^2/J^2S^2) - 1]}$ a dimensionless constant close to unity. Taking, as an example, $\Theta/JS = 10$ we have $K = 1.34$ and for $N = 100$ and $S = \frac{5}{2}$ Eq. (13) yields $k_B T^* = 0.728J$. For $J = 5$meV the crossover temperature $T^* \simeq 36$K. The above analysis suggests that the classical spiral ground state is reasonably stable and the more likely limiting factor in a realistic system will be the substrate superconducting critical temparature T_c which is below ~ 10K for most simple metals.

In closing several remarks are in order. In our calculation of the spin suscepti-

bility we have neglected the SC gap Δ and worked at $T = 0$. Inclusion of the former leads to changes in $\chi^{\alpha\beta}(q)$ near $q = 0$ which are small as long as $\Delta < JS$, which is a necessary condition for the topological phase. Such small changes do not significantly alter our conclusions regarding the spiral stability. Similarly, working at non-zero temperature has a negligible effect on the electron spin susceptibility as long as $k_B T \ll JS$ because the electrons are gapped. Since we found both $k_B T_{\mathrm{DM}}$ and $k_B T^*$ to be parametrically smaller than JS, our analysis is self-consistent in this regard. Finally, one may ask if other spin states might compete with the assumed spiral ground state. We have tried several possibilities, including a spiral with a constant out-of-plane spin component, but all were higher in energy.

6.4 Conclusions

Our results provide strong support for the notion of a self-organized topological state. Magnetic moments of atoms assembled into a wire geometry on a superconducting surface are indeed found to self-organize into a topological state under a wide range of experimentally relevant conditions. The emergent Majorana fermions can be probed spectroscopically by the same STM employed in building the structures and will show zero-bias peaks localized near the wire ends. The system can be tuned out of the topological phase by applying magnetic field $\vec{B}$ which, when strong enough, will destroy the helical order by polarizing the adatom magnetic moments. An attractive feature of this setup is the possibility of assembling more complex structures, such as T-junctions and wire networks that will aid future efforts to exchange and braid Majorana Fermions with the goal of probing their non-Abelian statistics [126]. We also note that the general self-organization principle described above should apply to other 1D structures, most notably quantum wires with nuclear spins considered in Ref. [116]; however the energy scales are expected to be much smaller due to the inherent weakness of the nuclear magnetism.

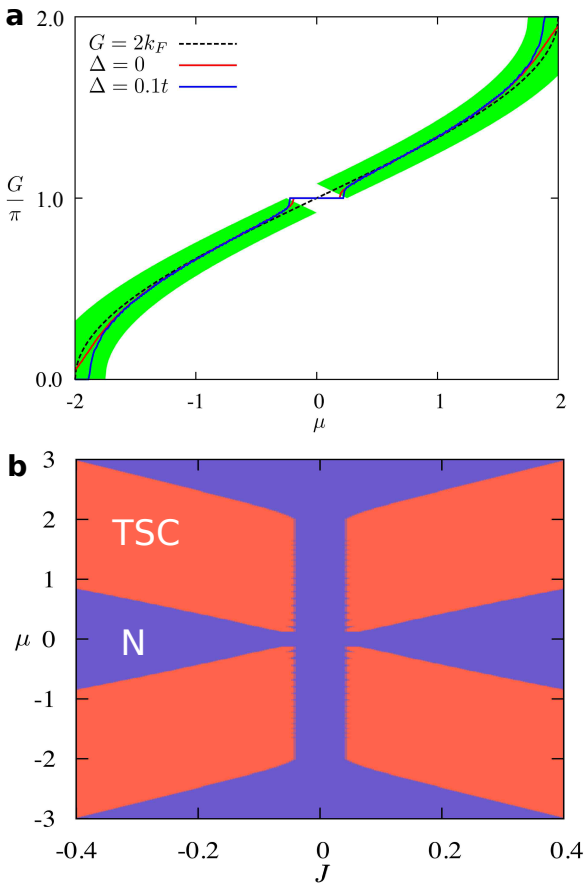

Figure 6.2: Panel **a** shows the spiral wavevector G that minimizes the system ground state energy $E_g(G)$ as a function of μ, the latter in units of t. The parameters are $S = 5/2$, $J = 0.1t$ and $\Delta = 0$ (red), $\Delta = 0.1t$ (blue). The dashed line represents $G = 2k_F$ while the green band shows the region in which G must lie for the system to be topological for a given μ. Panel **b** shows the topological phase diagram in the μ–J plane, both in units of t, for $\Delta = 0.1t$. To distinguish the two phases we have calculated the Majorana number $\mathscr{M}$ as defined in Ref. [69]. Topological phase (TSC) is indicated when $\mathscr{M} = -1$ while $\mathscr{M} = +1$ indicates the topologically trivial phase (N).

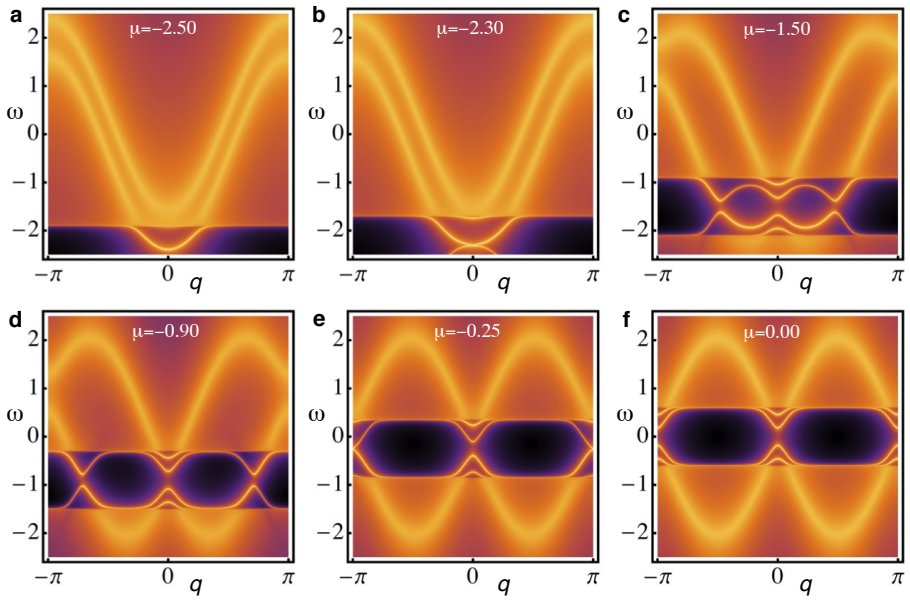

Figure 6.3: $A_{\text{eff}}(\omega, q)$ defined in Eq. (6.11) is represented as a density plot for several representative values of the chemical potential μ, with the appropriate self-consistently determined spiral pitch G shown in Fig. 6.2a. In panel **a** μ is below the bottom edge of the chain band and the system is in the trivial phase. When μ reaches the band edge a topological phase transition occurs through a gap closing shown in panel **b**. Further increase of μ puts the system into the topological phase illustrated in **c**, **d** until the gap closes again near half filling **e** placing the system back into the trivial phase **f**. A similar sequence of phases occurs for positive values of μ for which the spectral function can be obtained by simply flipping the sign of the frequency ω. The dark band around the chemical potential reflects the bulk SC gap. In all panels frequency ω is in units of t while $JS = 0.4t$, $\Delta_0 = 0.6t$, $\rho_0 r^2 = 0.05t$ and $\delta = 0.002t$ is used to give a finite width to the spectral peaks.

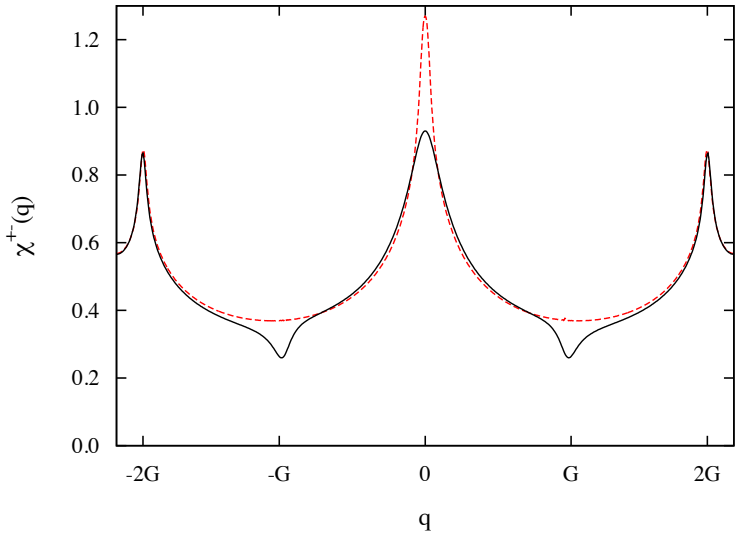

Figure 6.4: Spin susceptibility χ^{+-}(q) in the units of $1/t$ evaluated for the lattice model Eq. (5) with $\mu = 1.5t$, $\Delta = 0$ and $JS = 0$ ($JS = 0.1t$) for dashed (solid) line. A small temperature $T = 0.01t$ has been used to cut off the Lindhard divergences. q extends over the first Brillouin zone $(-\pi/a, \pi/a)$.

Chapter 7

Conclusions

7.1 Summary

In chapter 1 we gave a brief historical overview of the role of topology in condensed matter systems. We introduced basic concepts which are important to better understand the questions we address in this thesis. In chapter 2, we considered the topological electromagnetic response responsible for interesting quantized magneto-electric phenomena in the bulk and at the surface and showed that using simple assumptions this topological action must be quantized. We showed how this topological term can be factorized and written as a product of two first Chern numbers of the abelian electromagnetic gauge field. The quantization of the first Chern numbers follows with an argument which is similar to the Dirac proof of the quantization of monopole charges which arises by requiring that the electronic wave-functions of the constituent particles must be well-defined and therefore single-valued.

The same topological response described above also explains the exotic surface response where the topological phase terminates. This is possible if one considers a profile for the axion field which can be assumed to be constant at the two sides of the interface, i.e., zero at one side and π at the other side. Since θ changes from π to 0 time-reversal symmetry would be broken at the interface unless there is an opposite contribution which arises from the gapless surface modes. This establishes a connection between the bulk topological structure and the existence of odd num-

ber of gapless Dirac surface modes when TR is respected. Careful consideration of the lattice model in a topological phase shows that there is an interesting spin-momentum locking in these electronic surface modes which can be seen in their low energy Dirac Hamiltonian. In chapter 3 we studied one interesting signature of this spin-momentum entanglement which can be used as a sensitive probe of the small intrinsic gaps in their spectrum when the TR symmetry is broken. As we showed, there is a jump in the total magnetization arising from the existence of fully spin polarized LL. We proposed a Knight shift β-NMR measurement as an experimental technique to observe this signature.

In chapter 4 we discussed a toy model for realizing a Weyl semimetal with multiple pairs of isolated Weyl points separated in BZ. A interesting aspect of this model is that although Weyl points are separated in BZ, the system respects TR symmetry. This would not be possible in a system with a single pair of weyl points. As we show, Weyl points contribute oppositely to the anomalous Hall current because of their opposite separation in momentum space.

In chapter 5 we continued studying Weyl semimetals by focusing on their unusual electromagnetic response which had been predicted to exist by the field theoretical considerations based on the effective low energy theory for fermion fields coupled to the classical electromagnetic gauge field. We considered a simple cubic lattice model for a Weyl semimetal and we ruled out the possibility of a static equilibrium CME. However, we showed that the anomalous Hall effect is consistent with the predicted value from the effective field theory.

Finally in chapter 6 we considered a one dimensional system consisting of magnetic adatoms on top of an s-wave superconductor and introduced the notion of self-organized topological phase where the system energetically prefers to be in a topological phase. This phase supports MF at its ends and can be a promising platform for realizing these interesting localized modes.

7.2 Future works

Topological phases and their exotic boundary modes have opened a new promising avenue of research which is growing fast by new discoveries and the high volume of experimental and theoretical works. There are still many missing elements in the

topological table of phases which await discovery [55, 56, 127]. However, recent advances in experimental techniques promises a good future and more exciting discoveries in the field.

In all the discovered three dimensional TR symmetric TIs, an important remaining challenge is the existence of the mid-gap bulk states due to the bulk imperfections and impurities which are contributing to the conductance along with the surface modes [128]. Experimentalists are working to resolve these issues by growing higher quality samples and looking for better potential materials which can be in a TI phase. Another important aspect is to control surface states occupancy (the chemical potential) and also their Dirac masses which in the three dimensional case is very challenging. The magneto-electric response which arises due to existence of the quantized topological $E \cdot B$ action in the effective electromagnetic theory has potential for interesting technological applications [83, 85, 129] by considering various forms of TI interfaces.

In the two dimensional QSH TI phase the only example discovered so far is HgTe, which requires sophisticated experimental techniques which makes the experimental realization a formidable task. Experimentalists are investigating other theoretical proposals based on the deposition of heavy adatoms on top of graphene monolayers to hopefully induce a large SO gap desired for the QSH phase. [31, 32]

Although very recently a three dimensional Dirac phase has been discovered in Na_3Bi [97], a Weyl semimetal phase with isolated modes in momentum has not yet been discovered. However, some of the candidate systems seem experimentally feasible enough to make us believe that they will be discovered in the near future [55–57]. Recently, the negative magneto-resistivity observed in $Bi_{1-x}Sb_x$ near the topological phase transition has been attributed to the existence of a topological $E \cdot B$ term due to the isolated Weyl points which in theory can be formed by breaking the TR symmetry at the critical topological transition point [130]. However, this is still not a smoking gun proof for the existence of the isolated Weyl nodes.

On the other hand, one dimensional topological superconductors with MFs are also highly pursued. Manipulating Majorana states in a controlled fashion in order to exploit their interesting non-Abelian statistics is also an important topic and is another direction which has a good potential for being used in fault-tolerant quantum computation devices that might be invented in the future. More theoretical and

experimental works are required to achieve these goals. The model we described in chapter 6 can be realized with the current experimental techniques and might prove easier access to Majorana modes at its ends by constructing more sophisticated patterns which is possible by moving adatoms using an Scanning Tunnelling Microscopy (STM) tip [112, 113].

It is also important to note that all the phases we discussed here have been based on the assumption that the interaction does not play a major role and therefore can only describe non-interacting or weakly interacting systems. One can imagine more exotic possibilities like fractional topological insulators analogous to the fractional counterparts of the quantum Hall insulators in two spatial dimensions [131, 132]. As far as I understand no such fermion field model, that can arise from a condensed matter system lattice model, has been proposed yet. All the considerations so far have been based on the effective topological field theory for the electromagnetic gauge fields. In two dimensions, there has been some progress in this avenue and lattice models which can have flat bands have been proposed. Flat bands are essential ingredients to realize a fractional topological phase in a two dimensional system without a perpendicular magnetic field.

Overall, there remain several problems to be addressed and roads to be paved to see more exciting discoveries in the field of topological phases of matter.

Bibliography

[1] Ivar Martin and Alberto F. Morpurgo. Majorana fermions in superconducting helical magnets. *Phys. Rev. B*, 85:144505, Apr 2012. → pages iv, 70, 72

[2] S. Nadj-Perge, I. K. Drozdov, B. A. Bernevig, and Ali Yazdani. Proposal for realizing majorana fermions in chains of magnetic atoms on a superconductor. *Phys. Rev. B*, 88:020407, Jul 2013. → pages iv

[3] Mikio Nakahara. *Geometry, topology and physics*. CRC Press, 2003. → pages 1, 30

[4] Mark Anthony Armstrong. *Basic topology*. Springer, 1983. → pages 1

[5] David Scott Richeson. *Euler's Gem: The polyhedron formula and the birth of topology*. Springer, 2008. → pages 2

[6] K. v. Klitzing, G. Dorda, and M. Pepper. New method for high-accuracy determination of the fine-structure constant based on quantized Hall resistance. *Phys. Rev. Lett.*, 45:494–497, Aug 1980. → pages 3

[7] Klaus von Klitzing. Developments in the quantum Hall effect. *Philosophical Transactions of the Royal Society A: Mathematical, Physical and Engineering Sciences*, 363(1834):2203–2219, 2005. → pages 3, 7

[8] R. B. Laughlin. Quantized hall conductivity in two dimensions. *Phys. Rev. B*, 23:5632–5633, May 1981. → pages 6

[9] R.E. Prange and S.M. Girvin. *The quantum Hall effect:*. Springer-Verlag, 1987. → pages 69

[10] Tsuneya Ando, Yukio Matsumoto, and Yasutada Uemura. Theory of hall effect in a two-dimensional electron system. *Journal of the Physical Society of Japan*, 39(2):279–288, 1975. → pages 3

[11] D. J. Thouless, M. Kohmoto, M. P. Nightingale, and M. den Nijs. Quantized Hall conductance in a two-dimensional periodic potential. *Phys. Rev. Lett.*, 49:405–408, Aug 1982. → pages 4, 5, 105

[12] R. Kubo. The fluctuation-dissipation theorem. *Reports on Progress in Physics*, 29(1):255, 1966. → pages 4

[13] Yasuhiro Hatsugai. Chern number and edge states in the integer quantum hall effect. *Phys. Rev. Lett.*, 71:3697–3700, Nov 1993. → pages 5

[14] J. E. Avron, R. Seiler, and B. Simon. Homotopy and quantization in condensed matter physics. *Phys. Rev. Lett.*, 51:51–53, Jul 1983. → pages 5, 7

[15] Qian Niu, D. J. Thouless, and Yong-Shi Wu. Quantized Hall conductance as a topological invariant. *Phys. Rev. B*, 31:3372–3377, Mar 1985. → pages 5

[16] B. I. Halperin. Quantized hall conductance, current-carrying edge states, and the existence of extended states in a two-dimensional disordered potential. *Phys. Rev. B*, 25:2185–2190, Feb 1982. → pages 7

[17] F. D. M. Haldane. Model for a quantum Hall effect without landau levels: condensed-matter realization of the "parity anomaly". *Phys. Rev. Lett.*, 61:2015–2018, Oct 1988. → pages 8, 55, 57, 58

[18] P. R. Wallace. The band theory of graphite. *Phys. Rev.*, 71:622–634, May 1947. → pages 8, 13

[19] AH Castro Neto, F Guinea, NMR Peres, Kostya S Novoselov, and Andre K Geim. The electronic properties of graphene. *Reviews of modern physics*, 81(1):109, 2009. → pages 8, 13, 34

[20] K. S. Novoselov, A. K. Geim, S. V. Morozov, D. Jiang, Y. Zhang, S. V. Dubonos, I. V. Grigorieva, and A. A. Firsov. Electric field effect in atomically thin carbon films. *Science*, 306(5696):666–669, 2004. → pages 8

[21] C. L. Kane and E. J. Mele. Quantum spin Hall effect in graphene. *Phys. Rev. Lett.*, 95:226801, Nov 2005. → pages 8, 9

[22] C. L. Kane and E. J. Mele. $\mathbb{Z}_2$ topological order and the quantum spin Hall effect. *Phys. Rev. Lett.*, 95:146802, Sep 2005. → pages 9, 10

[23] Shuichi Murakami, Naoto Nagaosa, and Shou-Cheng Zhang. Spin-Hall insulator. *Phys. Rev. Lett.*, 93:156804, Oct 2004. → pages 9

[24] Liang Fu and C. L. Kane. Time reversal polarization and a z_2 adiabatic spin pump. *Phys. Rev. B*, 74:195312, Nov 2006. → pages 9, 13

[25] Rahul Roy. z_2 classification of quantum spin hall systems: An approach using time-reversal invariance. *Phys. Rev. B*, 79:195321, May 2009. → pages

[26] J. E. Moore and L. Balents. Topological invariants of time-reversal-invariant band structures. *Phys. Rev. B*, 75:121306, Mar 2007. → pages 12, 16, 17

[27] D. N. Sheng, Z. Y. Weng, L. Sheng, and F. D. M. Haldane. Quantum spin-hall effect and topologically invariant chern numbers. *Phys. Rev. Lett.*, 97:036808, Jul 2006. → pages 9

[28] Markus Konig, Steffen Wiedmann, Christoph Brune, Andreas Roth, Hartmut Buhmann, Laurens W. Molenkamp, Xiao-Liang Qi, and Shou-Cheng Zhang. Quantum spin Hall insulator state in HgTe quantum wells. *Science*, 318(5851):766–770, 2007. → pages 11, 12

[29] B. Andrei Bernevig, Taylor L. Hughes, and Shou-Cheng Zhang. Quantum spin Hall effect and topological phase transition in HgTe quantum wells. *Science*, 314(5806):1757–1761, 2006. → pages 11

[30] B. Andrei Bernevig and Shou-Cheng Zhang. Quantum spin Hall effect. *Phys. Rev. Lett.*, 96:106802, Mar 2006. → pages 11

[31] Conan Weeks, Jun Hu, Jason Alicea, Marcel Franz, and Ruqian Wu. Engineering a robust quantum spin hall state in graphene via adatom deposition. *Phys. Rev. X*, 1:021001, Oct 2011. → pages 12, 87

[32] Jun Hu, Jason Alicea, Ruqian Wu, and Marcel Franz. Giant topological insulator gap in graphene with ¡span class=”aps-inline-formula”¿¡math display=”inline”¿¡mn¿5¡/mn¿¡mi¿d¡/mi¿¡/math¿¡/span¿ adatoms. *Phys. Rev. Lett.*, 109:266801, Dec 2012. → pages 12, 87

[33] Liang Fu, C. L. Kane, and E. J. Mele. Topological insulators in three dimensions. *Phys. Rev. Lett.*, 98:106803, Mar 2007. → pages 12, 34

[34] Rahul Roy. Topological phases and the quantum spin Hall effect in three dimensions. *Phys. Rev. B*, 79:195322, May 2009. → pages 12

[35] Liang Fu and C. L. Kane. Topological insulators with inversion symmetry. *Phys. Rev. B*, 76:045302, Jul 2007. → pages 12, 35

[36] Shuichi Murakami. Phase transition between the quantum spin hall and insulator phases in 3d: emergence of a topological gapless phase. *New Journal of Physics*, 9(9):356, 2007. → pages 13, 18

[37] Xiao-Liang Qi, Taylor L. Hughes, and Shou-Cheng Zhang. Topological field theory of time-reversal invariant insulators. *Phys. Rev. B*, 78:195424, Nov 2008. → pages 13, 16, 17, 32, 33, 35

[38] D. Hsieh, Y. Xia, L. Wray, D. Qian, A. Pal, J. H. Dil, J. Osterwalder, F. Meier, G. Bihlmayer, C. L. Kane, Y. S. Hor, R. J. Cava, and M. Z. Hasan. Observation of unconventional quantum spin textures in topological insulators. *Science*, 323(5916):919–922, 2009. → pages 13, 14, 34

[39] D. Hsieh, Y. Xia, D. Qian, L. Wray, J. H. Dil, F. Meier, J. Osterwalder, L. Patthey, J. G. Checkelsky, N. P. Ong, A. V. Fedorov, H. Lin, A. Bansil, D. Grauer, Y. S. Hor, R. J. Cava, and M. Z. Hasan. A tunable topological insulator in the spin helical Dirac transport regime. *Nature*, 460(7259):1101–1105, 08 2009. → pages 13

[40] David Hsieh, Dong Qian, Lewis Wray, YuQi Xia, Yew San Hor, RJ Cava, and M Zahid Hasan. A topological dirac insulator in a quantum spin hall phase. *Nature*, 452(7190):970–974, 2008. → pages 14, 34

[41] Y. Xia, D. Qian, D. Hsieh, L. Wray, A. Pal, H. Lin, A. Bansil, D. Grauer, Y. S. Hor, R. J. Cava, and M. Z. Hasan. Discovery (theoretical prediction and experimental observation) of a large-gap topological-insulator class with spin-polarized single-Dirac-cone on the surface. *Nature Physics*, 5:398, 2009. → pages 14, 34, 59

[42] Y. L. Chen, J.-H. Chu, J. G. Analytis, Z. K. Liu, K. Igarashi, H.-H. Kuo, X. L. Qi, S. K. Mo, R. G. Moore, D. H. Lu, M. Hashimoto, T. Sasagawa, S. C. Zhang, I. R. Fisher, Z. Hussain, and Z. X. Shen. Massive Dirac Fermion on the surface of a magnetically doped topological insulator. *Science*, 329(5992):659–662, 2010. → pages 14, 18, 35, 43

[43] Rui Yu, Wei Zhang, Hai-Jun Zhang, Shou-Cheng Zhang, Xi Dai, and Zhong Fang. Quantized anomalous Hall effect in magnetic topological insulators. *Science*, 329(5987):61–64, 2010. → pages 35

[44] G. Rosenberg and M. Franz. Surface magnetic ordering in topological insulators with bulk magnetic dopants. *Phys. Rev. B*, 85:195119, May 2012. → pages 14, 16, 18

[45] Yuval Baum and Ady Stern. Magnetic instability on the surface of topological insulators. *Phys. Rev. B*, 85:121105, Mar 2012. → pages 14

[46] G. D. Morris, W. A. MacFarlane, K. H. Chow, Z. Salman, D. J. Arseneau, S. Daviel, A. Hatakeyama, S. R. Kreitzman, C. D. P. Levy, R. Poutissou, R. H. Heffner, J. E. Elenewski, L. H. Greene, and R. F. Kiefl. Depth-controlled $\beta-$nmr of ^{8}li in a thin silver film. *Phys. Rev. Lett.*, 93:157601, Oct 2004. → pages 14, 36

[47] T. J. Parolin, J. Shi, Z. Salman, K. H. Chow, P. Dosanjh, H. Saadaoui, Q. Song, M. D. Hossain, R. F. Kiefl, C. D. P. Levy, M. R. Pearson, and W. A. MacFarlane. Nuclear magnetic resonance study of li implanted in a thin film of niobium. *Phys. Rev. B*, 80:174109, Nov 2009. → pages 14, 36

[48] G. Rosenberg and M. Franz. Witten effect in a crystalline topological insulator. *Phys. Rev. B*, 82:035105, Jul 2010. → pages 16, 17, 32

[49] E. Witten. Dyons of charge $e\theta/2\pi$. *Phys. Rev. B*, 86(34):283 – 287, 1979. → pages 17, 32

[50] R. D. Peccei and Helen R. Quinn. Constraints imposed by CP conservation in the presence of pseudoparticles. *Phys. Rev. D*, 16:1791–1797, Sep 1977. → pages 17

[51] Steven Weinberg. A new light boson? *Phys. Rev. Lett.*, 40:223–226, Jan 1978. → pages

[52] F. Wilczek. Problem of strong P and T invariance in the presence of instantons. *Phys. Rev. Lett.*, 40:279–282, Jan 1978. → pages 17

[53] Frank Wilczek. Two applications of axion electrodynamics. *Phys. Rev. Lett.*, 58:1799–1802, May 1987. → pages 17, 25

[54] Xiao-Liang Qi, Rundong Li, Jiadong Zang, and Shou-Cheng Zhang. Inducing a magnetic monopole with topological surface states. *Science*, 323(5918):1184–1187, 2009. → pages 17, 35

[55] A. A. Burkov and Leon Balents. Weyl semimetal in a topological insulator multilayer. *Phys. Rev. Lett.*, 107:127205, Sep 2011. → pages 18, 20, 49, 55, 58, 61, 87

[56] A. A. Burkov, M. D. Hook, and Leon Balents. Topological nodal semimetals. *Phys. Rev. B*, 84:235126, Dec 2011. → pages 20, 61, 87

[57] A. A. Zyuzin, Si Wu, and A. A. Burkov. Weyl semimetal with broken time reversal and inversion symmetries. *Phys. Rev. B*, 85:165110, Apr 2012. → pages 18, 87

[58] Xiangang Wan, Ari M. Turner, Ashvin Vishwanath, and Sergey Y. Savrasov. Topological semimetal and fermi-arc surface states in the electronic structure of pyrochlore iridates. *Phys. Rev. B*, 83:205101, May 2011. → pages 18, 20, 61, 69

[59] Gang Xu, Hongming Weng, Zhijun Wang, Xi Dai, and Zhong Fang. Chern semimetal and the quantized anomalous hall effect in $hgcr_2se_4$. *Phys. Rev. Lett.*, 107:186806, Oct 2011. → pages 18

[60] Stephen L. Adler. Axial-vector vertex in spinor electrodynamics. *Phys. Rev.*, 177:2426–2438, Jan 1969. → pages 18, 20

[61] J.S. Bell and R. Jackiw. A pcac puzzle: 0 in the -model. *Il Nuovo Cimento A*, 60(1):47–61, 1969. → pages 20

[62] H.B. Nielsen and M. Ninomiya. A no-go theorem for regularizing chiral fermions. *Physics Letters B*, 105(23):219 – 223, 1981. → pages 18, 20

[63] A. A. Zyuzin and A. A. Burkov. Topological response in weyl semimetals and the chiral anomaly. *Phys. Rev. B*, 86:115133, Sep 2012. → pages 18, 20, 58, 61

[64] Gábor B. Halász and Leon Balents. Time-reversal invariant realization of the weyl semimetal phase. *Phys. Rev. B*, 85:035103, Jan 2012. → pages 18

[65] Chao-Xing Liu, Peng Ye, and Xiao-Liang Qi. Chiral gauge field and axial anomaly in a weyl semimetal. *Phys. Rev. B*, 87:235306, Jun 2013. → pages 18

[66] Stephen L. Adler. Axial-vector vertex in spinor electrodynamics. *Phys. Rev.*, 177:2426–2438, Jan 1969. → pages 20

[67] Kenji Fukushima, Dmitri E. Kharzeev, and Harmen J. Warringa. Chiral magnetic effect. *Phys. Rev. D*, 78:074033, Oct 2008. → pages 21

[68] Jason Alicea. New directions in the pursuit of majorana fermions in solid state systems. *Reports on Progress in Physics*, 75(7):076501, 2012. → pages 21, 22, 73, 74

[69] A Yu Kitaev. Unpaired majorana fermions in quantum wires. *Physics-Uspekhi*, 44(10S):131, 2001. → pages 21, 71, 73, 82

[70] Catherine Kallin. Chiral p-wave order in sr 2 ruo 4. *Reports on Progress in Physics*, 75(4):042501, 2012. → pages 21, 69

[71] Liang Fu and C. L. Kane. Superconducting proximity effect and majorana fermions at the surface of a topological insulator. *Phys. Rev. Lett.*, 100:096407, Mar 2008. → pages 21

[72] Yuval Oreg, Gil Refael, and Felix von Oppen. Helical liquids and majorana bound states in quantum wires. *Phys. Rev. Lett.*, 105:177002, Oct 2010. → pages 22, 72, 73

[73] V. Mourik, K. Zuo, S. M. Frolov, S. R. Plissard, E. P. A. M. Bakkers, and L. P. Kouwenhoven. Signatures of majorana fermions in hybrid superconductor-semiconductor nanowire devices. *Science*, 336(6084):1003–1007, 2012. → pages 23

[74] Y. Aharonov and D. Bohm. Significance of electromagnetic potentials in the quantum theory. *Phys. Rev.*, 115:485–491, Aug 1959. → pages 25

[75] J.D. Jackson. *Classical electrodynamics*. Wiley, 1999. → pages 27, 32

[76] Y.M. Shnir. *Magnetic monopoles*. Texts and Monographs in Physics. Springer, 2005. → pages 32

[77] Y. L. Chen, J. G. Analytis, J.-H. Chu, Z. K. Liu, S.-K. Mo, X. L. Qi, H. J. Zhang, D. H. Lu, X. Dai, Z. Fang, S. C. Zhang, I. R. Fisher, Z. Hussain, and Z.-X. Shen. Experimental realization of a three-dimensional topological insulator, Bi_2Te_3 . *Science*, 325(5937):178–181, 2009. → pages 34, 60

[78] M. Z. Hasan and C. L. Kane. *Colloquium*: topological insulators. *Rev. Mod. Phys.*, 82:3045–3067, Nov 2010. → pages 69

[79] Zhanybek Alpichshev, J. G. Analytis, J.-H. Chu, I. R. Fisher, Y. L. Chen, Z. X. Shen, A. Fang, and A. Kapitulnik. Stm imaging of electronic waves on the surface of bi_2se_3: Topologically protected surface states and hexagonal warping effects. *Phys. Rev. Lett.*, 104:016401, Jan 2010. → pages 34

[80] Zhigang Wang, Zhen-Guo Fu, Shuang-Xi Wang, and Ping Zhang. Magnetic quantum oscillations for the surface states of topological insulator bi_2se_3. *Phys. Rev. B*, 82:085429, Aug 2010. → pages 34, 36, 37

[81] Dung-Hai Lee. Surface states of topological insulators: the Dirac Fermion in curved two-dimensional spaces. *Phys. Rev. Lett.*, 103:196804, Nov 2009. → pages 35

[82] G. Rosenberg, H.-M. Guo, and M. Franz. Wormhole effect in a strong topological insulator. *Phys. Rev. B*, 82:041104, Jul 2010. → pages

[83] Wang-Kong Tse and A. H. MacDonald. Giant magneto-optical Kerr effect and universal Faraday effect in thin-film topological insulators. *Phys. Rev. Lett.*, 105:057401, Jul 2010. → pages 87

[84] Joseph Maciejko, Xiao-Liang Qi, H. Dennis Drew, and Shou-Cheng Zhang. Topological quantization in units of the fine structure constant. *Phys. Rev. Lett.*, 105:166803, Oct 2010. → pages

[85] Ion Garate and M. Franz. Inverse spin-galvanic effect in the interface between a topological insulator and a ferromagnet. *Phys. Rev. Lett.*, 104:146802, Apr 2010. → pages 35, 87

[86] Takehito Yokoyama, Yukio Tanaka, and Naoto Nagaosa. Anomalous magnetoresistance of a two-dimensional ferromagnet/ferromagnet junction on the surface of a topological insulator. *Phys. Rev. B*, 81:121401, Mar 2010. → pages 35

[87] I. Meinel, T. Hengstmann, D. Grundler, D. Heitmann, W. Wegscheider, and M. Bichler. Magnetization of the fractional quantum hall states. *Phys. Rev. Lett.*, 82:819–822, Jan 1999. → pages 35

[88] Ines Meinel, Dirk Grundler, Silke Bargstdt-Franke, Christian Heyn, Detlef Heitmann, and Bernd David. High-sensitive superconducting magnetometry on a two-dimensional electron gas up to 10 tesla. *Applied Physics Letters*, 70(24):3305–3307, 1997. → pages 35

[89] J. G. E. Harris, R. Knobel, K. D. Maranowski, A. C. Gossard, N. Samarth, and D. D. Awschalom. Magnetization measurements of magnetic two-dimensional electron gases. *Phys. Rev. Lett.*, 86:4644–4647, May 2001. → pages 35

[90] R. J. Abraham. Principles of magnetic resonance. *Magnetic Resonance in Chemistry*, 28(12):1078–1078, 1990. → pages 35, 45

[91] J. W. McClure. Diamagnetism of graphite. *Phys. Rev.*, 104:666–671, Nov 1956. → pages 36, 37

[92] Chao-Xing Liu, Xiao-Liang Qi, HaiJun Zhang, Xi Dai, Zhong Fang, and Shou-Cheng Zhang. Model hamiltonian for topological insulators. *Phys. Rev. B*, 82:045122, Jul 2010. → pages 36

[93] Jun Xiong, Yongkang Luo, YueHaw Khoo, Shuang Jia, R. J. Cava, and N. P. Ong. High-field shubnikovde haas oscillations in the topological insulator bi_2te_2se. *Phys. Rev. B*, 86:045314, Jul 2012. → pages 36

[94] Robert H Heffner and Donald G Fleming. Muon spin relaxation. *Physics Today*, 37(12):38–46, 2008. → pages 48

[95] HR Leider and DN Pipkorn. Mössbauer effect in mgo: Fe+ 2; low-temperature quadrupole splitting. *Physical Review*, 165(2):494, 1968. → pages

[96] H.-E. Mahnke. Introduction to pac/pad. *Hyperfine Interactions*, 49(1-4):77–102, 1989. → pages 48

[97] Z. K. Liu, B. Zhou, Y. Zhang, Z. J. Wang, H. M. Weng, D. Prabhakaran, S.-K. Mo, Z. X. Shen, Z. Fang, X. Dai, Z. Hussain, and Y. L. Chen. Discovery of a three-dimensional topological dirac semimetal, na3bi. *Science*, 343(6173):864–867, 2014. → pages 49, 87

[98] P. M. Ostrovsky, I. V. Gornyi, and A. D. Mirlin. Interaction-induced criticality in $\mathbb{Z}_2$ topological insulators. *Phys. Rev. Lett.*, 105:036803, Jul 2010. → pages 51

[99] Chang-Yu Hou, Claudio Chamon, and Christopher Mudry. Electron fractionalization in two-dimensional graphenelike structures. *Phys. Rev. Lett.*, 98:186809, May 2007. → pages 56

[100] Yajaira Sierra-Sastre, Sukgeun Choi, S. T. Picraux, and Carl A. Batt. Vertical growth of ge nanowires from biotemplated au nanoparticle catalysts. *Journal of the American Chemical Society*, 130(32):10488–10489, 2008. → pages 59, 60

[101] Sheng Xu, Yaguang Wei, Melanie Kirkham, Jin Liu, Wenjie Mai, Dragomir Davidovic, Robert L. Snyder, and Zhong Lin Wang. Patterned growth of vertically aligned zno nanowire arrays on inorganic substrates at low temperature without catalyst. *Journal of the American Chemical Society*, 130(45):14958–14959, 2008. → pages

[102] Cheng Li and Limin Qi. Colloidal-crystal-assisted patterning of crystalline materials. *Advanced Materials*, 22(13):1494–1497, 2010. → pages 59, 60

[103] William Witczak-Krempa and Yong Baek Kim. Topological and magnetic phases of interacting electrons in the pyrochlore iridates. *Phys. Rev. B*, 85:045124, Jan 2012. → pages 61

[104] Adolfo G. Grushin. Consequences of a condensed matter realization of lorentz-violating qed in weyl semi-metals. *Phys. Rev. D*, 86:045001, Aug 2012. → pages 61, 65

[105] Neil W. Ashcroft and David N. Mermin. *Solid state physics*. Thomson Learning, Toronto, 1st edition, January 1976. → pages 61

[106] Pallab Goswami and Sumanta Tewari. Axionic field theory of $(3+1)-$dimensional weyl semimetals. *Phys. Rev. B*, 88:245107, Dec 2013. → pages 61, 65

[107] Zhou Jian-Hui, Jiang Hua, Niu Qian, and Shi Jun-Ren. Topological invariants of metals and the related physical effects. *Chinese Physics Letters*, 30(2):027101, 2013. → pages 61

[108] Xiao-Liang Qi and Shou-Cheng Zhang. Topological insulators and superconductors. *Rev. Mod. Phys.*, 83:1057–1110, Oct 2011. → pages 62, 69

[109] Liang Fu and Erez Berg. Odd-parity topological superconductors: theory and application to $Cu_xBi_2Se_3$. *Phys. Rev. Lett.*, 105:097001, Aug 2010. → pages 62

[110] J.G. Esteve, Fernando Falceto, and C. Garca Canal. Generalization of the hellmannfeynman theorem. *Physics Letters A*, 374(6):819 – 822, 2010. → pages 68

[111] J. E. Moore. The birth of topological insulators. *Nature*, 464:194, 2010. → pages 69

[112] Kenjiro K Gomes, Warren Mar, Wonhee Ko, Francisco Guinea, and Hari C Manoharan. Designer dirac fermions and topological phases in molecular graphene. *Nature*, 483(7389):306–310, 2012. → pages 70, 88

[113] Marco Polini, Francisco Guinea, Maciej Lewenstein, Hari C Manoharan, and Vittorio Pellegrini. Artificial honeycomb lattices for electrons, atoms and photons. *Nature nanotechnology*, 8(9):625–633, 2013. → pages 70, 88

[114] T.-P. Choy, J. M. Edge, A. R. Akhmerov, and C. W. J. Beenakker. Majorana fermions emerging from magnetic nanoparticles on a superconductor

without spin-orbit coupling. *Phys. Rev. B*, 84:195442, Nov 2011. → pages 70

[115] S. Nadj-Perge, I. K. Drozdov, B. A. Bernevig, and Ali Yazdani. Proposal for realizing majorana fermions in chains of magnetic atoms on a superconductor. *Phys. Rev. B*, 88:020407, Jul 2013. → pages 70

[116] Bernd Braunecker, Pascal Simon, and Daniel Loss. Nuclear magnetism and electronic order in ^{13}c nanotubes. *Phys. Rev. Lett.*, 102:116403, Mar 2009. → pages 71, 75, 81

[117] Bernd Braunecker, George I. Japaridze, Jelena Klinovaja, and Daniel Loss. Spin-selective peierls transition in interacting one-dimensional conductors with spin-orbit interaction. *Phys. Rev. B*, 82:045127, Jul 2010. → pages 71

[118] Pascal Simon, Bernd Braunecker, and Daniel Loss. Magnetic ordering of nuclear spins in an interacting two-dimensional electron gas. *Phys. Rev. B*, 77:045108, Jan 2008. → pages 71, 75

[119] Matthias Menzel, Yuriy Mokrousov, Robert Wieser, Jessica E. Bickel, Elena Vedmedenko, Stefan Blügel, Stefan Heinze, Kirsten von Bergmann, André Kubetzka, and Roland Wiesendanger. Information transfer by vector spin chirality in finite magnetic chains. *Phys. Rev. Lett.*, 108:197204, May 2012. → pages 71

[120] P. Scheller, C. T.-M. Liu, G. Barak, A. Yacoby, N. Pfeiffer, L. W. West, K. and M. Zumbühl, D.˙ Possible evidence for helical nuclear spin order in gaas quantum wires. *Phys. Rev. Lett.*, 112:066801, Feb 2014. → pages 71

[121] Roman M. Lutchyn, Jay D. Sau, and S. Das Sarma. Majorana fermions and a topological phase transition in semiconductor-superconductor heterostructures. *Phys. Rev. Lett.*, 105:077001, Aug 2010. → pages 72, 73

[122] C.W.J. Beenakker. Search for majorana fermions in superconductors. *Annual Review of Condensed Matter Physics*, 4(1):113–136, 2013. → pages 73

[123] T D Stanescu and S Tewari. Majorana fermions in semiconductor nanowires: fundamentals, modeling, and experiment. *Journal of Physics: Condensed Matter*, 25(23):233201, 2013. → pages 73

[124] Hirokazu Tsunetsugu, Manfred Sigrist, and Kazuo Ueda. The ground-state phase diagram of the one-dimensional kondo lattice model. *Rev. Mod. Phys.*, 69:809–864, Jul 1997. → pages 75

[125] Kevin Ingersent. Behavior of magnetic impurities in gapless fermi systems. *Phys. Rev. B*, 54:11936–11939, Nov 1996. → pages 75

[126] Jason Alicea, Yuval Oreg, Gil Refael, Felix von Oppen, and Matthew PA Fisher. Non-abelian statistics and topological quantum information processing in 1d wire networks. *Nature Physics*, 7(5):412–417, 2011. → pages 81

[127] Andreas P. Schnyder, Shinsei Ryu, Akira Furusaki, and Andreas W. W. Ludwig. Classification of topological insulators and superconductors in three spatial dimensions. *Phys. Rev. B*, 78:195125, Nov 2008. → pages 87

[128] Dimitrie Culcer, E. H. Hwang, Tudor D. Stanescu, and S. Das Sarma. Two-dimensional surface charge transport in topological insulators. *Phys. Rev. B*, 82:155457, Oct 2010. → pages 87

[129] B. Seradjeh, J. E. Moore, and M. Franz. Exciton condensation and charge fractionalization in a topological insulator film. *Phys. Rev. Lett.*, 103:066402, Aug 2009. → pages 87

[130] Heon-Jung Kim, Ki-Seok Kim, J.-F. Wang, M. Sasaki, N. Satoh, A. Ohnishi, M. Kitaura, M. Yang, and L. Li. Dirac versus weyl fermions in topological insulators: Adler-bell-jackiw anomaly in transport phenomena. *Phys. Rev. Lett.*, 111:246603, Dec 2013. → pages 87

[131] D. C. Tsui, H. L. Stormer, and A. C. Gossard. Two-dimensional magnetotransport in the extreme quantum limit. *Phys. Rev. Lett.*, 48:1559–1562, May 1982. → pages 88

[132] Joseph Maciejko, Xiao-Liang Qi, Andreas Karch, and Shou-Cheng Zhang. Fractional topological insulators in three dimensions. *Phys. Rev. Lett.*, 105:246809, Dec 2010. → pages 88

Appendix A

Appendix

A.1 Berry phase

The Berry phase is the phase acquired by a state during an adiabatic change of the Hamiltonian in a closed loop in the parameter space. The rate of changing parameters must be in such a way that the state remains to be the eigenstate of the Hamiltonian at all times during the process meaning that the total time that it takes to go around the loop, i.e., T must be longer than other time scales defined by energy gaps. Quantitatively, we have

$$\Phi_B = i\int_0^T < n(t)|\frac{d}{dt}|n(t) > dt, \tag{A.1}$$

Where $|n(t) >$ is an eigenstate of the Hamiltonian $H(t)$ which depends on the parameter $t \in \mathbb{R}$. If the process of changing the Hamiltonian is slow enough, then the state remains to be the eigenstate of the Hamiltonian without acquiring energy from the environment. This is called an adiabatic process. Interestingly, Although t goes back to itself and therefore the initial and final Hamiltonians are the same after going around the loop in the parameter space, the final eigenstate is not necessarily the same as the initial one. In the abelian case the final state differ from the initial one by a phase which is called a Berry phase.

Let us consider a simple example. If you consider a general spinor state for $s = 1/2$ electron in the basis of S_z eigenstates we have

$$|n(\phi,\theta)>=\begin{pmatrix} e^{-i\phi}\cos\frac{\theta}{2} \\ \sin\frac{\theta}{2}\end{pmatrix}, \tag{A.2}$$

this state is the ground state for the Hamiltonian $H=-\zeta\vec{B}\cdot\vec{S}$ with $\vec{B}=B_0\hat{n}$. Now, adiabatic change of the direction of the magnetic field along a loop in the (ϕ,θ) space will change the phase of the initial state by Φ_B given by the following equation

$$\Phi_B = i\oint <\boldsymbol{n}|\nabla|\boldsymbol{n}>\cdot d\boldsymbol{n} = \oint \vec{A}\cdot d\boldsymbol{l}, \tag{A.3}$$

where we have defined $\vec{A}=i<\boldsymbol{n}|\nabla|\boldsymbol{n}>$. According to the stocks theorem one can rewrite it in terms of a surface integral

$$\Phi_B = \oint \vec{A}\cdot d\boldsymbol{l} = \int_S \nabla\times\vec{A}\cdot d\boldsymbol{a}, \tag{A.4}$$

It is easy to calculate $\vec{A}$ and then $\vec{B}$ from it

$$\vec{A}=(\cos\frac{\theta}{2})^2(\sin\theta)^{-1}\hat{\boldsymbol{\phi}} \quad\rightarrow\quad \vec{B}=\nabla\times\vec{A}=\frac{1}{2}\hat{\boldsymbol{r}}, \tag{A.5}$$

Therefore we have

$$\Phi_B = \int_S \vec{B}\cdot d\boldsymbol{a} = \frac{1}{2}\int d\Omega = \frac{\Omega}{2}, \tag{A.6}$$

This geometrical phase also shows up in the path integral representation. The Lagrangian describing the path integral contains a Berry phase term

$$\int \frac{d^2\hat{n}}{2\pi}|\hat{n}><\hat{n}| = \mathbb{1}_{2\times 2}, \tag{A.7}$$

The Green's function then is

$$\begin{aligned} G(\hat{n},\hat{n}_0,t,t_0) &= <\hat{n}|U(t,t_0)|\hat{n}_0> \qquad (A.8)\\ &= <\hat{n}|U(t,t-\Delta t)\cdot U(t-\Delta t,t-2\Delta t)\cdots U(t_0+\Delta t,t_0)|\hat{n}_0> \\ &= \frac{1}{(2\pi)^N}\int D[\hat{n}(t)]e^{i\int_{t_0}^{t}\mathscr{L}(\hat{n}(t),\dot{\hat{n}}(t),t)dt}, \end{aligned}$$

where for $H = 0$ the Lagrangian $\mathscr{L}$ is

$$\mathscr{L} = i < \hat{n}(t)|\frac{d}{dt}|\hat{n}(t) >, \tag{A.9}$$

which is surprisingly nonzero, and it is associated with the Berry phase and therefore is a topological term in the Lagrangian.

This geometrical phase reflects the frustration in choosing the same phase for all of the coherent states.

A.2 TKNN invariant for massive Dirac states

The low energy Hamiltonian describing a two dimensional Dirac state with mass m can be expressed as

$$H(\vec{k}) = \upsilon_x k_x \sigma_x + \upsilon_y k_y \sigma_y + m\sigma_z, \tag{A.10}$$

The eigenstates can be found by diagonalizing above two-by-two matrix. At half filling the occupied state as a function of k_x and k_y have the following spinor form

$$\chi_{\vec{k}} = \begin{pmatrix} e^{-i\phi_{bk}} \cos\frac{\theta_{\vec{k}}}{2} \\ \sin\frac{\theta_{\vec{k}}}{2} \end{pmatrix}, \tag{A.11}$$

where $\phi_{\vec{k}}$ and $\theta_{\vec{k}}$ are defined in terms of (k_x, k_y, m) as follows

$$\cos\theta_{\vec{k}} = \frac{m}{\sqrt{m^2 + \upsilon_x^2 k_x^2 + \upsilon_y^2 k_y^2}}, \tag{A.12}$$

and

$$\cos\phi_{\vec{k}} + i\sin\phi_{\vec{k}} = \frac{\upsilon_x k_x + i\upsilon_y k_y}{\sqrt{\upsilon_x^2 k_x^2 + \upsilon_y^2 k_y^2}}, \tag{A.13}$$

Using these expressions and the similarity between these states with the spinor states defined in the previous sections we can obtain the expressions for the pseudo-magnetic field

$$\vec{A}_{\vec{k}} = (\cos\frac{\theta_{\vec{k}}}{2})^2(\sin\theta_{\vec{k}})^{-1}\hat{\phi}_{\vec{k}} \quad \rightarrow \quad \vec{B} = \nabla_{\vec{k}} \times \vec{A} = \frac{1}{2}\hat{\boldsymbol{r}}_{\vec{k}}, \tag{A.14}$$

where $\hat{\phi}_{\vec{k}}$ and $\hat{\boldsymbol{r}}_{\vec{k}}$ are the unit vectors defined in the spherical coordinate system of (k_x, k_y, m) space.

Using the expression given for the TKNN invariant in Eq. (1.4) we can evaluate this invariant. After some careful consideration and by summing the contribution from all the occupied states we find

$$n = \frac{\mathrm{sgn}(m\upsilon_x\upsilon_y)}{2}. \tag{A.15}$$

A.3 Electrons in a periodic potential

In the absence of the magnetic field and any spin orbit interaction, the Hamiltonian describing noninteracting electrons in a periodic potential can be written as

$$H = (-\frac{\hbar^2}{2m}\vec{\nabla}^2 + V(\vec{r})) \otimes \mathbb{1}_{2\times 2}, \tag{A.16}$$

in which the potential satisfies the following periodicity relation for the three lattice vectors, $\vec{a}_i \quad i = 1,2,3$

$$V(\vec{r} + \vec{a}_i) = V(\vec{r}), \tag{A.17}$$

This periodicity implies that the Hamiltonian is invariant under a symmetry group of discrete translations defined by the same lattice vectors. The generators of this Abelian symmetry group are three translations in each direction given by

$$T_{\vec{a}_i} f(\vec{r}) = f(\vec{r} + \vec{a}_i), \tag{A.18}$$

According to the Bloch theorem this symmetry implies that the eigenstates of the Hamiltonian are also eigenstates of these symmetry operators, therefore they satisfy the following relation

$$\psi_{n\vec{q}}(\vec{r} + \vec{a}_i) = e^{i\vec{q}\cdot\vec{a}_i}\psi_{n\vec{q}}(\vec{r}), \tag{A.19}$$

where n is the band index and $\vec{q}$ is called the lattice wave-vector. Therefore, one can write these Hamiltonian eigenfunctions in terms of the periodic Bloch functions

$$\psi_{n\vec{q}}(\vec{r}) = e^{i\vec{q}\cdot\vec{r}} u_n(\vec{q},\vec{r}), \tag{A.20}$$

The invariance of the wave-function under translation by the system length requires that the lattice momentum can only take discrete values

$$\vec{q} = 2\pi(\frac{n_1}{L_1}, \frac{n_2}{L_2}, \frac{n_3}{L_3}), \tag{A.21}$$

where (L_1, L_2, L_3) are the dimensions of the system. Shifting $\vec{q}$ vectors by the reciprocal vectors $\vec{G}_i$ does not change the wavefunction since

$$e^{i\vec{G}_i.\vec{a}_i} = e^{2\pi i} = 1, \tag{A.22}$$

The lattice constructed by these $\vec{G}_i$ vectors is called the reciprocal lattice. The $\vec{q}$ points in the unit cell of the reciprocal lattice is called Brillouin Zone (BZ). The $\vec{q}$ points in the BZ are the distinct quantum numbers which label the Bloch wavefunctions. The energy as a function of $\vec{q}$ for each band n, i.e., $\varepsilon_n(\vec{k})$ is called the band spectrum.

A.4 Generalized Bloch states

Turning on a perpendicular magnetic field in a two dimensional electron system breaks the discrete translational symmetry of the two dimensional lattice. If the magnetic field is commensurate meaning that the magnetic flux going through a unit cell is a rational multiple of quantum of magnetic flux, i.e., $(m/n)\cdot(h/e)$, then it is possible to define a generalized version of the Bloch states. For this to happen one needs to use a Landau gauge, $\vec{A} = (0, eBx)$. The eigenfunctions of the Hamiltonian describing such a system can be chosen in a way that they satisfy a generalized version of the Bloch condition for the translations along x [11]

$$\psi_{k_1k_2}(x+ma, y) = exp(2\pi imy/b + ik_1na)\psi_{k_1k_2}(x,y), \tag{A.23}$$

One can then define periodic functions with a generalized periodicity given by

$$u_{k_1k_2}(x+ma,y) = exp(2\pi imy/b)u_{k_1,k_2}(x,y), \tag{A.24}$$

These are the generalized Bloch functions and are eigenfunctions of the following Hamiltonian

$$H(k_1,k_2) = \frac{1}{2m}\left(-i\hbar\frac{\partial}{\partial x}+\hbar k_1\right)^2 + \frac{1}{2m}\left(-i\hbar\frac{\partial}{\partial y}+\hbar k_2 - eBx\right)^2 + V(x,y), \tag{A.25}$$

In fact one uses these generalized Bloch functions to get non-zero Hall conductance in Eq. (1.2).

A.5 From discrete to continuum limit

Consider a 1D lattice system with lattice spacing a and we can define a quantity f on each site, i.e., f_n is the f value on nth site. The average of this quantity on this lattice would be

$$\bar{f} = \frac{1}{N}\sum_{n=1}^{N} f_n, \tag{A.26}$$

Now if $N = L/a$ is very large we can approximate a continuum theory for the above expression as follows

$$\bar{f} = \frac{1}{L}\int_0^L dx f(x), \tag{A.27}$$

Note that this has been obtained using the following substitution

$$\sum_{n=1}^{N} \to \int_{-\infty}^{\infty} dx\rho(x) = \frac{1}{a}\int_0^L dx, \tag{A.28}$$

$f(x)$ is the average of f_n in a dx segment with a center at x.

we can generalize this to a case like the following

$$< fg >= \frac{1}{N}\sum_{n=0}^{N} f_n g_n \to \frac{1}{N}\int_{-\infty}^{\infty} dx\rho(x)f(x)g(x) = \frac{1}{L}\int_0^L dx f(x)g(x), \tag{A.29}$$

Note that here we are approximating $f(x)g(x)$ as being the product of the averages of the f_n and g_n over a dx segment centred at x which would be equal to the average of the $f_n g_n$ if the quantities does not vary radically over a length scale dx and they can be approximated by linear functions.

another form which is a bit trickier is the following quantity

$$F_p = \frac{1}{N}\sum_{n=1}^{N}(f_n - f_{n-1})^p, \tag{A.30}$$

which becomes

$$F_p = \frac{1}{N}\int_{-\infty}^{\infty} dx\rho(x)[f(x) - f(x-a)]^p = \frac{1}{L}\int_0^L dx(\partial_x f(x))^p, \tag{A.31}$$

Now let see what happens to a function like $f_n = V\delta_{nl}$ where δ_{nl} is the Kronecker function so f_n is only non-zero at lth site

$$\bar{f} = \frac{1}{N}\sum_{n=1}^{N} V\delta_{nl} = \frac{V}{N}, \tag{A.32}$$

Now in the continuum limit we still need to find the same value

$$\bar{f} = \frac{1}{L}\int_0^L f(x)d(x) = \frac{V}{N}, \tag{A.33}$$

It turns out that $f(x)$ has all the properties of the Dirac's delta function as we take the limit, i.e., $f(x) = aV\delta(x - x_l)$.

Now as we take a to zero if $Va = \mathscr{V}$ remains constant we get

$$f(x) = \mathscr{V}\delta(x - x_l), \tag{A.34}$$

This happens when V grows linearly with N this way we have

$$\lim_{a\to 0} Va = V_0 Na = V_0 L, \tag{A.35}$$

Now we use above arguments to derive the famous integral representation of Dirac delta function, namely,

$$\delta(k-k_0) = \frac{1}{2\pi}\lim_{L\to\infty}\int_{-L/2}^{L/2} dx e^{i(k-k_0)x}, \tag{A.36}$$

we define a lattice with a lattice spacing $2\pi/L$ when we take L to infinity we can make every $k_n \equiv k_0 + (2\pi n)/L$ sufficiently close to any k

this way we have

$$I = \frac{1}{2\pi}\int_{-L/2}^{L/2} dx e^{i2\pi nx/L} = \frac{-iL}{(2\pi)^2}\oint z^{n-1}dz = \frac{L}{2\pi}\delta_{k_n k_0} = \frac{\delta_{k_n k_0}}{a}, \tag{A.37}$$

Now according to our continuum conversion we have

$$I = \frac{\delta_{k_n k_0}}{a} = \delta(k_n - k_0), \tag{A.38}$$

which proves Eq. (A.36). For finite L we need the periodic boundary condition in x (i.e., $x = x + L$) in order to get the kronecker function form of Eq. (A.36)

A.6 Fourier transform of the step function

The F.T. of a step function, i.e., $\Theta(t)$ can be expressed as

$$\Theta(\omega) = \int_0^\infty e^{i\omega t - 0^+ t} = \frac{i}{\omega + i0^+}, \tag{A.39}$$

A.7 Fourier transform of the product

Consider two functions $f(t)$ and $g(t)$. The F.T. of the product can be written in terms of an integral of the product of the F.T.s components as follows

$$\begin{aligned}
[f.g](\omega) &= \int_{-\infty}^{\infty} f(t)g(t)e^{i\omega t}dt \\
&= \int_{-\infty}^{\infty}\frac{d\omega'}{2\pi}f(\omega')\int_{-\infty}^{\infty}dt g(t)e^{i(\omega-\omega')t} \\
&= \int_{-\infty}^{\infty}d\omega' f(\omega')g(\omega-\omega'),
\end{aligned} \tag{A.40}$$

Now by using what we have got in the previous section we find

$$\int_0^\infty dt f(t) e^{-i\omega t - 0^+ t} = \int_{-\infty}^\infty d\omega' \frac{f(\omega')}{\omega - \omega' + i0^+}. \tag{A.41}$$

A.8 Green's function for Schrodinger equation

$$i\hbar \frac{\partial \Psi(t)}{\partial t} = \mathscr{H}\Psi(t), \tag{A.42}$$

$$i\hbar \partial_t \hat{U}(t,t_0) = \mathscr{H}\hat{U} \qquad \Psi(t) = \hat{U}(t,t_0)\Psi(t_0), \tag{A.43}$$

where $\hat{U}(t,t_0)$ for time independent Hamiltonian takes the following form

$$\hat{U}(t,t_0) = e^{i\mathscr{H}(t-t_0)/\hbar}, \tag{A.44}$$

for a time-dependent Hamiltonian for which $[\hat{\mathscr{H}}(t), \hat{\mathscr{H}}(t')] = 0$ for all t, t' we have

$$\hat{U}(t,t_0) = e^{i\int_{t_0}^t \hat{\mathscr{H}}(t')dt'/\hbar}, \tag{A.45}$$

for the case where $[\hat{\mathscr{H}}(t), \hat{\mathscr{H}}(t')] \neq 0$ we get the dyson series

$$\hat{U}(t,t_0) = 1 + \sum_{n=1}^{\infty} (-\frac{i}{\hbar})^n \int_{t_0}^t dt_1 \int_{t_0}^{t_1} dt_2 ... \int_{t_0}^{t_{n-1}} dt_n \hat{\mathscr{H}}(t_1)\hat{\mathscr{H}}(t_2)\hat{\mathscr{H}}(t_3)...\hat{\mathscr{H}}(t_n), \tag{A.46}$$

using the time-ordering operator it can be written as

$$\hat{U}(t,t_0) = \mathscr{T}(e^{i\int_{t_0}^t \hat{\mathscr{H}}(t')dt'/\hbar}), \tag{A.47}$$

$$i\hat{G}(t,t_0) \equiv \hat{U}(t,t_0)\Theta(t-t_0), \tag{A.48}$$

where $\Theta(t)$ is the step function

$$i(i\hbar\partial_t - \hat{\mathscr{H}})\hat{G}(t,t_0) = -\hbar\delta(t-t_0)\hat{U}(t,t_0) = -\hbar\delta(t-t_0)\mathbb{1}, \tag{A.49}$$

Therefore we get

$$(i\hbar\partial_t - \hat{\mathscr{H}})G(t,t_0) = i\hbar\delta(t-t_0)\mathbb{1}, \tag{A.50}$$

In position basis it becomes

$$(i\hbar\partial_t - \hat{\mathscr{H}}(\vec{x}))G(\vec{x},t;\vec{x}_0,t_0) = i\hbar\delta(t-t_0)\delta(\vec{x}-\vec{x}_0), \tag{A.51}$$

If we F.T. the time we get

$$\hat{G}(\omega) = \int_{-\infty}^{\infty} \hat{G}(t_0+t,t_0)e^{i\omega t-\eta t}, \tag{A.52}$$

and from Eq. (A.50) we obtain the following equation for $\hat{G}(\omega)$

$$(\hbar\omega - \hat{\mathscr{H}} + i\eta)\hat{G}(\omega) = i\hbar, \tag{A.53}$$

$$\hat{G}(\omega) = \frac{i\hbar}{\hbar\omega - \hat{\mathscr{H}} + i\eta}. \tag{A.54}$$

A.9 Density of states function from the Green's function

The density of the states function can be defined as follows

$$D(E) = \sum_i \delta(E-\varepsilon_i) = \mathrm{tr}[\delta(E-\hat{\mathscr{H}})], \tag{A.55}$$

but we also have the following limit definition of the Dirac delta function

$$\frac{1}{x \pm i0^+} = P.V.(\frac{1}{x}) \mp \pi\delta(x), \tag{A.56}$$

So from the previous section we find that

$$D(E) = -\frac{1}{\pi}\mathrm{tr}[\mathrm{Im}(\hat{\bar{G}}(\omega = \frac{E}{\hbar}))], \tag{A.57}$$

Where $i\hbar\bar{G} = G$

A.10 Green's function for a perturbed system

$$(\hbar\omega - \hat{\mathscr{H}_0} - \hat{V} + i\eta)\hat{G}(\omega) = i\hbar \quad \rightarrow \quad \hat{G}(\omega) = \hat{G}_0(\omega) - \frac{i}{\hbar}\hat{G}_0(\omega)\hat{V}\hat{G}(\omega), \tag{A.58}$$

we can also write it as

$$\hat{G}(\omega) = \frac{1}{1 + \frac{i}{\hbar}\hat{G}_0(\omega)\hat{V}}\hat{G}_0(\omega), \tag{A.59}$$

Note that we can recover more well-known equation for this if we replace G with $i\hbar G$

$$\hat{G}(\omega) = \frac{1}{1 - \hat{G}_0(\omega)\hat{V}}\hat{G}_0(\omega) \qquad \hat{G}(\omega) = \hat{G}_0(\omega) + \hat{G}_0(\omega)\hat{V}\hat{G}(\omega), \tag{A.60}$$

for a time dependent perturbation $\hat{V}$ it takes the following form

$$\hat{G}(\omega) = \hat{G}_0(\omega) - \frac{i}{\hbar}\int_{-\infty}^{\infty}\frac{d\omega'}{2\pi}\hat{G}_0(\omega)\hat{V}(\omega')\hat{G}(\omega - \omega'). \tag{A.61}$$

A.11 Quantum linear response theory

Consider the following Hamiltonian

$$H = H_0 + \hat{O}_1 f(t), \tag{A.62}$$

where H_0 is the base Hamiltonian where its ground-state is known. One can ask what would be the effect of this additional term on the expectation value of another operator like $\hat{O}_2$ at an arbitrary time t

$$\begin{aligned} \delta < |\hat{O}_2(t)| > &\equiv < \Psi(t)|\hat{O}_2|\Psi(t) > - < \Psi_0(t)|\hat{O}_2|\Psi_0(t) > \\ &= < \delta\Psi(t)|\hat{O}_2|\Psi(t) > + < \Psi(t)|\hat{O}_2|\delta\Psi(t) >, \end{aligned} \tag{A.63}$$

where $|\Psi(t) >= |\Psi_0(t) > +|\delta\Psi(t) >$ and it is easy to see that $|\delta\Psi(t) >$ in linear order is given by

$$|\delta\Psi(t)>=-ie^{-iH_0(t-t_{-\infty})}\int_{t_{-\infty}}^{t}dt'\hat{O}_1(t')f(t'), \tag{A.64}$$

where $\hat{O}_1(t')=e^{iH_0(t'-t_{-\infty})}\hat{O}_1e^{-iH_0(t'-t_{-\infty})}$ therefore by substituting the above into Eq.(A.63) we get

$$\delta<|\hat{O}_2(t)|>=-i\int_{t_{-\infty}}^{t}dt'<\Psi_0|[\hat{O}_2(t),\hat{O}_1(t')]|\Psi_0>f(t'), \tag{A.65}$$

which can be written as

$$\delta<|\hat{O}_2(t)|>=\int_{-\infty}^{\infty}dt'D(t,t')f(t'), \tag{A.66}$$

where $D(t,t')$ is defined as

$$D(t,t')=-i\Theta(t-t')<\Psi_0|[\hat{O}_2(t),\hat{O}_1(t')]|\Psi_0>, \tag{A.67}$$

So the response function $D(t,t')$ is relation to the correlation function

A.12 Coupled systems and the effective theory

Consider two systems described by Hamiltonians H_1 and H_2 coupled through $\mathscr{H}_{int}$

$$\mathscr{H}=\underbrace{H_1\otimes\mathbb{1}+\mathbb{1}\otimes H_2}_{\mathscr{H}_0}+\mathscr{H}_{int}, \tag{A.68}$$

any observable operator A defined in the system 1 Hilbert space has the following expectation value

$$<|A|>=\mathrm{tr}(\rho\cdot A\otimes\mathbb{1})=\mathrm{tr}_1\mathrm{tr}_2(\rho\cdot A\otimes\mathbb{1})=\mathrm{tr}_1(\rho_1A), \tag{A.69}$$

where $\rho_1=\mathrm{tr}_2(\rho)$. This can be understood from

$$[A\otimes B]_{ijlk}=<\phi_l,\varphi_k|A\otimes B|\phi_i,\varphi_j>=<\phi_l|A|\phi_i>\cdot<\varphi_k|B|\varphi_j>=A_{il}B_{jk}, \tag{A.70}$$

$$\mathrm{tr}(A\otimes B)=\mathrm{tr}_1(A)\mathrm{tr}_2(B), \tag{A.71}$$

So the system described by ρ_1 is an effective theory in which we have integrated out the degrees of freedom we had from the second system.

To understand this better, consider it in the position basis in which we have

$$< x_b|\hat{\rho}_1|x_a >= \mathrm{tr}_2 < x_b|\hat{\rho}|x_a >= \int < x_b, X|\hat{\rho}|x_a, X > dX, \tag{A.72}$$

Consider for example the canonic ensemble where we can have a path integral for its partition function and therefore relate it to the classical action for the system.

So from the path integral representation for the effective partition function obtained from the effective density operator $\rho_1 = \mathrm{tr}_2(\rho)$ (for example ρ_1 can be $e^{-\beta H}$ when you integrate out the system 2 being the thermal bath) we can find the effective action describing the system where we integrate all degrees of freedom available for system 2.

So we have the following for the partition function

$$Z = \int \mathscr{D}[x(t)]\mathscr{D}[X(t)]e^{i[S_1(x)+S_2(X)+S_{int}(x,X)]}, \tag{A.73}$$

where $(x,X)(t) = (x,X_b)$, $(x,X)(t_0) = (x,X_a)$,

$$S_1(x) = \int_{t_0}^{t} L_1(x,\dot{x},t)dt, \quad S_2(X) = \int_{t_0}^{t} L_2(X,\dot{X},t)dt, \tag{A.74}$$

and

$$S_{int}(x,X) = \int_{t_0}^{t} L_{int}(x,\dot{x},X,\dot{X},t)dt, \tag{A.75}$$

We can write $Z = Z_{eff}Z_X$ in which the two systems are decoupled in a sense and the system 1 through Z_{eff} carries information from its interaction with the system 2.

$$Z = \int \mathscr{D}[x(t)]\mathscr{D}[X(t)]e^{i[S_1(x)+S_2(X)+S_{int}(x,X)]} = \underbrace{\int \mathscr{D}[x(t)]e^{iS_{eff}(x)}}_{Z_{eff}} \cdot \int \mathscr{D}[X(t)]e^{iS_2(X)}, \tag{A.76}$$

where $S_{eff}(x) = S_1(x) + S_I(x)$ and $S_I(x)$ is defined as

$$e^{iS_I(x)} = \frac{\int \mathscr{D}[X(t)] e^{i[S_2(X)+S_{int}(x,X)]}}{\int \mathscr{D}[X(t)] e^{iS_2(X)}}, \tag{A.77}$$

The effective quantum theory for system 1 is in fact approximately a theory in which the interaction of it with system 2 has been averaged over the canonical ensemble of system 2

$$Z_{eff} = < | \int \mathscr{D}[x(t)] e^{i[S_1(x)+S_{int}(x,X)]} | >_2, \tag{A.78}$$

where $< \star >_2$ is

$$< \star >_2 = \frac{\int \mathscr{D}[X(t)] \star e^{iS_2(X)}}{\int \mathscr{D}[X(t)] e^{iS_2(X)}}. \tag{A.79}$$

A.13 Topologically protected semi-metal

At low energies, the minimal Hamiltonian describing the unstable 3D gapless system at the TI-OI transition point with a pair of energy crossing points would have the following form

$$\mathscr{H} = \sum_{\alpha=\pm} \sum_{|\vec{k}-\vec{w}_\alpha|<\Lambda} \Psi^\dagger_\alpha(\vec{k}) [\vec{\lambda}_\alpha . (\vec{k} - \vec{w}_\alpha)] \Psi_\alpha(\vec{k}), \tag{A.80}$$

where $\vec{\lambda}_\alpha$ are 2-by-2 matrices given by

$$\vec{\lambda} = (\upsilon_x \sigma_x, \upsilon_y \sigma_y, \upsilon_z \sigma_z), \tag{A.81}$$

in which $\vec{w}_+ = \vec{w}_- = \vec{w}_0$ are the positions of the Weyl points with opposite chirality ($= \mathrm{sgn}(\upsilon_x \upsilon_y \upsilon_z)$) in the BZ. This Hamiltonian consists of doubly degenerate Dirac cones with the Dirac points located at $\vec{w}_0$. The two component spinor operator $\Psi^\dagger_\pm$ is associated with the modes on the Dirac cone with chirality $\alpha = \pm$. This Hamiltonian describes the gapless phase at the phase transition point between a topological insulator and an ordinary insulator. When the opposite chirality Weyl points happen at the same point in the BZ there is no topological protection and even momentum conserving perturbations that connect the degenerate states can drive the system to an insulator phase. Now if somehow the opposite chirality

points become separated ($\vec{w}_+ - \vec{w}_- = \vec{q} \neq 0$) then the system would be in a gapless topological phase where small local momentum conserving perturbations cannot produce a gap in the spectrum and would only shift the position of the Weyl points in the BZ.

Using the mathematical properties of the Clifford algebra it is possible to see how such protection can occur for a gapless system containing a pair of separated opposite chirality Weyl points. The local Hamiltonian matrix in the BZ describing the low energy states in the topological semi-metal phase containing a pair of opposite chirality Weyl points can be written as follows

$$\mathscr{H}(\vec{k}) = k_x\gamma_1 + k_y\gamma_2 + k_z\gamma_3 + \frac{q}{2}\gamma_3', \tag{A.82}$$

where for simplicity and without the loss of the generality we have put $|\upsilon_{x,y,z}| = 1$. Note that by writing the Hamiltonian in this fashion we implicitly exclude any perturbation that connects two Weyl nodes which might arise from the e-e interactions and scattering sources and can potentially gap out the Weyl nodes. This Hamiltonian has three terms (4-by-4 hermitian matrices) which are anti-commuting with each other, i.e., $\gamma_{1,2,3}$. It also has a term which is essential to separate the Weyl points in the BZ. This term commutes with one of the terms and anti-commutes with all others. So we have $\{\gamma_i, \gamma_j\} = \{\gamma_{1,2}, \gamma_3'\} = 0$ and $[\gamma_3, \gamma_3'] = 0$. The last term separates the Weyl points along the k_z axis by q and the resulting spectrum is given by

$$\varepsilon_{\vec{k},s} = \pm\sqrt{k_x^2 + k_y^2 + (k_z + \frac{sq}{2})^2}, \qquad s = \pm 1, \tag{A.83}$$

In order to open up a gap by adding a local momentum conserving term to the Hamiltonian in a way that doesn't merge the Weyl points there must be a hermitian matrix that anti-commutes with all of the terms in the above Hamiltonian. The statement we want to prove here is that no such term exist and any 4-by-4 hermitian matrix which can be written as a superposition of the normalized Clifford algebra matrices, γ_g, (${\gamma_g}^2 = I_{4\times 4}$) would commute with at least one of the terms in this Hamiltonian and therefore cannot produce a gap in the spectrum and only shifts the position of the Weyl nodes. In order to prove this statement consider the most

general form of a normalized matrix that anti-commutes with $\gamma_{1,2,3}$ and we show that it cannot at the same time anti-commute with γ_3'. In order to do so we need to choose a representation of the present matrices. We can choose a basis in which both γ_3 and γ_3' are diagonal since they commute with each other. This way we have $\gamma_3 = \text{diag}[1, a_1, a_2, -1-a_1-a_2]$ and $\gamma_3' = \text{diag}[1, b_1, b_2, -1-b_1-b_2]$. It turns out that only three independent choices can satisfy the commutation condition, i.e., $(a_1, a_2, b_1, b_2) = (1,-1,-1,1), (-1,1,1,-1), (-1,1,-1,-1)$. For each of these choices only two independent normalized matrices exist that anti-commute with γ_3 and γ_3' and with themselves. This would then imply that no other matrices exist that anti-commutes with all the existing matrices in the Hamiltonian. To see how this works consider the most general normalized matrix satisfying the aforementioned conditions for the first choice of (a_1, a_2, b_1, b_2). For this particular representation it would be in the following form

$$\gamma_p = \begin{pmatrix} 0 & 0 & 0 & e^{i\phi} \\ 0 & 0 & e^{i\theta} & 0 \\ 0 & e^{-i\theta} & 0 & 0 \\ e^{-i\phi} & 0 & 0 & 0 \end{pmatrix}, \tag{A.84}$$

Matrices of this form that anti-commute with each other must satisfy $|\phi_i - \phi_j| = |\theta_i - \theta_j| = \pi/2$. It is easy to see that only two independent matrices can be found in this representation to mutually satisfy this equations. These matrices are already exploited in the Hamiltonian therefore no other matrices can be added to the Hamiltonian given in Eq. (A.82) that anti-commutes with all the present matrices. The same argument can be established for the other two choices of (a_1, a_2, b_1, b_2). Therefore, Weyl nodes cannot be annihilated unless two of them with opposite chirality merge together at the same point in the BZ. This would not be possible without the sufficiently strong local perturbations ($\sim |\hbar v_F q|$) and the system would be in a topological semimetal phase in at least a region of the phase space. The above proof is a generalization of the argument in which one considers only one of the isolated Weyl nodes in a two band model using two-by-two Pauli matrices. Here we have considered all the four bands that are present in the low energy theory describing a pair of Weyl fermions; therefore, it is on a more solid ground.

A.14 Mean-field treatment of H_{int}

The interaction term in the Hamiltonian is made up of some quadratic terms like $\Psi_1^\dagger\Psi_1\Psi_2^\dagger\Psi_2$. There are various ways to decouple these terms. In the following, we consider one specific decomposition channel.

First we use the anti-commutation relations, i.e., $\{\Psi_\alpha,\Psi_\beta^\dagger\}=\delta_{\alpha\beta}$, $\{\Psi_\alpha,\Psi_\beta\}=\{\Psi_\alpha^\dagger,\Psi_\beta^\dagger\}=0$ to get

$$\Psi_1^\dagger\Psi_1\Psi_2^\dagger\Psi_2=\frac{1}{2}[\Psi_1^\dagger\Psi_1+\Psi_2^\dagger\Psi_2]+\frac{1}{2}[\Psi_1\Psi_2^\dagger\Psi_1^\dagger\Psi_2+\Psi_2\Psi_1^\dagger\Psi_2^\dagger\Psi_1], \tag{A.85}$$

Now one can rewrite $\Psi_1\Psi_2^\dagger\Psi_1^\dagger\Psi_2$ as follows

$$\begin{aligned}\Psi_1\Psi_2^\dagger\Psi_1^\dagger\Psi_2 &= (\Psi_1\Psi_2^\dagger-<\Psi_1\Psi_2^\dagger>)(\Psi_1^\dagger\Psi_2-<\Psi_1^\dagger\Psi_2>) \\ &+ <\Psi_1\Psi_2^\dagger>\Psi_1^\dagger\Psi_2+<\Psi_2\Psi_1^\dagger>\Psi_2^\dagger\Psi_1+|\Psi_1\Psi_2^\dagger|^2,\end{aligned} \tag{A.86}$$

Now we assume that the first term is negligible according to the MF approximation so if we do the same thing for the other term and sum up after some simple commutations we get

$$\begin{aligned}\Psi_1^\dagger\Psi_1\Psi_2^\dagger\Psi_2 &= \frac{1}{2}[\Psi_1^\dagger\Psi_1+\Psi_2^\dagger\Psi_2]+<\Psi_1\Psi_2^\dagger>\Psi_1^\dagger\Psi_2 \\ &+ <\Psi_2\Psi_1^\dagger>\Psi_2^\dagger\Psi_1+|\Psi_1\Psi_2^\dagger|^2,\end{aligned} \tag{A.87}$$

Where we have chosen $<\Psi_1\Psi_2^\dagger>=\mathscr{M}_{12}$ as the order parameter. We can also drop the first two terms in the RHS since they are independent of the order parameter and they can be considered as an overall shift in the energy. (we cannot drop the last term though since although it is an overall shift but, it depends on the order parameter so it plays a role in when the order parameter varies) So this way we end up with

$$\Psi_1^\dagger\Psi_1\Psi_2^\dagger\Psi_2=\mathscr{M}_{12}\Psi_1^\dagger\Psi_2+\mathscr{M}_{12}{}^\star\Psi_2^\dagger\Psi_1+\mathscr{M}_{12}\mathscr{M}_{12}{}^\star. \tag{A.88}$$